A Photonic Generation and Transmission System for Millimetre-Wave Futuristic Communications

By

Rasha Khalid Mohammed Al-Dabbagh

A Thesis Submitted in fulfilment of the requirements

For the Degree of Doctor of Philosophy (PhD)

Department of Electronic and Computer Engineering

College of Engineering, Design and Physical Sciences

Brunel University London

Supervised By: Professor Hamed Al-Raweshidy

May 2018

Abstract

In this thesis, a fully millimetre-wave (mm-wave) generation and transmission system is proposed for futuristic communications. Significant challenges have been dealt with regarding the proposed system, including designing the mm-wave generation and transmission technique, and its application in cellular networks. These challenges are presented through five main contributions and validated via Optiwave Design Software and MATLAB simulation tools.

Firstly, three novel photonic generation methods are proposed and designed based on the characteristics of Brillouin fibre laser and the Stimulated Brillouin Scattering (SBS) effects with phase modulation. The mm-wave carriers are successfully generated with a tuning capability from 5 to 90 GHz. Also, these carriers are with good Signal to Noise Ratio (SNR) up to 51 dB, and low noise signal power of about -40 dBm. The impact of these methods is obtaining stable mm-waves appropriate for Radio over Fibre (RoF) transmission systems in 5G optical networks.

Secondly, a full-duplex RoF system with the generation of a 64 GHz mm-wave is proposed. Successful transmission of the mm-wave over a fibre link is achieved for up to 100 km of fibre with a data rate of 5 Gbits/s. The main impact of this system is cost reduction and performance improvement by simplifying mm-wave generation and transmission over fibre. Also, it ensures a useful communication link for small cell networks.

Thirdly, a hybrid Fibre/Free-space optical (FSO) system for the generation and transmission of 64 GHz mm-wave is proposed. This optical system provides a low latency communication link and overcomes mm-wave high path losses. A successful mm-wave transmission is achieved over a 10 km fibre length, and 2 km FSO link length with a good Bit Error Rate (BER) of about 1.5×10^{-13} and a data rate of 10 Gbits/s. This system increases the network coverage area by transmitting the mm-wave over the FSO link to the areas with natural obstacles the laying of fibre cables impossible. Also, it can be used as an effective solution under emergency disaster conditions.

Fourthly, a comprehensive study of the wireless propagation performance for different mm-wave bands (28, 60, and 73 GHz) as cellular networks is investigated and compared with the 2.4 GHz Ultra-High Frequency band (UHF). A map-based scenario is proposed for the deployment of Base Stations (BSs) within the Brunel University London Campus map to consider real blockage effects. This investigation involved specifying which mm-wave spectrum can enhance the futuristic cellular networks, by evaluating the coverage and rate trends. Comparative results show that the 73 GHz bands can achieve the higher rate with good coverage and the lowest interference effects than the other mm-wave bands.

Finally, a simplified path loss model is proposed to estimate precisely the 28 GHz mm-wave performance, which is considered a key component in 5G networks in outdoor applications. The proposed path loss model captures the diffraction and specular reflection impacts on mm-wave wireless propagation.

Table of Contents

Dedication

To

My father (Khalid Al-Dabbagh)

For making me be who I am, and for supporting me all the way.

To

The memory of my mother (Samira)

The strong and gentle soul who taught me to believe in myself.

To

My beloved Husband (Dhafer Mohammed)

Without him, none of my success would be possible.

To

My treasure, my wonderful blessing from the God,

My daughters

(Farah and Rafal)

Acknowledgements

First of all, I would like to thank my principal supervisor Professor Hamed Al-Raweshidy for his valuable advice and guidance during the PhD period. He has been very helpful and supportive for all these years.

I am thankful to my second supervisor Dr Rajagopal Nilavalan for his encouragement and support. I would also like to acknowledge the Estates Department at Brunel University London for their help in providing the information of the campus map. Also, my gratitude goes to my colleagues in the Wireless Networks and Communications Centre (WNCC), who have been supportive throughout this period. I would like to acknowledge the great attitude of all the staff members that I have interacted with at Brunel University London and specifically in the Department of Electronic and Computer Engineering.

I would like to express my appreciation and gratefulness to the Iraqi Ministry of Higher Education and scientific research for funding my PhD study.

Finally, to my father, brothers, sisters, relatives, friends: thank you for being beside me as a source of care, love, motivation and encouragement, which travel the distance that separates us, and fill me with patience and commitment.

London, May 2018

Rasha Al-Dabbagh

Declaration

I declare that this thesis is my own work and is submitted for the first time to the Post-Graduate Research Office. The study was originated, composed and reviewed by myself and my supervisors in the Department of Electronic and Computer Engineering, College of Engineering, Design and Physical Sciences, Brunel University London, UK. All the information derived from other works has been properly referenced and acknowledged.

SIGNED: Rasha K. M. Al-Dabbagh

DATE: May 2018

List of Figures

List of Tables

List of Abbreviations

5G	Fifth Generation
APD	Avalanche Photodiode
BER	Bit Error Rate
BSs	Base Stations
BW	Bandwidth
CS	Central Station
CW	Continuous Wave
DFBLDs	Distributed Feedback Laser Diodes
EAM	Electro-Absorption Modulator
EDFA	Erbium-Doped Fibre Amplifier
FBG	Fibre Bragg Grating
FOBS	First Order Brillouin Stokes
FSO	Free Space Optics
GVD	Group Velocity Dispersion
HetNets	Heterogeneous Networks
LMDS	Local Multipoint Distribution Service
LO	Local Oscillator
LoS	Line of Sight
MZM	Mach-Zehnder Modulator
MIMO	Multiple Input Multiple Output
mm-wave	Millimetre-Wave
NLoS	Non-Line of Sight
OC	Optical Coupler
OSA	Optical Spectrum Analyser
PD	Photo Detector
PM	Phase Modulator
PRBSs	Pseudo-Random Bit Sequences
QoS	Quality of Service

RAUs	Radio Access Units
RF	Radio Frequency
RoF	Radio over Fibre
RSA	Radio Spectrum Analyser
RX	Receiver
SBS	Stimulated Brillouin Scattering
SINR	Signal to Interference Plus Noise Ratio
SMF	Single Mode Fibre
SNR	Signal to Noise Ratio
SOBS	Second Order Brillouin Stokes
SRS	Stimulated Raman Scattering
TX	Transmitter
UHF	Ultra-High Frequency

List of Symbols

α	Fibre Attenuation Coefficient
α_L	LoS Path Loss Exponent
α_N	NLoS Path Loss Exponent
α_{UHF}	UHF Path Loss Exponent
γ	Atmospheric Attenuation
$\Delta\phi$	Phase Deviation
ε_0	Electric Field Constant
ε_p	Relative Permittivity
ε_r	Optical Receiver Efficiency
ε_t	Optical Transmitter Efficiency
θ	Divergence Angle
λ	Wavelength
μ	Squared Envelope of the Multipath Fading
ρ	Fixed Path Loss
ϕ	Phase Shift
ω	Angular Frequency
ω_c	Carrier Angular Frequency
A_{eff}	fibre Effective Area
c	Light Speed
D	FSO Receiver Diameter
C_p	Coverage Probability
D_{fibre}	Fibre Dispersion
E_0	Electric Field Amplitude
$E_{out}(t)$	Output optical Signal
$E_p(t)$	Output Optical Field
E_{ph}	Photon Energy
f	Frequency
f_c	Carrier Frequency

G	Antenna Gain
g	Brillouin Gain
h	Planck's Constant
$I(t)$	Electric Wave Intensity
$J_n(m)$	First Kind Bessel Function of Order n
k_p	Polarisation Factor
L	FSO Link Length
L_{fibre}	Fibre Length
L_{eff}	Interaction Effective Length
L_{FS}	Free Space Path Loss
LM	Link Margin
m	Modulation Index
n_1	Air Refractive Index
n_2	Refractive Index of the Surface Material
$n(\omega)$	Fibre Refractive Index
N_b	Receiver Sensitivity
P_{in}	Input Optical Power
P_r	Received Power
P_t	Transmitted Power
P_{th}	SBS Threshold Power
PL_{mm}	mm-Wave Path Loss
PL_{UHF}	UHF Path Loss
R	Link Data Rate
R_p	Rate Probability
r	Distance between Transmitter and Receiver
$V(t)$	Electronic Modulating Signal
t	Time
Th_r	Rate threshold
Th_s	SINR threshold
V_π	Switching Voltage
ν_b	SBS Interaction Bandwidth

$v_p(\omega)$	Phase Velocity
v_s	Laser Linewidth
X_L	LoS Shadow Fading
X_N	NLoS Shadow Fading
X_{UHF}	UHF Shadow Fading

Chapter 1

Introduction

1.1 Overview

Owing to the explosive evolution of mobile communications, the mobile data traffic in the futuristic networks is estimated to experience a significant tenfold increase in current networks [1, 2]. To cope with this communication growth, the capacity of the wireless communication link needs to be enhanced. Spectrum congestion in the current microwave band and the global bandwidth shortage facing current wireless carriers have motivated interest in the development and implementation of an underutilised millimetre-wave (mm-wave) frequency spectrum for futuristic communication networks [3, 4]. The mm-wave spectrum (3-300 GHz) is considered a vital solution for the next era of the communication system, i.e. the Fifth Generation (5G) due to its large available bandwidth [5]. Within the mm-wave spectrum, many bands can be suitable for the application in the futuristic mobile broadband, and there are several tens of gigahertz (bandwidth) available in different mm-wave bands. Including: the local multipoint distribution service band (LMDS) at 28-30 GHz, the oxygen absorption band at 57-64 GHz, the E-bands at 71-76 GHz, 81-86 GHz, and 92-95 GHz [1, 6, 7]. Figure 1.1 presents different mm-wave spectrum bands with the available bandwidth for each.

The application of mm-wave frequencies in futuristic communication networks requires the designing of a compact and low-cost system for the generation and transmission of the mm-waves. To this end, extensive research has recently undertaken aimed at developing technologies for mm-wave signals generation and transmission. Fortunately, there is advantageous integration between the

optical fibre and mm-waves that will facilitate the generation methods and support the mm-waves transmission in providing a high data rate. The radio over fibre (RoF) system provides high bandwidth through fibre links for long distances, while mm-wave communication provides very high bandwidth in wireless networks in comparison with microwave bands [8, 9, 10]. However, there are still some challenges relating to the implementation of mm-waves in the RoF system. That is, mm-wave propagation faces serious difficulties in the wireless channel due to its physical characteristics, such as high path losses, high signal attenuation, and blockage by solid materials [8, 10]. Figure 1.2 shows the attenuation and atmospheric absorption of mm-wave band propagation. Rain, fog, and any moisture in the air make the mm-wave signal attenuation very high, and this will limit the wireless transmission distances. It can be seen from the curve in Figure 1.2 that the attenuation is high especially at the 60 GHz band, because of oxygen absorption, while the water absorption is responsible for increasing the attenuation in the other mm-waves peaks. Owing to this, selecting the lowest attenuation mm-wave frequencies within the curve can minimise the propagation losses [3, 11, 12]. These characteristics will add a new challenge to address of inventing new components and applying advanced antennas with beamforming [13, 14]. In general, achieving a practical, simple, and cost-effective system design is essential for the success of mm-wave application in futuristic communication systems.

The rest of this chapter is organised as follows: In Section 1.2, the motivations for this study are explained, and the aim with objectives are presented in Section 1.3. Section 1.4 includes the thesis scope and contributions. Finally, the thesis outline is provided in Section 1.5

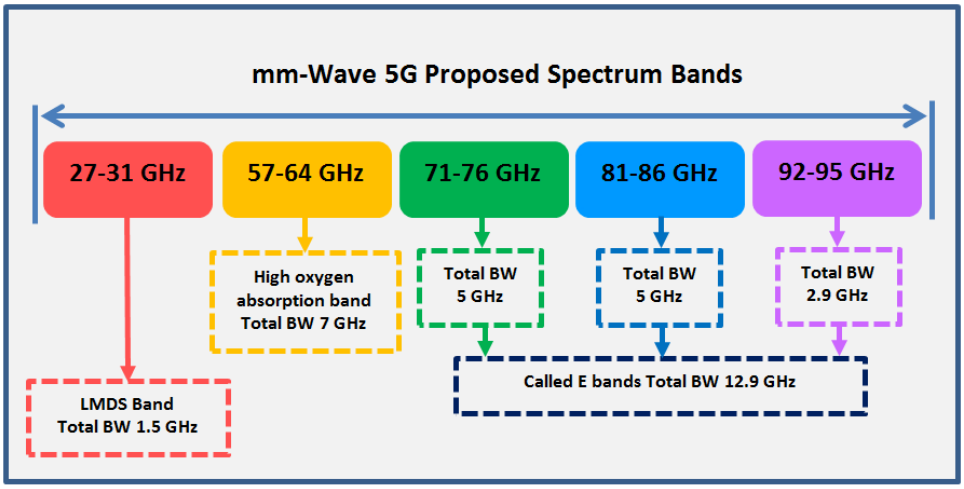

Figure 1.1 The proposed mm-wave spectrum bands for 5G networks with the available bandwidth (BW).

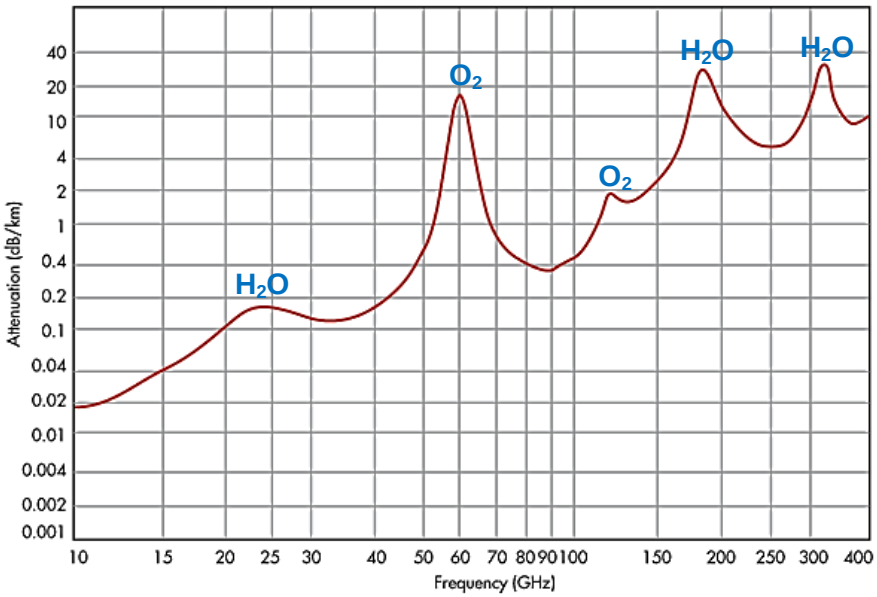

Figure 1.2 Atmospheric absorption across mm-wave frequencies [12].

1.2 Motivations

As the upcoming mobile networks will migrate to the higher frequencies, i.e. the mm-wave bands, this new spectrum will compensate for the bandwidth lack of the current wireless carriers. The use of mm-wave frequencies will greatly help in increasing the communication system capacity. Also, the mm-wave communication imposes some challenges and thus, when considering mm-waves for futuristic mobile networks, many issues must be addressed to verify these networks.

Firstly, mm-wave signals generation is considered challenging in the electrical generation domain and consequently, the optical generation method is preferred for obtaining high-frequency signals with high quality [8, 15, 16]. Various methods for mm-wave generation have been proposed recently, but the application of mm-waves in communication systems still needs feasible and cost-effective methods to simplify the system setup. To address this, studying the integration between mm-wave and RoF system is needed to generate and deliver mm-waves, thereby taking advantage of the benefits of high capacity fibre cables. Also, the mm-wave transmission through fibre cable will be advantageous in it overcoming mm-wave high path losses in wireless propagation. Unfortunately, transmitting mm-wave over RoF systems also faces some limitations due to fibre nonlinearity effects and this drives the necessity of developing new photonic generation methods with the RoF system to reduce these effects (as will be explained in the first and second contributions).

Secondly, the realising of a low latency communication link is an important consideration in futuristic communication networks to support massive and various delay-sensitive applications. Latency in fibre-optic networks comes from three main parts: the fibre itself, the optical components, and the optoelectronics components. The applications of long fibre link will increase the latency and will add extra complexity to the networks. In addition, long fibre link needs the use of further components to improve the performance of

the communication system, such as amplifiers, dispersion compensator, and repeaters. As a result, the further use of fibre will not support the 5G requirements for achieving low latency (below 1 ms) [2, 17, 18, 19]. The application of Free Space Optical (FSO) systems can provide a low latency communication link due to the possibility of applying a direct optical communication link. Considering the high bandwidth of FSO transmission link with short range distance is beneficial to obtain low latency communications. Also, there is no need to consider licence obligations and deployment permissions. However, there is stills need for a comprehensive investigation to apply these systems in futuristic networks. Moreover, laying fibre cables is not possible in some areas with natural obstacles so applying an FSO link instead will enable to increase network coverage area to reach the last-mile. In addition, under emergency and disaster conditions there is a crucial need for verifying an efficient communication link, so applying an FSO system could provide a vital solution for these cases. The latest studies have investigated the use of such a system for the transmission of high data rate between two fixed points over a long distance [20, 21, 22], but currently there has been investigation on the collaboration between mm-wave frequency and the FSO link [23]. All these issues raised the importance of designing a new system capable of integrating mm-wave frequencies with the RoF system and FSO link (as will be explained in the third contribution).

Thirdly, applying mm-wave in cellular networks will need extensive research in this field to achieve significant improvement in network performance. Millimetre-wave frequency can provide high bandwidth as a carrier signal. Data rates of around multi Gbits/s could be achieved by applying an mm-wave wireless link, but it will suffer from high path loss and have a low wireless propagation range [10, 24]. Thus, the use of the new mm-wave bands for indoor and outdoor wireless propagation will require a full understanding of all characteristics and propagation performance for each mm-wave band as an electromagnetic wave. Some of the new research has had the intention of integrating the mm-wave application with advanced antenna techniques by

applying new beamforming and advanced Multiple Input Multiple Output (MIMO) technique. This needs a design of new and compact components with consideration of the production cost [25, 26, 27]. However, the application of the mm-wave frequencies in the next generation communication networks will differ from the existing one, regarding its high propagation loss, sensitivity to blockage, and high directivity. Accordingly, a comprehensive study of mm-wave wireless propagation as a cellular network with considering blockages effects is important for successfully verifying mm-wave wireless network (as will be explained in the fourth and fifth contributions).

Finally, all these characteristics of mm-wave frequencies add significant challenges to the futuristic communication networks, including the design, the generation and transmission system and the application in cellular networks. All these challenges stand behind the motivation for this PhD study, with the aim of proposing a solution and design for a fully mm-wave communication system for futuristic communication networks.

1.3 Aim and Objectives

In the light of the above overview on the application of mm-waves in futuristic communication, the overall aim of this study is to design a fully mm-wave communication system for futuristic communication networks. The focus of this work with its objectives is as follows:

1. To generate photonically stable mm-wave carriers with low noise by proposing practical generation methods. This process includes proposing novel photonic generation methods with a simple and cost-effective setup to obtain high-quality mm-wave carriers.

2. To verify multi Gbits/s data transmission with the design of the mm-wave over fibre system. This process includes designing a practical full

duplex RoF system with mm-wave generation and transmission. The proposed system is demonstrated by using the Optiwave Software.

3. To verify a low latency and high capacity communication link. This process includes proposing a novel system for mm-wave generation and transmission over a hybrid Fibre/FSO link. The latency is reduced by decreasing the fibre length and proposing an FSO link instead.

4. To estimate precisely the mm-wave propagation performance in a cellular network. This process includes proposing a realistic scenario for the deployment of different bands of mm-wave Base Stations (BSs) using MATLAB simulation tools to evaluate coverage and rate trends.

5. To estimate precisely the diffraction and specular reflection impacts on 28 GHz mm-wave wireless propagation. This process includes proposing a simplified path loss model with applying a map-based scenario for BSs deployment to evaluate coverage and rate trends.

1.4 Thesis Scope and Original Contributions

As a direct impact of this study, there are five main original contributions presented in this thesis, which can be summarised as follows:

1. Three novel photonic mm-wave generation methods have been designed. The proposed generation methods are based on characterisations of the Brillouin fibre laser and Stimulated Brillouin Scattering (SBS) effects with phase modulation. Very stable mm-wave carriers with low noise and frequency tuning capability have been obtained. A single laser source is used in the generation methods, thereby overcoming the fibre nonlinearity

effects. The proposed full setup and explanation of these methods with the theoretical analysis and simulation results are discussed in Chapter 3.

2. A feasible full-duplex RoF system with the photonic generation of 64 GHz mm-wave has been proposed. One laser source is utilised, and a Fibre Bragg Grating (FBG) is used for the wavelength reuse for the uplink connection. A stable mm-wave transmission over fibre link is successfully achieved that with verifies a high data transmission rate. Cost reduction and performance improvement are achieved by simplifying the mm-wave generation method with the proposed RoF technique. The proposed simulation setup of this system with the theoretical analysis and simulation results is discussed in Chapter 4.

3. A novel hybrid Fibre/FSO system has been designed to generate and transmit mm-waves. The proposed system provides a low latency and high capacity communication link. The mm-wave frequency is integrated with the RoF system and FSO link to achieve a successful high data transmission rate. The proposed simulation setup of this hybrid system with the obtained results is discussed in Chapter 5.

4. A comprehensive study of applying different mm-wave bands in the cellular networks has been carried out by evaluating the coverage and rate trends. A map-based scenario is proposed for analysing the deployment of BSs. Different mm-wave performances in outdoor applications have been estimated and compared. The full theoretical analysis and mathematical calculation with the simulation results are provided in Chapter 6.

5. A simplified path loss model is proposed to estimate precisely the diffraction and specular reflection impacts on 28 GHz mm-wave performance in outdoor applications. The coverage and rate trends have been calculated, with a subsequent proposal for a map-based scenario for

the deployment of BSs. The full theoretical analysis and mathematical calculation with the simulation results are presented in Chapter 7.

The thesis scope is summarised in Figure 1.3, which explains the integration of all the contributions and the importance for each.

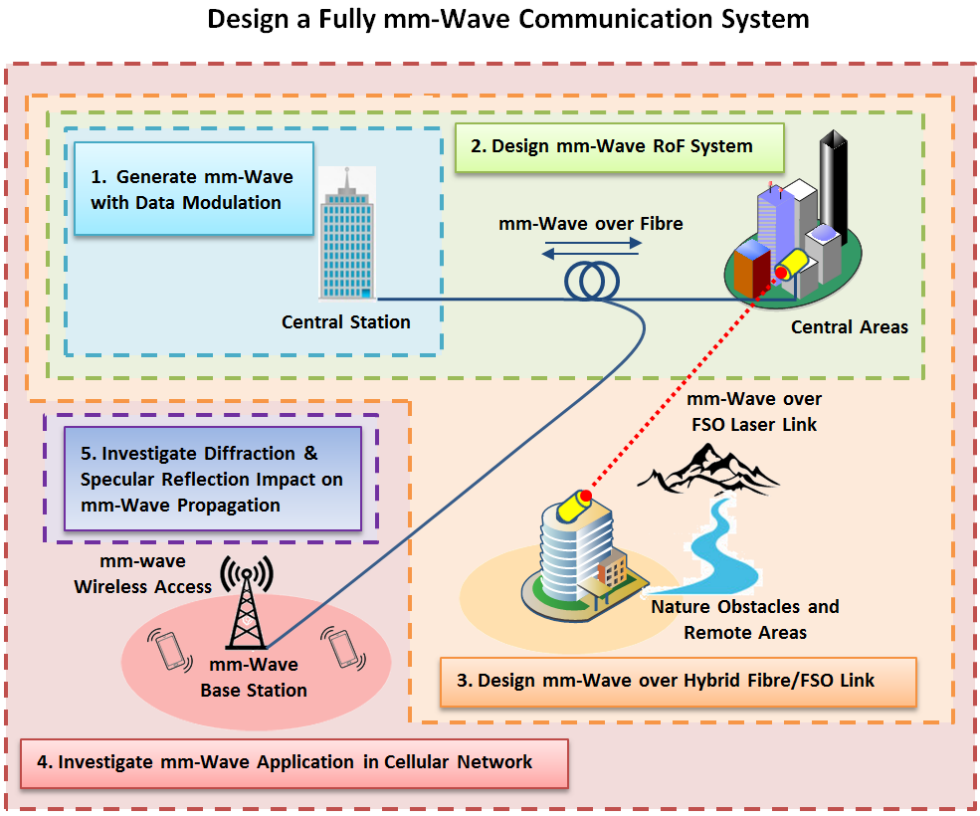

Figure 1.3 Thesis scope.

1.5 Thesis Outline

The work in this thesis is organised into eight chapters. Each chapter will start with a brief introduction providing an overview of the main points and highlighting its contribution. At the end of each chapter, a summary is presented.

The thesis outline is summarised below:

Chapter 2: includes the main concepts, which are key to the development of the work presented in this thesis. This chapter first provides a detailed background about the mm-wave generation and transmission systems. A more comprehensive explanation about the RoF and the FSO systems is also included. Then, it describes the challenges with mm-wave wireless networks. Finally, this chapter provides a discussion of the previous related works.

Chapter 3: introduces the proposed three novel photonic methods for the mm-wave generation, which are based on the characteristics of Brillouin fibre laser and SBS effects with phase modulation. The design of the generation methods with the mathematical and simulation analysis is explained with all details. The effectiveness of these methods is discussed and the simulation results presented.

Chapter 4: presents the design of a full-duplex RoF system with the generation of a 64 GHz mm-wave. The simulation setup of the RoF system is described with the mathematical analysis, whilst the benefits of proposing this system are discussed and the simulation results presented.

Chapter 5: presents the design of a novel system for mm-wave generation and transmission over a hybrid Fibre/FSO link. The impact of proposing this low latency and high capacity communication link is explained. The simulation setup of this hybrid system is described with a results discussion.

Chapter 6: introduces a comprehensive study of the application of mm-wave bands in the cellular networks. The coverage and rate trends are evaluated to investigate mm-wave propagation performance. A map-based scenario is proposed for the deployment of BSs and to estimate the effectiveness of mm-wave outdoor applications. The comparative results are presented and

discussed along with the mm-wave challenges and their advantages in cellular networks, specifically.

Chapter 7: presents the proposed simplified path loss model to estimate precisely the 28 GHz mm-wave performance in outdoor applications. The impact of the diffraction and specular reflection on the mm-wave wireless propagation is calculated and compared with the traditional path loss model. Simulation results are presented and discussed.

Chapter 8: provides a summary of the findings of this thesis, and some suggestions for the future work, with a final commentary on this research's impact.

Chapter 2

Background and Literature Review

2.1 Introduction

Due to the enormous increase in both the number of wireless communication subscribers and the bandwidth needed, applying the underutilised mm-wave carriers is a vital solution to the overcrowded current frequency spectrum [3]. A prospective high-bandwidth communication system known as the RoF system has been proposed as the significant solution for mm-wave generation and transmission [28]. As the mm-wave spectrum bands have channels sizes capable of improving the wireless data speeds, they provide an attractive opportunity due to the available large bandwidth. This vast mm-wave spectrum could be used within the next few years for the 5G cellular networks and WiFi communications [29]. In addition, RoF systems with mm-wave applications can increase the capacity, bandwidth and mobility as well, which has gained tremendous attention recently [17, 24, 30].

The simplified RoF system is explained in Figure 2.1. The mm-wave signals will be transmitted directly between the Central Station (CS) and the Radio Access Units (RAUs) using optical fibres. The signal generation and processing will be at the CS, which contains data resources, Optical Transmitters (TXs) and Receivers (RXs) with lasers and Photo Detectors (PDs). This configuration means the RAUs are simplified to deal with only the process of signals conversion and amplification, and transmitting the mm-wave signals to the mobile terminal end users [8, 15, 31].

The application of mm-wave in communication networks poses two main challenges. Firstly, the generation and the transmission of such high-frequency mm-wave signals is a very significant issue. Regarding which, the common

methods of the generation by using cheap components would result in significant Bit Error Rate (BER) degradation [15]. Secondly, whilst mm-wave carriers provide large bandwidth, they suffer from high path losses in the wireless propagation, which would require an increase in the number of the RAUs. As a result, the cellular network cells should be split into smaller cells, and whilst this will provide high bandwidth per user, it will lead to an increase in the network complexity and the infrastructure costs [2, 10].

This chapter presents a detailed background to the fundamentals of mm-wave generation methods and RoF with the FSO technologies. Also, it discusses the physical characteristics of the mm-wave propagation, which vary with different frequencies due to the electromagnetic mm-wave wave nature. Then, it presents a discussion about the related previous studies that were aimed at improving mm-wave generation and transmission systems, whilst also highlighting the significant gaps in the previous research.

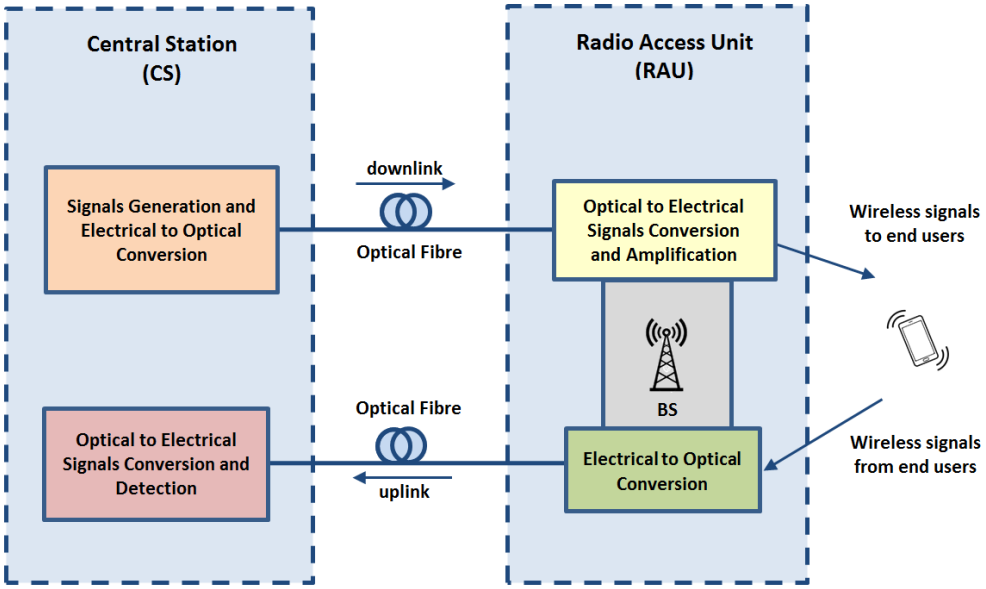

Figure 2.1 A simplified RoF system architecture.

2.2 Optical Millimetre-Wave Generation Techniques

The electrical generation methods of mm-waves are considered challenging because they need fast electronic processing. Also, most of the extant electronic mm-wave generation methods use oscillators and frequency multiplexers, which make the mm-wave sources huge and heavy. Moreover, applying of mm-waves in wireless networks requires a large number of BSs due to the mm-wave high path losses. Owing to this requirement, the electrical generation will increase the infrastructure cost and the complexity of the BSs [32]. As a result, the optical generation technique is the most promising solution to simplify the BSs. Over the past few years, many studies have been conducted to develop and improve the optical mm-wave generation and transmission systems. Recently, optically generated mm-waves have attracted considerable attention specifically for high carrier frequency above 60 GHz, because of the high available bandwidth [33]. There are four main methods for the optical generation of mm-wave signals over fibre links: direct modulation; external modulation; optical heterodyning; and multimode light sources [8, 15, 16, 34].

2.2.1 Direct Modulation

The direct modulation technique is based on modulating a laser source directly with the downlink data signal at a mm-wave carrier frequency and then, the mm-wave signal can be recovered at the photodiode by direct detection. The method is explained simply in Figure 2.2.

This technique is simple and cheap, but it has some limitations. The bandwidth of the directly modulated laser limits the frequency range of the modulating signals by the laser resonance peak. Due to this, all the reported RoF systems with deploying the direct modulation technique are limited to low mm-wave frequencies [8, 15, 35, 36, 37]. This impairment will also increase the nonlinearities, the frequency chirp, as well as causing poor frequency stability

and transmission integrity [38]. Owing to this, to generate and transmit high mm-wave frequencies a viable option is the use of the external modulation technique, which is explained in the next section.

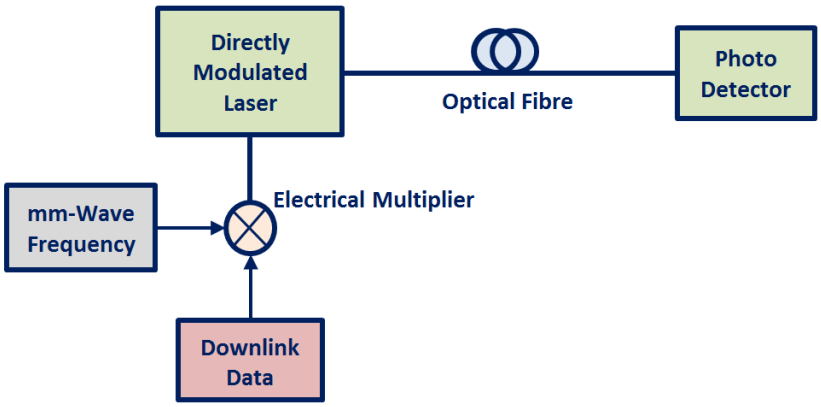

Figure 2.2 Direct modulation.

2.2.2 External Modulation

The external modulator is commonly one of the intensity modulator types, which can be a Mach-Zehnder Modulator (MZM), a Phase Modulator (PM), or an Electro-Absorption Modulator (EAM), as reported in [8, 15, 39, 40]. Simply, the external modulation technique includes a Continuous Wave (CW) laser source followed by an external modulator that modulates the laser light with the mm-wave signal, as explained in Figure 2.3.

With this technique, the main drawback relates to the transmission of the optical signal, which is derived from the external modulator. Due to the fibre nonlinearity characteristics, the transmission of the laser light will generate high order harmonics and these harmonics might be undesired or required depending on the system architecture. Hence, the power of these harmonics should be controlled by the bias voltage of the external modulator and the modulation index. Also, optical filters are required to eliminate undesired harmonics.

Whilst external modulation generates high mm-wave frequencies, this technique is considered more expensive and complicated than direct modulation [8, 41, 42]. Recently, an external modulation technique is reported in [43] for generating a 40 GHz dual-tone optical mm-wave by quadrupling a local radio-frequency oscillator via single dual-electrode MZM. Another approach is proposed in [44], that of generating microwave and mm-wave signals by using an MZM modulator and a filtering technique based on the Brillouin sideband. Regarding another way, as in [45], a generation scheme is proposed to generate a high-frequency mm-wave up to 120 GHz by using a dual-parallel MZM, but this still affects the complexity and cost of the system. Also, the researchers in [46] studied mm-wave signal generation based on frequency doubling by using an MZM modulator, whilst trying to overcome fibre chromatic dispersion.

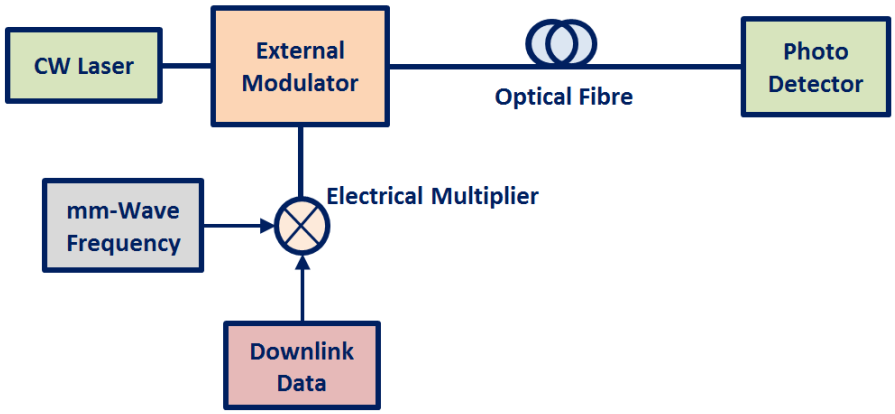

Figure 2.3 External modulation.

2.2.3 Optical Heterodyning

With this technique, two laser sources emitting different frequencies can be mixed by an optical coupler to generate the mm-wave signal. The generated mm-wave will have a frequency equal to the difference between the emission frequencies of the two lasers sources. In radio frequency signal detection, the

electromagnetic field drives the oscillatory motion of electrons in the antenna; so the captured electromagnetic field is then electronically mixed with a local oscillator by any proper nonlinear circuit element with a quadratic term. Unlike RF band detection, optical frequencies oscillate too rapidly to directly measure and process the electric field electronically. Instead optical photons are (usually) detected by absorbing the photon's energy, thus only revealing the magnitude, and not by following the electric field phase. Hence the primary purpose of heterodyne mixing is to down shift the signal from the optical band to an electronically tractable frequency range [8, 15]. The heterodyning generation technique is explained in Figure 2.4.

In optical detection, the desired nonlinearity is inherent in the photon absorption process. Conventional light detectors, which named square-law detectors, respond to the photon energy to free the bound electrons, and then the energy flux scales as the square of the electric field, so does the rate at which electrons are freed. A difference frequency appears only in the detector output current after both of the local oscillator and signal illuminate the detector at the same time, which will causing the square of their combined fields to have a difference frequency modulating the average rate at which free electrons are generated.

The optical heterodyning technique can assure the generation of high mm-wave frequencies with the advantage of avoiding the use of high-frequency components or broad bandwidth optical devices. The problem with the optical heterodyning technique is the limited spectral purity and frequency accuracy by the laser linewidth and the temperature controls. Due to this limitation, low phase noise and narrow linewidth lasers sources are required [16]. Another approach to the optical heterodyning technique is to use a single laser source with optical sidebands to generate an optical double sideband. This approach requires high-speed optoelectronic components, most of which are expensive such as modulators, photo detectors, optical mixers and filters, as proposed in [47, 48, 49, 50, 51].

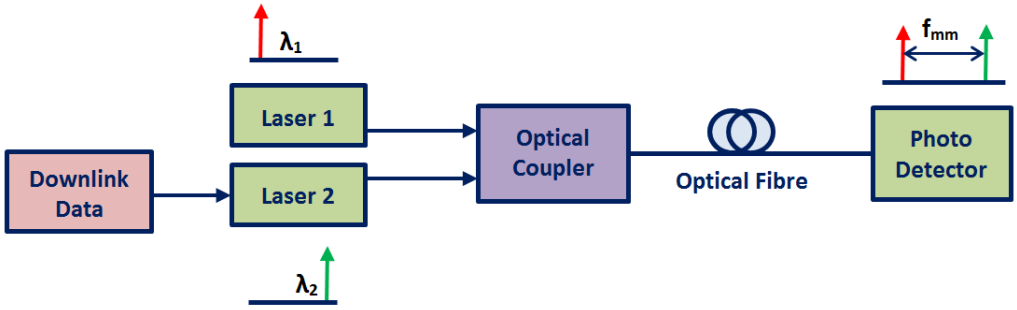

Figure 2.4 The optical heterodyning technique.

2.2.4 Multimode Light Sources

Multimode lasers sources include different types, such as Fabry-Perot lasers, mode-locked lasers and dual-mode lasers. These sources have been considered a low-cost alternative to expensive external modulators. Multimode light sources can be used to generate different optical tones and combine them at the PD. This process will generate a mm-wave signal based on the laser multi-modes that are separated by the desired mm-wave frequency, as in [32, 52, 53]. Figure 2.5 shows the general multimode laser source technique.

The advantage of using this technique is the possibility of obtaining tuneable mm-wave frequencies. Also, it can reduce the cost and the power consumption of the whole system, because high-frequency components and broad bandwidth optical devices are not required. This technique has some drawbacks, given its limited spectral purity and frequency accuracy by the multimode laser linewidth. In addition, it requires the use of an external modulator with optical filters [8].

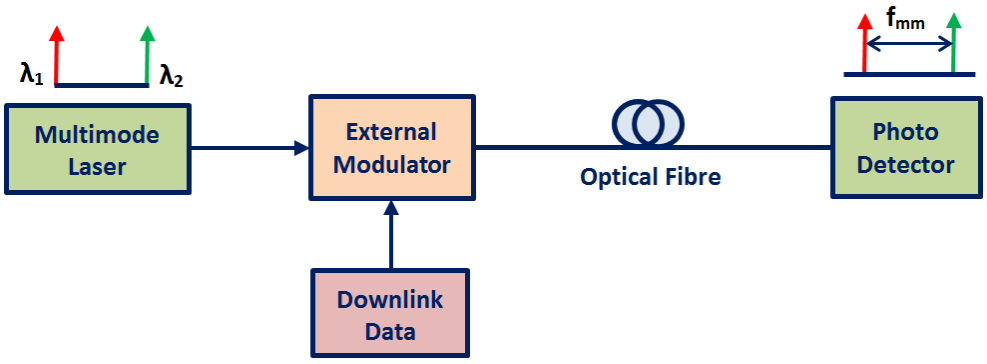

Figure 2.5 The multimode light sources technique.

2.3 Brillouin Fibre Laser and SBS Effects

To reduce the power consumption, and to obtain low cost with a reliable setup for the mm-wave generation system, the Brillouin fibre laser source has been proposed recently in several studies with SBS effects [54]. It is well known that SBS is one of the nonlinear effects in optical fibre and it happens due to the process of interaction between the laser light with the propagating density waves or acoustic phonons [55]. This process dependably exists in each optical fibre, because of the microscopic defects and thermal fluctuations. Due to these effects, Brillouin Stokes are generated inside the fibre with a frequency difference of about 11 GHz in a 1550 nm laser wavelength. This frequency difference between these Stokes can help in obtaining a simple generation method of mm-waves because it is close to its range [56].

SBS is commonly known as one of the limiting factors on the system performance in fibre-optic networks, due to the effect of the backscattering signal, which is transferred with the signal energy. The generated backwards propagating Stokes carry most of the input energy until the Brillouin threshold is reached [55]. Hence, SBS limits the amount of the optical power that can be entered into the optical fibre without reducing the signal quality. The adverse effects of SBS have been widely studied in transmission systems [15, 44, 45, 49]. Fortunately, it has also some beneficial features, such as frequency

selective amplification, which can be utilised in mm-wave photonics applications [56].

Different methods of mm-wave generation have been proposed in the literature taking the advantages of using the fibre laser, like those based on applying a dual-wavelength Q-switched Erbium-doped fibre laser, as in [52, 57]. This method offers tuneable mm-wave signal generation from 30 to 82.5 GHz, but at the same time it needs accurate control of the two FBGs, which need to have the same centre wavelength and this makes the structure more complicated. In contrast, a design that uses an optical phase modulator and a Brillouin-assisted notch-filtering technique is proposed in [58], but it generates only a limited mm-wave frequency equal to 18 GHz. The method, which replaces those components with optical splitters and circulators, is proposed in [49]. It needs an Erbium-Doped Fibre Amplifier (EDFA), and it generates a maximum mm-wave carrier frequency of 64.4 GHz with a phase noise of −57.17 dBc/Hz.

Recently, the generation of the mm-wave based on SBS has been demonstrated in some of the research. An approach for mm-wave generation based on SBS has been proposed in [59] by heterodyning the output modes of a dual-wavelength fibre laser. They used a simple configuration by the optical heterodyning of two lasers, but the generated signal has poor characteristics due to the phased mismatching of the two free-running lasers. Another technique is presented in [60] to generate a mm-wave by interfering two spectral lines of a frequency comb generated by a femtosecond fibre laser. Whilst a transmission system, based on the SBS effect with injection-locked distributed feedback laser, is proposed in [61] to achieve single optical sideband modulation. In other research work, an SBS amplification method for improving the resolution of the Brillouin-based spectral analysis is proposed, as found in [62]. Also, a method has been presented for the tuneable generation of high-quality millimetre- and THz- waves with an ultra-narrow linewidth in another study [63]. In their work, they presented the electrical characteristics of the generated waves as well as the generation and transmission of a 200 GHz and a 1 THz wave over a distance of 24.5 cm.

2.4 Comparison of Millimetre-Wave Generation Techniques

To summarise the benefits and the limitations of the different mm-wave generation techniques, Table 2.1 gives a comparison between all the reported techniques of the most cited studies to improve mm-wave generation. From this comparison, it is obvious that the simplest generation technique is operating with a directly modulated laser, which provides practical and low-cost system, but the frequency of the generated mm-wave is limited by the laser and the modulator bandwidth.

Table 2.1 Comparison of the reported mm-wave generation techniques

Techniques	Reported References	Benefits	Limitations
Direct Modulation	[8], [15], [35], [36], [37], [38]	- Simple setup - Cheap components	- Limited to low mm-wave frequency - Poor mm-wave frequency stability and transmission integrity
External Modulation	[8], [15], [39], [40], [41], [42], [43], [44], [45], [46]	- Generate high frequency mm-wave - Flexible setup	- Harmonic generation affects mm-wave efficiency - Needs an optical filter
Optical Heterodyning	[16], [47], [48], [49], [50], [51]	- Achieves a high frequency mm-wave - High scalability and avoids the use of high frequency devices	- Frequency is limited by laser linewidth - Needs complex and expensive components
Multimode Light Sources	[8], [52], [53]	- Reduce the system cost and the power consumption - Achieve tuneable mm-wave frequency	- Low scalability - Limited frequency accuracy
Brillouin Fibre Laser	[49], [52], [54], [56], [57], [58], [59], [60], [61], [62], [63]	- Reduces the power consumption - Reliable setup	- Signal power limitations due to SBS effects - Needs optical splitters

Most of the schemes reported up until now are either complicated or require a radio frequency source at the transmitter for the remote generation of the radio frequency signal. Due to this limitation, there is a significant need to design a practical generation method of obtaining high-quality mm-wave carriers with a cost-effective RoF system.

In recent work by this researcher [64], novel mm-wave generation methods were proposed and demonstrated based on the SBS nonlinearity effects in the optical fibre with fibre laser properties and the phase modulation technique. The generation of mm-waves with different frequencies was achieved for the first time with a straightforward optical communications setup, as proven in the demonstration explained in detail in Chapter 3. These mm-wave generation methods can reduce the systems cost, as well as have the possibility of generating mm-wave carriers with low signal noise and very high stability, which could improve mm-wave RoF technology, thereby meeting futuristic network requirements.

2.5 Millimetre-Wave over Fibre Links

The propagation of a laser through the optical fibre channel is affected by the fibre characteristics and impairments. As a result, the mm-wave over fibre system is affected by these fibre features as well [15]. These impairments include the fibre attenuation, dispersion, nonlinearities and noise, as will be explained in the following subsections.

2.5.1 Fibre Channel Attenuation

The reduction in the power of the transmitted signal is an important parameter during the transmission of the optical signal through fibre. Due to this, the fibre attenuation is the measure of the loss of laser power as travels along the optical fibre link. Fibre attenuation is caused by one or more of these reasons: a) fibre material absorption, b) waveguide imperfections, c) fibre bending and/or, d)

Rayleigh scattering [9, 31]. If an optical signal, with transmitted power (P_t), enters the optical fibre, the received optical power (P_r) after the signal has been propagated through the fibre link length (L_{fibre}) in [km] can be calculated by [15]:

$$P_r = P_t \exp(-\alpha L_{fibre}) \tag{2.1}$$

where, α is the fibre attenuation constant, which has a value of 0.2 [dB/km], typically.

2.5.2 Fibre Dispersion

Fibre dispersion is the widening out of the light pulse over time as it travels through the fibre. The refractive index $n(\omega)$ of the fibre changes, as the angular frequency (ω) of the propagating optical wave changes, where the frequency (f) of the propagating optical wave is $f = \frac{\omega}{2\pi}$. As a light pulse widens, it can interfere with the other pulses through the fibre, leading to the limitation of the maximum transmission rate of the communication system [56].

Mathematically, the phase velocity $v_p(\omega)$ of the optical wave propagates through the fibre is denoted by [28]:

$$v_p(\omega) = \frac{c}{n(\omega)} \tag{2.2}$$

where, c is the speed of the light.

Thus, the propagation velocity depends on the optical frequency (f), and this phenomenon results in the dispersion. The amount of the fibre dispersion is quantified by the parameter (D_{fibre}) in [ps/(km.nm)], which is calculated by [28]:

$$D_{fibre} = -\frac{2\pi}{\lambda^2}\left[\left(2\frac{dn}{d\omega} + \omega\frac{d^2n}{d\omega^2}\right)\right] \tag{2.3}$$

This fibre dispersion is also named as Group Velocity Dispersion (GVD) or chromatic dispersion. There are several other kinds of dispersion in optical communication systems, such as intermodal, and polarisation dispersion [28, 38, 46].

2.5.3 Fibre Nonlinearity

The fibre medium, which is an electrical insulator, can be polarised by the applied electric field. Due to this, fibre nonlinearity results from a nonlinear function of the electric field of the light, especially when the optical intensity is high. This polarisation leads to the nonlinear effects, such as nonlinear variation of the refractive index as a function of the total propagating signal power, which varies with time. This variation makes a phase shift and optical frequency deviation known as frequency chirping [15]. These nonlinearities include the self-phase modulation and the cross-phase modulation. Also, the interaction between multiple signals that are propagated through the fibre leads to the generation of optical signals at new frequencies, which is typically called the Four-Wave Mixing [65]. Finally, there are other important nonlinear effects including SBS, which have been explained previously in Section 2.3, and Stimulated Raman Scattering (SRS). SRS occurs where the optical energy as photons is transferred from the signal propagating via fibre at a particular optical frequency to a signal at a lower one [56].

Fibre nonlinearity can be very useful in some applications, such as amplification, multiplexing, wavelength conversion, and pulse regeneration [66]. In fact, the futuristic optical communication systems need the trade-off between the advantages and disadvantages of the nonlinear effects which should be carefully considered so as select communication system with the desired performance and transmission capacity.

2.5.4 Fibre Link Noise

Many noises are added in the fibre link, which affect the mm-wave over fibre system. Figure 2.6 presents these fibre link noises, including the Relative Intensity noise (RIN), Amplified Spontaneous Emission (ASE) noise, Phase noise, Shot noise, and Receiver Thermal noise [8].

The propagating laser light inside the fibre has a noise that results from the random fluctuation of the intensity and the phase of the optical signal. The RIN

is the ratio of the mean square of power fluctuation per unit bandwidth to the square of the signal power average. The main source of this, is the spontaneous emission of photons, where the intensity noise causes Signal to Noise Ratio (SNR) degradation. The non-zero spectral linewidth around the output frequency arises due to the phase noise, the effects of which depend on the ratio of the total linewidth to the bit rate. Moreover, the optical field and the electric current consist of photons and electrons that result in a quantum noise effect in the photo-detected signal, and this is called Shot noise. The random motion of the electrons, which depends on the temperature, results in the thermal noise, which is added by the load resistor and the amplifiers at the optical receiver side [36, 56].

Therefore, the transmission system integrity can be divided into two stages based on two separate physical channels: the optical channel (fibre and FSO), and the RF channel (mm-wave). In the optical channel, noise can cause the link performance degradation. The primary sources of noise in the optical path of the RoF transmission link are photodetector shot and thermal noise, the ASE noise of the optical amplifiers, and the RIN of the light source. Also, the beating of the different optical components at the photodetector produces a phase-to-amplitude conversion, and hence frequency chirp and fibre induced dispersion will increase the output noise power. While in the wireless domain, the RF (mm-wave) power amplifier is an important element to set the link budget and the power requirements for obtaining acceptable SNR levels. Nevertheless, the maximum amplifier gain is constrained by the maximum transmitter noise of the wireless system specification. Furthermore, the base station and mobile terminal stability specifications limit the power levels, as a high gain for the uplink and the downlink directions may lead to oscillation [8, 36].

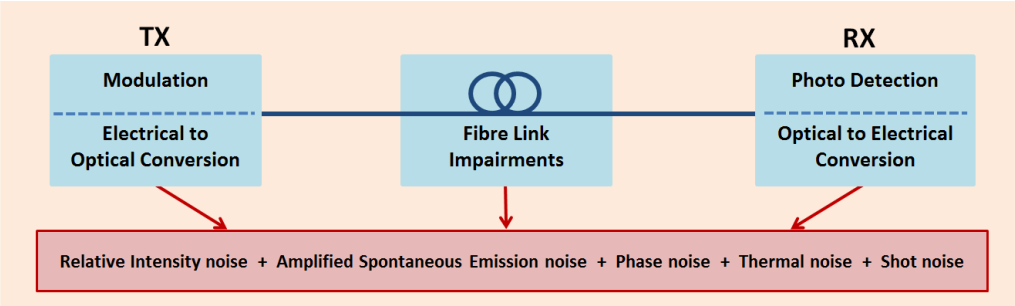

Figure 2.6 Fibre link noises.

2.6 Strengths and Challenges of a mm-Wave over Fibre System

The application of a mm-wave in RoF communication systems has the significant advantage of increasing the capacity of a wireless communication system [25]. The main benefits from doing so are [8, 28]:

- Low attenuation mm-wave signals can be transmitted through optical fibres;
- Simple and cost-effective setup;
- The possibility of sharing the resources centralised at the CS with simple BSs;
- High capacity systems due to use the higher frequencies of mm-waves;
- High flexibility because the same RoF network can be used for many services.

The major drawback of mm-wave over fibre systems is the requirement of high-speed optical components for high-frequency mm-wave signals. Millimetre-wave generation techniques are considered more sophisticated, in comparison with the generation methods of low-frequency radio waves. As has

been explained in Section 2.2. Also, there is a need to increase the number of BSs, which should be supported by broad bandwidth PDs, to cover the service area. In addition, the problem of the fibre chromatic dispersion affects the link even with short fibre cables, and hence; the application of advanced optical modulation and transmission schemes is necessary [31, 54].

All these requirements have led to the development of new optical devices and components operating at the mm-wave bands. Accordingly, mm-waves with a RoF system became the subject of many studies in the literature. Several structures have been proposed to develop mm-wave communications, but there remain many challenges regarding the verifying of an effective mm-wave over fibre communication system. These include the generation and the transmission of the mm-wave signal over the optical channel. Several techniques have been proposed for improving the fibre link performance regarding the throughput increase, overcoming the fibre impairments or digitising the RoF system. Table 2.2 presents a list of the seminal studies in the literature that has discussed performance improvement of mm-wave over fibre systems. These studies are considered the basis for the latest studies that followed.

In general, the mm-wave over fibre system still poses some challenges in terms of implementation, such as the complexity of devices and the high cost of the optical components. Also, the stability and quality of the mm-waves transmitted over fibre are considered very effective factors for obtaining successful transmission system. Hence, overcoming the nonlinearity of the optical fibre is an important issue. In recent work [67], this researcher proposed a full-duplex RoF system up to 100 km with a photonic generation method of a 64 GHz mm-wave with low noise power of less than -75 dBm. The demonstration of this system is explained in detail in Chapter 4. A stable mm-wave RoF system is achieved successfully with a high-quality mm-wave carrier. A reduction in fibre nonlinearity effects is also obtained, with a practical mm-wave RoF system, which could be appropriate for small cell 5G networks.

Table 2.2 mm-Wave over fibre techniques

Techniques	Reported References	Contributions
Carrier Suppression	Jia, *et al.* [68]	Designed a bidirectional RoF system with the generation of 40 GHz and a transmission data rate of about 2.5 Gbits/s over 10 km up to 40 km fibre length.
Optical Injection Locking	Braun, *et al.* [69]	Proposed the 60 GHz band for a RoF system with data rate 140-155 Mbits/s and obtained a signal with low phase noise less than -100 dBc/Hz.
Optical Filtering	Chen, *et al.* [70]	Used the optical filtering scheme in a RoF system, with optical generation of 40 GHz and transmission of 2.5 Gbits/s over 40 km fibre length.
Overcoming Chromatic Dispersion	Smith, *et al.* [71]	Presented an efficient 38 GHz fibre-wireless transmission system of 155 Mbits/s over 50 km fibre and a 5 m wireless link.
Digital RoF	Nirmalathas, *et al.* [72]	Proposed a digitised RoF system with the mm-wave signal as a prospective technology.
Overcoming Fibre Nonlinearity	Schneider, *et al.* [73]	Generated 40-100 GHz from the sidebands of a laser wave by the nonlinearity of an optical modulator, using two pump lasers over 50 km of fibre.

2.7 Free Space Optical Link

An FSO link is a wireless communication link, which transfers the data by using optical carriers (usually laser light) through the free space. It is established between two optical transceivers, which provide the full duplex capability. The data is modulated onto the optical carrier, and then, it is transmitted through the optical wireless channel to the other side [20, 74]. The basic configuration of the FSO system is shown in Figure 2.7. Recently, this system has garnered significant attention due to its high security, flexibility,

and fast deployment period [75, 76]. In addition, an FSO wireless channel applies the unlicensed spectrum in the range of the visible to the infrared laser light spectrum. Hence, the FSO laser spectrum does not need complicated regulations and it is considered cheap in comparison with the radio frequency licensed spectrum. The FSO laser communication system operates on a LoS link at laser wavelengths of 850 nm, 1300 nm, and 1550 nm, which have the lowest attenuation (less than 0.2 dB/km) [77, 78].

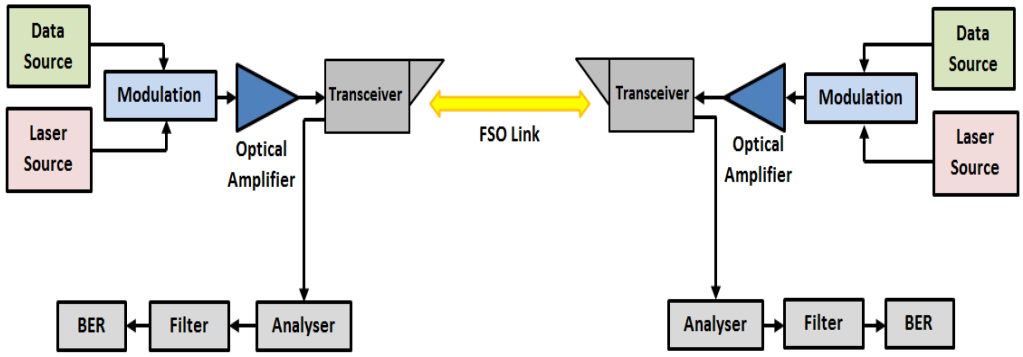

Figure 2.7 The basic structure of the FSO system.

2.8 FSO Laser Channel Analysis

The wireless optical channel of FSO system consists of two main components, the: optical transmitter and optical receiver. Between these two components, the modulated laser beams are transmitted through the atmosphere to verify the optical communication link, as illustrated in Figure 2.8. The optical power of the carrier, which is launched from the transmitter, is affected by various factors before arriving at the receiver. These affecting factors include system losses, noise, atmospheric turbulence, and misalignment loss [22, 79]. System losses are highly dependent on the design specifications, while misalignment loss depends on the condition of the LoS link and it increases as the distance between the transmitter and the receiver becomes greater. Atmospheric effects are presented by the attenuation factor which is affected by the distance as

well. The attenuation factor is used to analyse the effect of weather, like rain, fog, or wind, when transmitting data through FSO laser links [80].

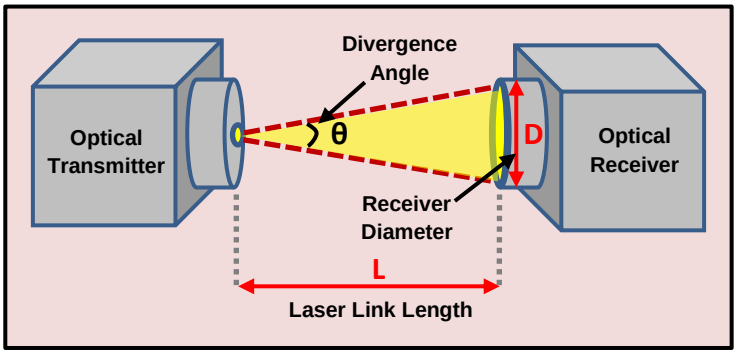

Figure 2.8 FSO laser channel.

Applying an FSO system enhances the quality of service (QoS) of mobile networks, especially in the remote areas, by reducing the length of the fibre link. To obtain proper data transmission to the remote destination, it is necessary to deal with the limitation of the laser beam divergence angle. In the FSO link, the beam divergence angle is considered as a critical issue, because it affects the data transmission and the accepted amount of BER [81]. Moreover, it is essential to specify the physical characteristics for both the optical transmitter and the receiver to reach a perfect link performance.

The laser wavelength is a very significant factor in the FSO link, because the propagation attenuation is related to it. Also, the components' availability and costs, such as detectors and transmitters, are based on this wavelength. Using a laser beam with a 1550 nm wavelength is suited for both the fibre and FSO links, because of its low attenuation. Also, cheap components that work at this laser wavelength are available and this will reduce the overall cost [74, 80]. In addition, this laser wavelength is well-suited with the EDFA technology, which is necessary for a futuristic communication system that needs high power and a multi-Gbits/s data rate.

The link attenuation and capacity are considered the most important parameters affecting the performance of the optical communication link and thus, these need to be evaluated to obtain the best performance. The propagation of the laser light through the atmosphere is affected by the absorption and the scattering of air molecules or liquid particles. Beer-Lambert's law describes a laser's power loss through the air. By considering the laser transmitted at a wavelength 1550 nm over a distance (L) in [m] between two points in free-space with a laser transmitting power (P_{tlaser}) in [W], the laser received power (P_{rlaser}) in [W] at the optical detector can be expressed by [74]:

$$P_{rlaser} = P_{tlaser} \frac{D^2}{\theta^2 L^2} 10^{-\gamma L/10} \varepsilon_t \varepsilon_r \tag{2.4}$$

where, D represents the receiver diameter [m], θ is the divergence angle [rad], γ is the atmospheric attenuation factor [dB/km], ε_t and ε_r are the optical efficiencies of the transmitter and receiver, respectively.

Another important factor in FSO link analysis is the link margin. This factor specifies the ratio of the available received power to the receiver power that is required to obtain a quantified BER with the given data rate. The link margin (LM) can be calculated by [81]:

$$LM = \left[\frac{P_{tlaser}\,\lambda}{N_b R h c}\right] \times \left[\frac{D^2}{\theta^2 L^2}\right] 10^{-\gamma L/10} \varepsilon_t \varepsilon_r \tag{2.5}$$

where, λ is the laser wavelength, h is a Planck's constant (6.626×10^{-34} m^2kg/s), c is the light velocity (3×10^8 m/s), and N_b is the receiver sensitivity [photon/bits or dBm]. While R is the link data rate [bits/s] which can be found from [81]:

$$R = \frac{P_{tlaser}\, P_{rlaser} 10^{-\gamma L/10} D^2}{\pi(\frac{\theta}{2})^2 L^2 E_{ph} N_b} \tag{2.6}$$

where, $E_{ph}=hc/\lambda$ represents the photon energy [eV] at wavelength λ.

Another challenge affects the FSO channel performance is the atmospheric turbulence. This turbulence, which affects the optical FSO link power, is a result of the thermal gradient within the propagation path because of the variations of air density and temperature. This variation can drive the refractive index fluctuations. The refractive index structure parameter, which is widely used to quantify the strength of scintillation, is altitude dependent. Therefore it

is greater at lower altitudes due to the added heat transfer between the air and the surface [82]. The turbulence effect also depends on the link distance and the wavelength of the light source. Fortunately, several atmospheric turbulence mitigation techniques at physical layer have been discussed recently such as employing some modulation schemes in FSO system, the forward error correction code, and the spatial diversity [20, 83].

2.9 Importance and Challenges of the FSO System

The FSO system is used efficiently for the transmission of a high data rate between two fixed points instead of applying optical fibre cables. The wide optical bandwidth has allowed for obtaining much higher data rates by using an FSO link. FSO systems also have attracted attention to solve the problem of last mile coverage in remote areas or under disaster emergencies. The integration of fibre optic infrastructure with the FSO system could help in resolving these issues as well [80, 84]. The performance of the FSO systems has been studied previously in some research, which has proposed different ways to improve it [82, 85, 86].

Despite the potential of the FSO system, it faces some challenges that relate to the transmission of the optical signals via different atmospheric conditions. The transmitted optical signal is affected by various factors, such as geometric losses, attenuation losses, and atmospheric turbulence [20, 80, 87]. Recently, in some literature, different solutions to mitigate these affecting factors have been proposed [21, 82]. In some studies, different atmospheric conditions have been incorporated into the design their models to improve the FSO system [75, 88, 89]. Also, the background radiation is another affecting factor in the performance of the FSO links. Regarding which, the receiver lens collects some background radiation that may consist of direct, reflected, or scattered sunlight with the FSO laser signal. This degrades the performance of the FSO link and some solutions are proposed in [80, 90, 91].

The importance of applying FSO links in futuristic communication systems is due its ability of providing a low latency link, which easily reaches the last mile coverage. The latest studies [20, 21, 22] have involved investigating the use of an FSO system for the transmission of a high data rate between two fixed points over a long distance, but there has been no investigation up until now for regarding the collaboration between mm-wave frequency and an FSO link. All these issues have raised the salience of the design in the current proposed new system being able to integrate mm-wave frequencies with a RoF system and FSO link. Accordingly, a novel hybrid Fibre/FSO system is proposed to generate and transmit mm-waves in Chapter 5. The simulation results with the mathematical analysis will show that this new system could provide a low latency communication link.

2.10 Millimetre-Wave Wireless Channel

Despite mm-wave frequencies being considered attractive for futuristic mobile networks, they have faced serious difficulties in terms of wireless propagation. Millimetre-wave signals have significant propagation losses and high power consumption of hardware [92, 93]. Hence, understanding the physical features of each mm-wave band is an important issue to specify which band able to achieve the best performance for the outdoor application.

Technically, there have been some important suggestions for understanding the characterisation of the mm-wave wireless channel, which include, studying the propagation loss, mm-wave penetration, Doppler effects and multipath, as will be explained in the next subsections.

2.10.1 Millimetre-Wave Propagation Losses

The main challenge in the application of mm-wave bands in futuristic 5G communication systems and beyond is the high path losses compared to the

microwave bands. In general, the free space path loss (L_{FS}) in [dB] is estimated by [2]:

$$L_{FS} = 20\log_{10}(\frac{4\pi}{c}) + 20\log_{10}(f_c) + 20\log_{10}(r) \quad (2.7)$$

where, f_c is the carrier frequency [GHz], and r represents the distance between the transmitter and the receiver in [m] [2, 7, 94]. It seems that the higher mm-wave frequencies have higher free space propagation losses than the lower ones. Furthermore, recent studies have explained that the directional transmission of narrow beams (high-frequency mm-wave) reduces interference and increases the possibility of applying spatial multiplexing techniques [6, 95]. This is why the mm-wave frequency can be used with highly directional antennas with line of sight (LoS) transmission, which means an unobstructed link between the transmitter and receiver, thereby improving performance. While the mm-wave non-line of sight (NLoS) transmission, which means there is a blockage between the transmitter and the receiver, is considered a weak transmission link. Figure 2.9 explains the LoS and the NLoS communication links. However, mm-wave propagation performance depends on several other factors, like the separation distance between the transmitter and the receiver, the communication link margin with the receiver's sensitivity, and the multipath diversity [1, 24].

Another challenge regarding mm-wave propagation via the wireless channel is the mm-wave high signal attenuation, especially at higher-frequency bands. This high attenuation is considered a serious problem, because it limits the signal propagation through the air [2, 11, 96]. The molecules of the oxygen and water vapour absorb mm-wave energy. The oxygen molecule can absorb the energy of the mm-wave band around 60 GHz; accordingly, the free-licensed mm-wave band (57-64) GHz has high oxygen absorption with high attenuation, reaching approximately 15 dB/km. Furthermore, the water vapour absorbs the mm-wave energy at frequencies between 164 and 200 GHz with higher attenuation [1, 12, 97] (as explained previously in Chapter One by Figure 1.1 and Figure 1.2).

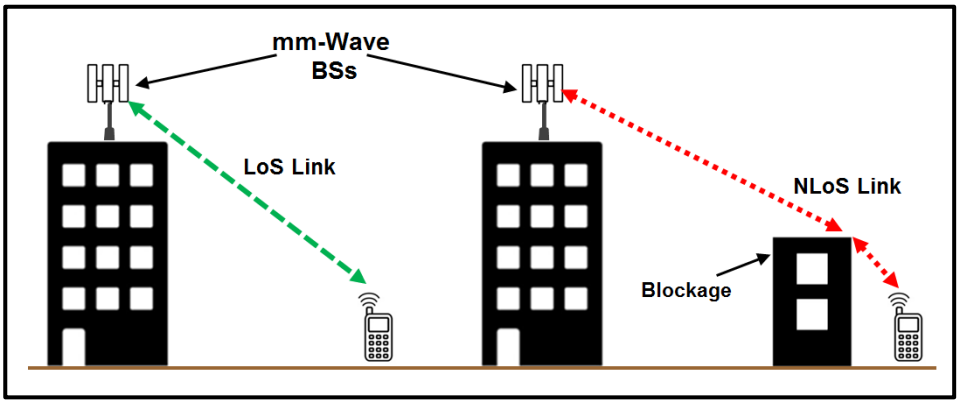

Figure 2.9 The LoS and NLoS communication links.

In the case of the mm-wave, the path loss calculation is based on the communication link between the transmitter and the receiver. Hence, the model of evaluating path loss for the mm-wave (PL_{mm}) wireless link is calculated by [98]:

$$PL_{mm}(r) = \rho + 10\alpha_L \, log_{10}(r) + X_L \tag{2.8}$$

where, ρ is the fixed path loss, which is given by [$(20log_{10}(4\pi/c))+20log10(f_c)$], f_c is the mm-wave frequency, α_L is path loss exponent for LoS, and X_L represents the shadow fading for LoS. While the received power of mm-wave (P_{rmm}) that is assumed to be transmitted wirelessly with the LoS path condition is calculated by [3]:

$$P_{rmm}(r) = \frac{P_{tmm} G \mu}{PL_{mm}(r)} \times \left(\frac{\lambda}{4\pi}\right)^2 \tag{2.9}$$

where, P_{tmm} is the mm-wave transmitted power, G is the transmit antenna gain, λ is the wavelength of mm-wave signal, and μ is the squared envelope of the multipath fading.

2.10.2 Millimetre-Wave Penetration

For understanding the mm-wave propagation in various environments, it is very important to determine the signal behaviour in the indoor and outdoor applications. For a 5G network and beyond, the deployment of mm-wave networks requires specification of the effects of diffraction, scattering,

penetration, and reflection in different environmental conditions [99]. Millimetre-wave signals can penetrate difficultly through solid materials, which causes very high losses and hence, makes these signals very sensitive to blockages, such as buildings and objects [3, 4, 100]. Recently, several studies investigated the reflection effects in mm-wave indoor and outdoor applications by comparing the penetration of mm-waves through various building materials, including glass, brick, wood and metals. These studies [101, 102, 103, 98, 104, 105] showed that the application of a mm-wave in an outdoor environment is more restricted than with an indoor application. However, it was also found that with some indoor applications, human bodies create a considerable blockage to mm-wave propagation, because of their movement, which generates some shadowing effects [106].

Small cells architecture is considered one of the best-proposed solutions to deal with mm-wave high losses [107]. Specifically, dense small cells deployment in urban areas with cell diameter around 200 metre can mitigate this problem [24, 108, 109]. The application of LoS propagation in small cells deployment seems promising for mm-wave communications. Ensuring the LoS condition would need a massive antenna deployment to reduce the NLoS condition and strengthen the mm-wave signal propagation. Figure 2.10 presents a diagram showing the dense deployment of mm-wave small cells in comparison with microwave deployment in a macro cell.

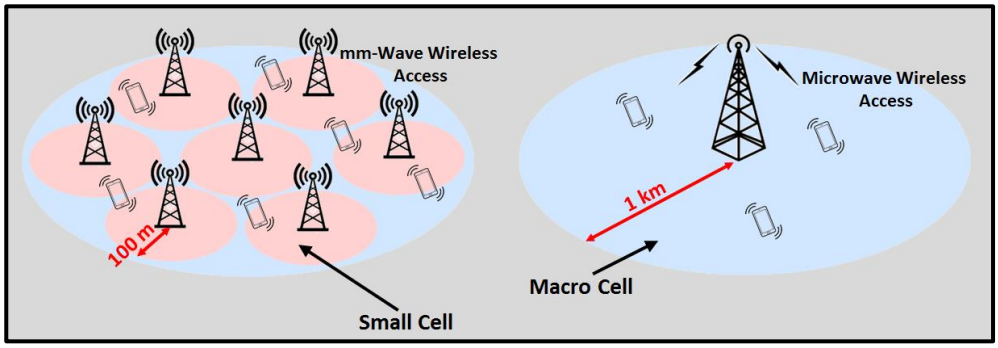

Figure 2.10 Dense deployment of mm-wave small cells inside a macro cell.

2.10.3 Doppler Effects and Multipath

In wireless communications, Doppler effects result from the relative motion between the receiver and signal source, which depend on the carrier frequency and mobility. The received waves have different shift values, which lead to Doppler spread. Fortunately, in the futuristic networks, there is no significant challenge in the mm-wave with Doppler effects, because of the narrow beam characteristics of the mm-wave, which can inherently reduce the angular spread [1, 7, 110].

There is another effect on the mm-wave wireless channel, which is multipath signal reception by multiple paths [7]. Channel multipath characteristics can be described by the root mean square of the power delay profiles, which helps in examining the effects of multipath in mm-wave wireless communication. This power delay profile presents the intensity of the mm-wave signal that is received through a multipath channel as a function of a time delay, which represents the difference in the travel time between all multipath arrivals [1, 101]. Because LoS links are not always possible, understanding the NLoS links problem is important. The NLoS link is obstructed by building edges and corners. Also, human activities and mm-wave reflection from different surfaces cause shadowing. Due to this, the NLoS links require the use of equalisers to improve the performance, as suggested in [1, 106], which adds more challenges to the mm-wave communication owing to an increase in the power consumption and the need to develop modulation techniques.

2.11 Challenges with Millimetre-Wave Wireless Channel

The underutilised mm-wave frequency bands have raised new challenges in wireless communications. The main difficulty with the mm-wave wireless channel is the unavailability of a standard channel model to understand the behaviour of mm-wave wireless networks. Hence, there has been a need to develop new techniques to understand mm-wave propagation through the air

interface [1, 3, 111]. Table 2.3 summarises the literature relating to understanding the mm-wave wireless channel with the most important key points in each work.

Table 2.3 Related work on the mm-wave wireless channel

mm-Wave Key Points	Reported References
5G Cellular Networks	[3], [5], [18], [94], [95], [102], [98], [109], [112], [113], [114]
Beamforming Techniques	[13], [14], [111], [92], [115], [116]
Massive MIMO	[25], [26], [108], [117], [118], [119]
Path Loss Models	[99], [101], [103], [104], [120], [121], [122], [123], [124], [125]

In addition, studying the thermal characteristic of mm-waves frequency so as to address safety concerns is an important issue. Regarding which, some of the latest research has been focused on examining the effects of mm-wave radiation on the human body, in particular and creatures in general [126, 127]. The behaviour of mm-wave wireless propagation has added new aspects for investigation in relation to the new communication system, including: the height of transmitters (i.e. BSs or antennas); nature of areas (urban, suburban or dense), and the interaction of mm-wave with objects materials in the neighbour surroundings [120, 128]. Specifically, blockage effects are a major reason for an increase in mm-wave path losses. The power of the mm-wave signal decreases because of their reflection and diffraction with buildings' walls or the ground in the environment. Consequently, the propagation of the mm-wave under these effects involves the NLoS condition. In response, a comprehensive investigation into the application of different mm-wave bands in the futuristic cellular networks is provided in detail in Chapter 6, as carried

out for this thesis [129]. A map-based scenario is applied, with a proposed simplified path losses model for precisely estimating the performance of mm-waves in outdoor applications. The mathematical and simulation results are presented and evaluated in Chapter 7, with consideration of the diffraction and specular reflection effects of the mm-wave to validate the proposed model, as presented by this researcher in recent research [130].

2.12 Summary

This Chapter has presented the fundamentals of mm-wave optical generation methods. The strength and challenges of mm-wave with RoF system and the FSO technologies are also discussed. Furthermore, the characteristics of mm-wave wireless propagation are presented. A detailed background is discussed with explaining the theoretical principles and mathematical analysis. The significant gaps in the previous related research are reported to improve mm-wave generation and transmission systems. So, the following chapters will provide the proposed work by this thesis to fulfil the mm-wave communication system requirements.

Chapter 3

Proposed Photonic Methods of mm-Wave Generation

In this chapter, three novel photonic methods of mm-wave generation are proposed and demonstrated by using the Optiwave Design Software for photonics. These generation approaches are based on the characterisations of a Brillouin fibre laser and SBS effects with phase modulation. According to the presented theoretical analysis and proposed simulation setups, stable mm-wave carriers are achieved successfully in the three proposed methods with different frequencies ranging from 5 GHz to 90 GHz. The proposed methods increased the stability and the quality of the generated mm-waves by using a single laser source as a pump wave and reducing the fibre nonlinearity effects. Simulation results show that all these carriers have a good SNR, low noise, and tuning capability in comparison with mm-waves that are generated by the previous methods, which are reported in this thesis. In addition, the proposed generation methods are profitable for RoF transmission systems, which make them appropriate for application in 5G optical networks.

3.1 Introduction

Millimetre-wave spectrum bands can improve wireless 5G cellular communications due to the wide available bandwidth within [29]. In addition, the application of mm-waves in RoF systems has gained substantial attention, because of its ability to increase the capacity, bandwidth and mobility of these systems [30, 131, 132]. In particular, the generation of high-frequency mm-waves has attracted considerable attention recently [33].

The photonic generation of mm-waves is considered the desired generation scheme for futuristic RoF networks, due to its capability of generating high-

frequency signals with a reduction in power consumption [8]. Many optical mm-wave carrier generation techniques have been proposed in the past few years, as explained previously in Chapter 2. However, there are still challenges to generating high-frequency mm-waves. Hence, there remains a significant need to achieve a simple, practical and cost-effective generation method to integrate it with RoF systems. Most of the schemes reported up until now are either complicated or require expensive components and thus, the development of a relatively simple low cost method for optically generating mm-waves remains a challenge worth pursuing.

In this chapter, three novel mm-wave generation schemes are proposed and examined with the simulation setups as in recent work by this researcher [64]. These proposed setups use one of the fibre nonlinearities, which is the SBS effect to give the benefit of the photonic generation of the mm-wave. In addition, the proposed methods are completely different from the previous work, because they are based on the characteristics of the Brillouin fibre laser and the SBS effect that exists in the optical fibre with the phase modulation technique. The proposed generating methods require only standard components of optical telecommunications, which makes their setup very simple and economical. The performance of the generation techniques is analysed and discussed with mathematical explanations and simulation results. The obtained results provide evidence that these methods of mm-wave generation can reduce systems cost and have the potential to create very stable high-frequency carriers with low noise which could meet the 5G optical network specifications.

The rest of this chapter is organised as follows: in Section 3.2, the mathematical theory and principle of the proposed mm-wave generation methods are explained. Section 3.3 is divided into three subsections, which describe the generation systems analyses and simulation setups for each generation method. Also, the obtained results and discussions of these are provided in each subsection. Finally, the chapter conclusions are presented in Section 3.4.

3.2 Mathematical Principles of the Generation Methods

Many methods have been proposed for the generation of mm-waves such as direct-modulation, external modulation, optical heterodyning and multimode light sources, as explained previously in Chapter 2. This study is focused on generating mm-wave carriers based on the SBS effect that exists in optical fibre with characterisation of the phase modulation technique.

Brillouin scattering occurs from the interaction of the light with the propagating density waves or acoustic phonons [56]. This process exists in each optical fibre, because none is free from microscopic defects or thermal fluctuations, which motivate the scattering, as explained previously in Chapter 2. The SBS effects are considered the dominant nonlinearity among the other nonlinear effects in optical fibre [73]. The standard for the Brillouin threshold power is specified as when the input optical power to the fibre equals the backward Stokes power [57]. Hence, the SBS threshold power (P_{th}) is considered from the point that SBS turns out to be a limiting factor. The use of a laser source with narrow linewidths makes SBS have low threshold power in the schemes. When the linewidth of the laser source is smaller than the Brillouin bandwidth, P_{th} can be assessed by [133]:

$$P_{th} = 21\frac{k_p A_{eff}}{g L_{eff}} \ (1 + \frac{v_s}{v_b}) \tag{3.1}$$

where, k_p is the polarisation factor, A_{eff} is the fibre core effective area, g is the Brillouin gain, v_s is the linewidth of the laser source, and v_b is the SBS interaction bandwidth. L_{eff} is the effective interaction length, which can be defined and calculated by [133]:

$$L_{eff} = \frac{1-exp(-\alpha L_{fibre})}{\alpha} \tag{3.2}$$

where, α is the attenuation coefficient, and L_{fibre} is the length of the fibre.

Accordingly, this nonlinear effect is utilised for generating mm-waves by optical heterodyning of the Brillouin Stokes with pump laser signals. The principle of optical heterodyning depends on the frequency difference between two optical signals [16]. These signals are combined in a photodiode to

produce an electrical signal which has a frequency equal to the frequency spacing between the two optical signals.

Assuming two optical waves, ($E_1(t)$ and $E_2(t)$), which have different angular frequencies (ω_1 and ω_2) and phases (ϕ_1 and ϕ_2), these are expressed by the following [49, 134]:

$$E_1(t) = E_{01}\cos(\omega_1 t + \phi_1) \tag{3.3}$$

$$E_2(t) = E_{02}\cos(\omega_2 t + \phi_2) \tag{3.4}$$

where, E_{01} and E_{02} are the electric field amplitudes, and t is the time. These two waves are converted from the optical domain to the electrical one by a photodiode, which registers the intensity ($I(t)$), as explained by the following [135]:

$$I(t) = \varepsilon_0 \varepsilon_p c|E_1(t) + E_2(t)|^2 \tag{3.5}$$

where, ε_0 is the electric field constant, ε_p is the relative permittivity, and c is the velocity of light. By substituting (3.3) and (3.4) into (3.5), the final expression of the generated electrical wave is represented by [135]:

$$I(t) \cong [E_{01}^2 + E_{02}^2 + 2E_{01}E_{02}\,cos\{(\omega_2 - \omega_1)t + (\phi_2 - \phi_1)\}] \tag{3.6}$$

Thus, the generated difference frequency (f), which represents that of the mm-wave, is calculated by $f = \frac{\omega_2 - \omega_1}{2\pi}$.

In an alternate technique, the SBS effect can be used for generating mm-waves by heterodyning with the phase modulated signals. The phase modulator function has the same principle as MZM, except that it has a single arm. The phase modulator has a switching voltage (V_π) and is fed by a laser signal with an optical power level of (P_{in}), so the output optical field ($E_p(t)$) of it can be calculated by [15]:

$$E_p(t) = e^{j\frac{\pi V(t)}{2V_\pi}}\sqrt{2P_{in}}e^{j\omega_c t} \tag{3.7}$$

where, ω_c is the carrier angular frequency, and $V(t)$ is the electronic modulating signal. Theoretically, the complex optical field envelope at the output of an optical phase modulator can be represented by [136]:

$$E(t) = \exp[jm\cos(\omega_m t)] \tag{3.8}$$

where, m is the modulation index, and ω_m is the angular frequency of the modulating microwave signal. So, the phase modulated signal contains the main optical carrier at ω_0 and the sidebands at $\omega_0 \pm n\omega_n$, which will generate the electrical signal when it is directly beating at a photodiode as in the following [58]:

$$E(t) = \sum_{n=-\infty}^{\infty} j^n J_n(m)\, exp(jn\omega_m t) \tag{3.9}$$

where, $J_n(m)$ is the Bessel function of the first kind of order n.

3.3 Simulation Analyses of the Proposed Generation Schemes

To design and analyse the proposed generation methods the concepts are built by using the Optisystem simulation tool. Optisystem simulation, which is a part of the Optiwave Design Software, is an advanced optical communication simulation package that designs, tests, and optimises, virtually, any type of optical link in the physical layer of a broad spectrum of optical networks.

For this study, as aforementioned, the nonlinearity effect in optical fibre is investigated by modelling and simulating three novel methods of mm-wave generation. System performance and characterisation are simulated by utilising the SBS effect for the generation and amplification of mm-waves. Applying the generated mm-wave with RoF technology is suggested in this work for the next generation optical communication systems. For this reason, two main issues are taken into considerations the frequency fluctuation and spurious sidebands suppression ratio. As it is explained in the literature review in Chapter 2, the most straightforward way for mm-wave generation is the use of two laser sources by the heterodyning technique. The mm-wave fluctuates around its central frequency because of phase mismatch between the two lasers and relative frequency instability. This fluctuation adds the residual frequency offset and increases the single sideband phase noise. In some research [65, 68],

suppression methods have been presented to cancel the undesired optical sidebands and to generating mm-waves. However, in this case, suppression ratio limits the influence of the whole mm-wave generation system. The analysis of the latest research has been presented evidence that the suppression ratio of the optical sideband can go above 37 dB and that of the radio frequency sideband exceeds 31 dB [45].

In this work, avoiding this situation is done by using a single laser source as a pump wave source. In the system simulation, the used CW laser source works with the parameters that are presented in Table 3.1. This laser source has a spectrum of 1550 nm, which is chosen because it has the lowest attenuation and dispersion inside the fibre [15]. The laser light is injected into a bidirectional single mode fibre (SMF) having a length around 25 km, which is considered ideal for a long-haul communication link [8]. This bidirectional SMF is activated by simulation with the Brillouin scattering effects to allow for the light to propagate in the forward and the backward directions. The simulation parameters considered for the SMF in this work are presented in Table 3.2, which are divided into two types: physical and numerical. The physical parameters are considered based on some recent studies [7, 8, 15, 49, 57], whereas the numerical parameters have been chosen based on enabling high accuracy of the simulator calculations. While the input power of the laser is set to 8 dBm, which is chosen to ensure that it is close to the Brillouin threshold. Then, the Brillouin threshold power is calculated by equation (3.1) to consider the SBS effect inside the optical fibre.

By ensuring that the laser power is high enough, i.e. beyond the SBS threshold, the transmitted light inside the SMF starts generating the backscattered Stokes-shifted signals. These optical signals generate sidebands due to the nonlinear characteristic inside the SMF. Then, the interactions among the pump wave, acoustic wave and Stokes wave will produce the SBS effect.

This effect of the SBS is involved in the Optisystem simulation tool and hence, its setting used in this work is based on the nonlinear Schrödinger equations. These are well known as mathematical equations that describe the changes in a

physical system over the time [56, 137]. They are solved in the simulator program by the utilisation of the symmetrised non-iterative split-step Fourier method. In the designed simulation setup, the step size has been selected with a variable amount, which is changed depending on the value of the maximum nonlinear phase shift and the calculation process, because in this case, it is more flexible and faster. If the step size is fixed, it will be calculated once, just when the simulation starts. Accordingly, a variable step size has been used and the SMF numerical parameters set up as presented in Table 3.2.

The simulation setup for each of the three proposed schemes is explained and discussed in the following subsections, 3.3.1, 3.3.2, and 3.3.3, respectively.

Table 3.1 Laser source simulation parameters

Parameter	**Optical Source**	**Wavelength**	**Linewidth**	**Power**
Value	CW Laser	1550 nm	1 MHz	8 dBm

Table 3.2 Bidirectional SMF simulation parameters

Physical Parameters		**Numerical Parameters**	
Parameter	**Value**	**Parameter**	**Value**
Fibre Length	25 km	Number of iterations	50
Fibre Attenuation	0.2 dB/km		
Fibre Dispersion	16.75 ps/nm.km	Number of steps	200
Effective Core Area	80 μm^2		
Brillouin Gain	46×10^{-12} m/W	Step accuracy	0.001
SBS Interaction Bandwidth	31.7 MHz		
Frequency Shift	11 GHz	Step size	Variable
Polarisation Factor	1.85		

3.3.1 First Proposed Method and Results Discussion

The simulation setup of the first proposed method of mm-wave carrier generation is presented in Figure 3.1. This generation scheme, which is based on SBS, is aimed at being quite simple and easy to implement. The obtained results of the output signals are visualised by using components from the simulation visualiser library, including the Optical Spectrum Analyser (OSA) and the Radio Spectrum Analyser (RSA). The spectrum analyser result in the simulation for each inset in Figure 3.1 (a, b, c, and d) is presented in Figure 3.2 (a, b, c, and d).

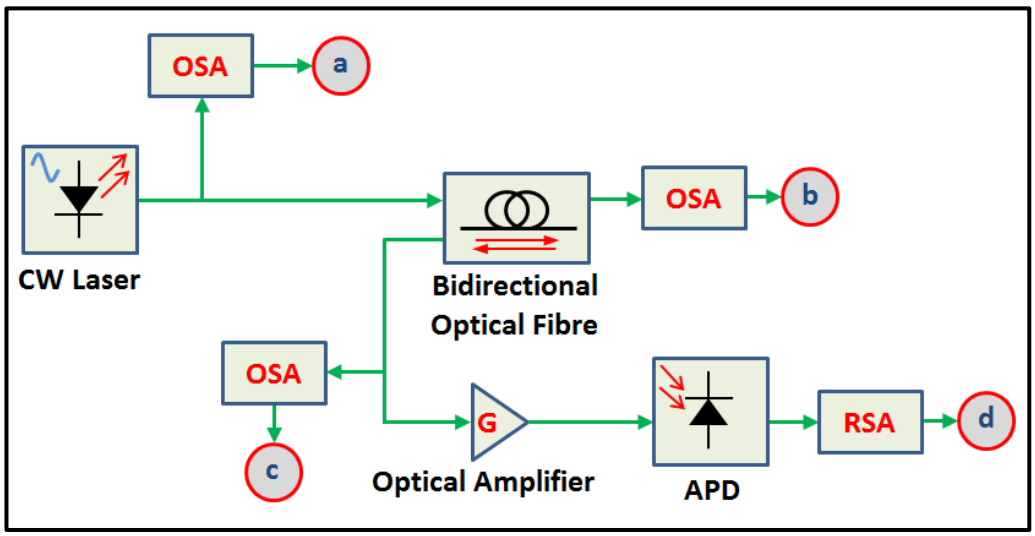

Figure 3.1 The first simulation structure of mm-wave generation.

Point (a) in Figure 3.1 shows the optical spectrum of the laser source output with power equal to 8 dBm at 1550 nm wavelength, with the results being given in Figure 3.2(a). This laser optical signal enters the bidirectional SMF with this sufficient amount of power to generate the First Order Brillouin Stokes (FOBS) signal spontaneously, as shown in point (b) in Figure 3.1 and the results are presented in Figure 3.2(b).

The FOBS signal is created through the light which is backscattered at a downshifted frequency. This first Stokes signal oscillates in the fibre cavity, and when it reaches a certain threshold for generating the second order Stokes waves, the same process will be repeated. Hence, it will produce another Stokes signal in the opposite direction inside the fibre. The Second Order Brillouin Stokes (SOBS) signal is generated when the optical signals returned to the bidirectional SMF in the opposite direction, as illustrated in point (c) in Figure 3.1.

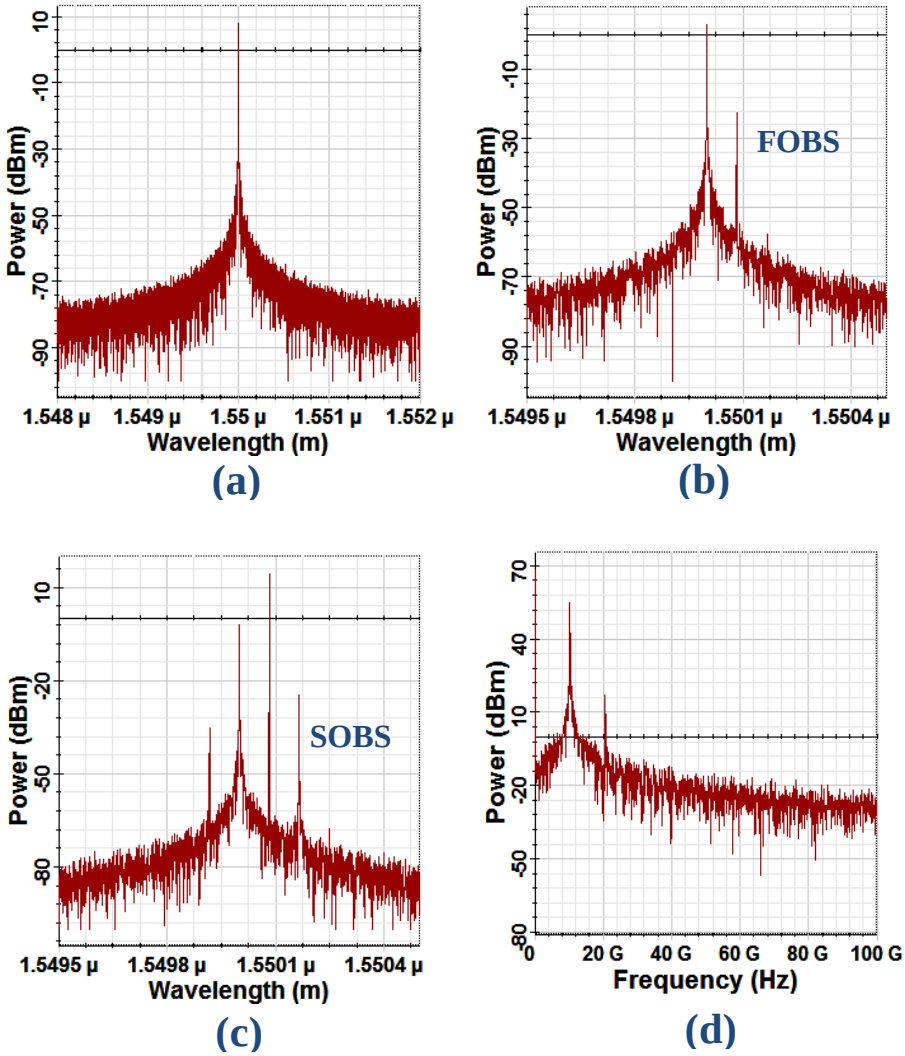

Figure 3.2 The analyser results at the corresponding points (a, b, c, and d) in Figure 3.1.

The outcomes generated SOBS with the amplified FOBS are provided in Figure 3.2(c). Then, these two Stokes signals are amplified by an EDFA amplifier, which has a gain of 30 dB and a noise figure of 4 dB. After that, the output signals are heterodyned and combined by the avalanche photodiode (APD) to generate mm-waves. The APD is considered in the proposed setup to provide the built-in gain through the avalanche multiplications process. This will increase the responsivity and provide the high sensitivity of the detection, but it will also increase the response time as well in comparison with using PIN photodiode. While considering PIN is possible, but it is not preferable in the proposed setup because it has lower responsivity and sensitivity of the detection. The point (d) in Figure 3.1 represents the generated mm-wave carriers at the output of the electrical spectrum analyser, and the results are given in Figure 3.2(d).

This method generates two mm-wave carriers, the first at 10 GHz, and the second at 20 GHz, which can be simply filtered with any filtering components. Also, the received power of these two carriers is good, which equals 53 dBm and 16 dBm for the first and second carrier, respectively. These carriers have a good signal to noise ratio of up to 51 dB. Therefore, both of these mm-waves have low noise signal power, which is averaged at -20 dBm as shown in Figure 3.3. As a result, this new method is very simple and cost-effective in comparison with the method of generation used in [49].

Nevertheless, the limited number of low frequencies that are generated brings forth the idea of improving this approach, as demonstrated in the next subsection, which contains the second proposed scheme.

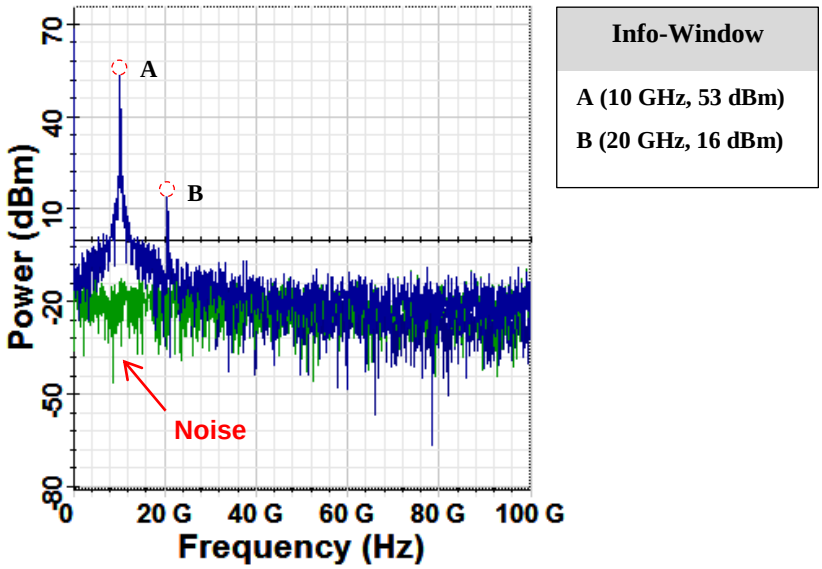

Figure 3.3 The generated mm-wave carriers with the noise signal.

3.3.2 Second Proposed Method and Results Discussion

To improve upon the previous generation method, adding the effects of the phase modulation technique is proposed in the second approach. Figure 3.4 represents the second proposed method, which is based on the coupling of the phase modulated signals with the Brillouin Stokes that is based on the SBS effects of the fibre laser. The spectrum analyser results in the simulation for each inset in Figure 3.4 (a, b, c, d, e, and f) are represented in Figure 3.5 (a, b, c, d, e, and f) respectively.

With this method, the laser optical spectrum is generated at the output of the diode laser, as in the point (a) in Figure 3.4, and the analyser's results are provided in Figure 3.5(a). Then, this signal is directed towards the first optical coupler component (OC1) and, this laser signal will be split into two equal parts by using the OC1 with a coupling coefficient that equals 0.5 in the simulation. The optical spectrum of these two signals, as in the two insets marked with a (b) in Figure 3.4, delivers the results presented in Figure 3.5(b).

Subsequently, one of these optical signals enters the bidirectional SMF to generate the Brillouin Stokes, as explained in the previous proposed method. Point (c) in Figure 3.4 represents the output optical spectrum from the bidirectional SMF, and the result is provided in Figure 3.5(c). At the same time, the second optical signal enters the phase modulator component. In the Optisystem simulation model, the electrical modulating signal imposes a phase modulation on an optical carrier and, the behaviour of this model is described by [64]:

$$E_{out}(t) = E_{in}(t).exp\big(j.\Delta\phi.modulation(t)\big) \quad (3.10)$$

where, $E_{out}(t)$ is the output optical signal, E_{in} is the input optical signal, $\Delta\phi$ is the phase deviation, and *modulation(t)* is the electrical input signal. In the Optisystem simulation, the normalisation of the electrical input signal is between 0 and 1, while the phase modulator does not affect the noise bins signals in this case. It is driven by radio frequency (RF) sinusoidal signals with the parameters of 20 GHz frequency and a phase of 90 degrees.

The spectrum analyser results at the output of the phase modulator in point (d) in Figure 3.4, are shown in Figure 3.5(d). Then, the Brillouin Stokes signals are combined with the phase modulated optical signals by using another optical coupler (OC2), as point (e) in Figure 3.4. The combined optical signals are shown in Figure 3.5(e), which are amplified by using the EDFA and then heterodyned at the APD (Figure 3.4 point (f)) to generate mm-wave carriers, as illustrated in Figure 3.5(f). This figure represents the generated mm-wave carriers presented by the electrical spectrum analyser. It can be seen that there are spectral lines appeared very close to the generated carriers. These lines appeared because of considering the Brillouin Stokes and anti-Stokes in this generation method by using the bidirectional fibre. Particularly, Brillouin anti-stokes might have frequency shift differs a little which leads to this spectral lines.

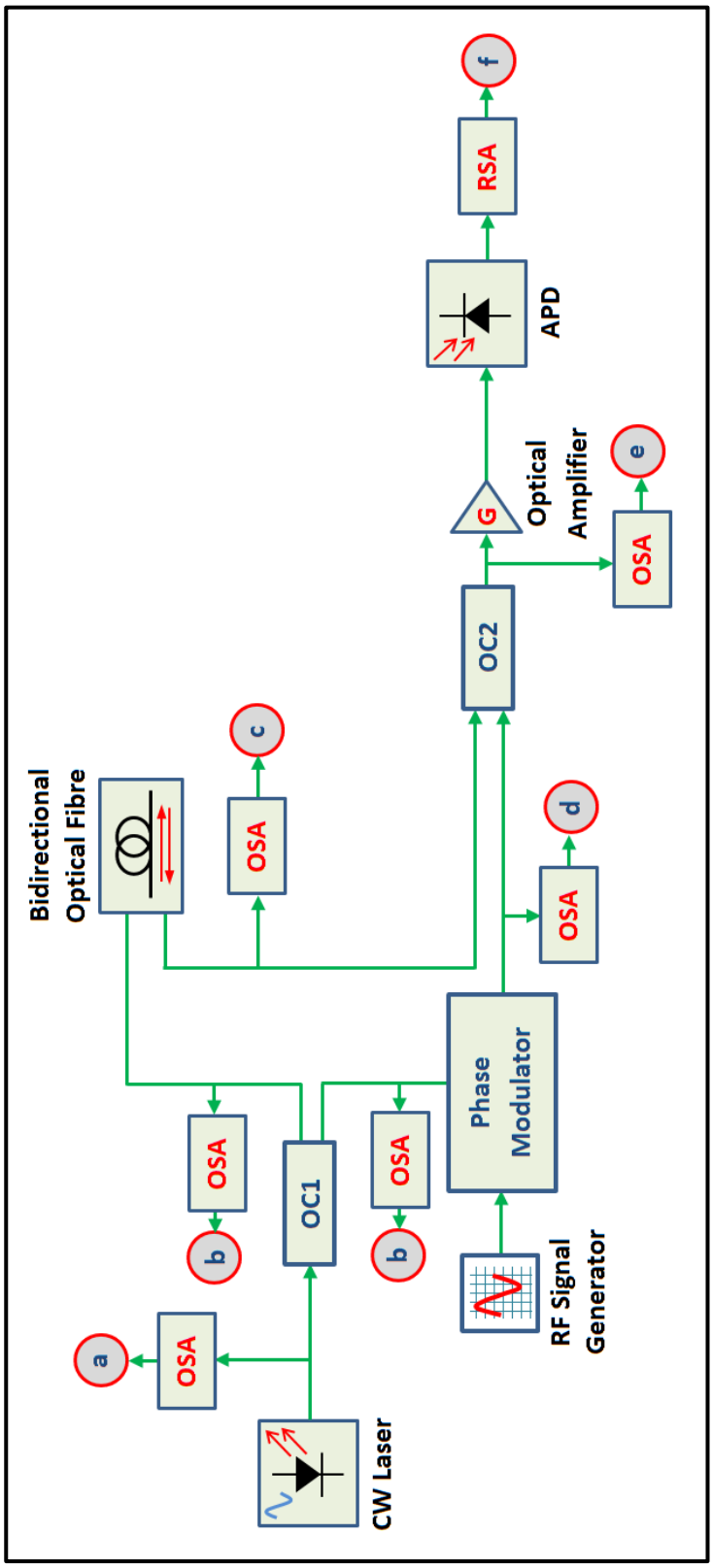

Figure 3.4 The second simulation structure of mm-wave generation.

The results obtained from this generation method show the possibility of generating high-frequency mm-wave carriers with improving tuning capability of up to 90 GHz, as shown in Figure 3.6(a). The generated mm-wave carriers are at different frequencies, according to the different order Brillouin Stokes and Brillouin anti-Stokes signals that are combined with the phase modulated signals. These carriers have a good signal to noise ratio of up to 39 dB. That is, these mm-waves have low noise power, which is averaged at -20 dBm, as shown in Figure 3.6(a). All the different mm-wave carries have a very low noise with good peak power, and this generation method represents a cost-effective setup in comparison with the method presented in [45], except that the obtained frequency was less than 100 GHz. Also, to investigate the effect of SBS on this generation method, the simulation setup is connected without the activation of the Brillouin scattering parameters inside the bidirectional SMF. The obtained result, in this case, has been compared with the proposed method, as shown in Figure 3.6(a,b). This comparison shows the advantages of considering the SBS effects, which increased the tuning capability of the generated mm-waves, with the ability to generate a higher frequency of up to 90 GHz, as can be seen in Figure 3.6(a). In contrast, Figure 3.6(b) shows a limited number of generated mm-waves due to the effect of just phase modulation.

In trying to obtain even more improvement, a third scheme is proposed in the next subsection.

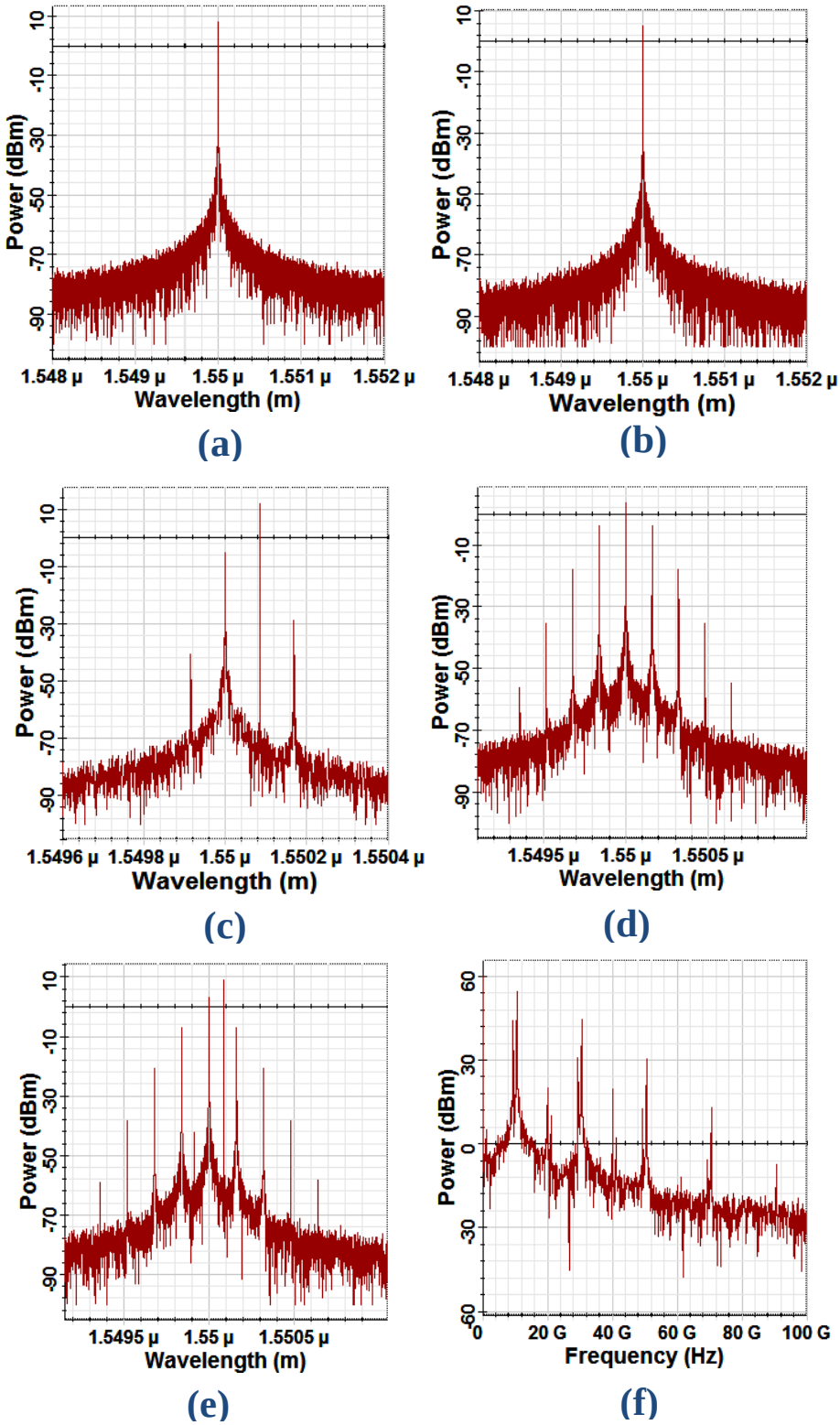

Figure 3.5 The analyser results at the corresponding points (a, b, c, d, e, and f) in Figure 3.4.

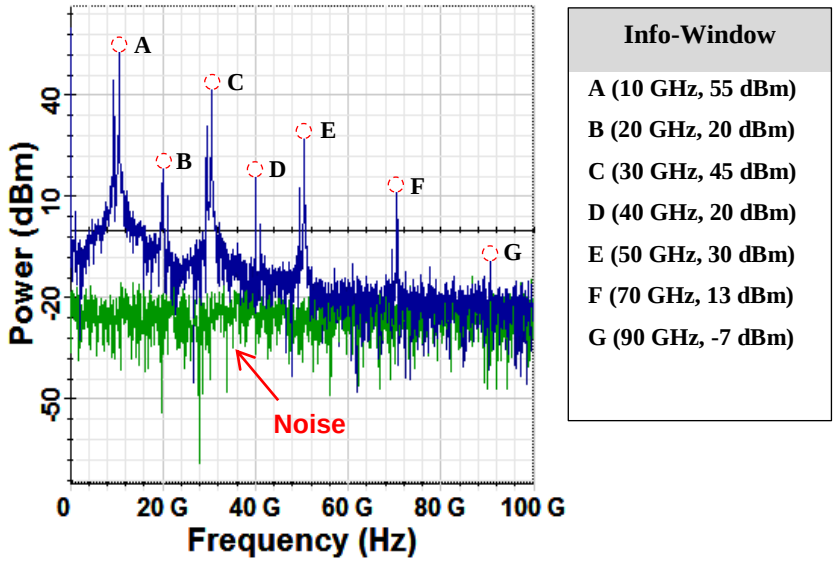

(a) With SBS effects

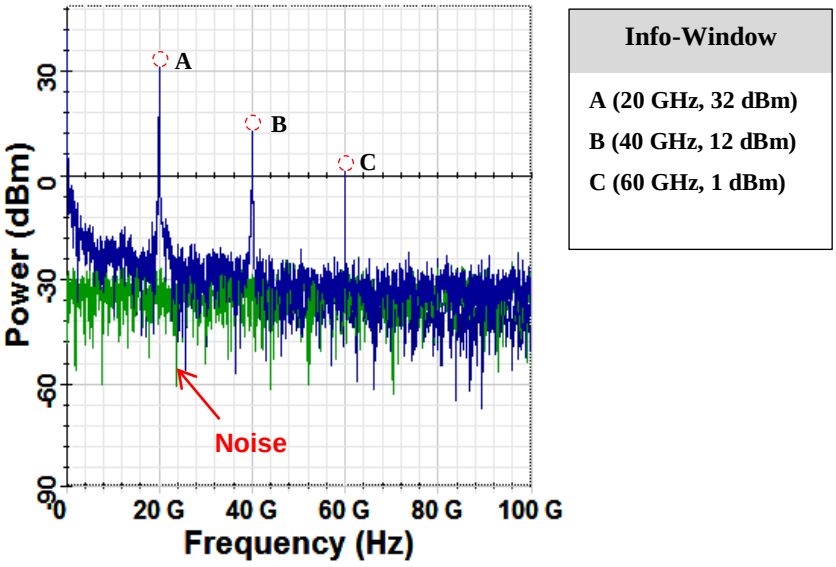

(b) Without SBS effects

Figure 3.6 The generated mm-wave carriers with the noise signal.

3.3.3 Third Proposed Method and Results Discussion

A third generation approach is proposed to optimise the performance of the generation system, which will improve the productivity of a stable mm-wave. In this case, the laser input signal enters the phase modulator, and the modulated signals are then injected to the SMF, as shown in Figure 3.7.

To have the maximum benefit of SBS, Brillouin Stokes is considered in this generation method for two schemes. The first, is with using unidirectional fibre, and the second, by deploying a bidirectional fibre. In sum, the third approach is based on the phase modulated signal using the SBS effects in the optical fibre.

Firstly, the effect of Brillouin Stokes in the unidirectional fibre is studied and simulated, which is followed by considering this effect when the bidirectional fibre is added and the results are compared. The spectrum analyser results in the simulation for each inset in Figure 3.7 (a, b, c, d, e, and f) are presented in Figure 3.8 (a, b, c, d, e, and f), respectively.

The laser optical spectrum is generated at the output of the diode laser as in point (a) in Figure 3.7, and the analyser's results are illustrated in Figure 3.8(a). Then, this signal is directed towards the phase modulator, which is driven by RF sinusoidal signals, having parameters of 20 GHz frequency and a phase of 90 degrees. Inset (b) in Figure 3.7 shows the output of the phase modulated signals, the results of which are provided in Figure 3.8(b). Next, these signals are propagated through the SMF with sufficient amount of power to generate the Brillouin Stokes, as in inset (c) in Figure 3.7, with the outcomes being given in Figure 3.8(c). These optical signals are amplified by using the EDFA and then heterodyned at the APD (Figure 3.7 point (e)) to generate mm-wave carriers, as can be seen in Figure 3.8(e). Note that the blue dash line in Figure 3.7 represents the simulation process for the unidirectional fibre case.

This SBS effect leads the obtaining of mm-wave carriers, as in inset (e) in Figure 3.7, the results of which are displayed in Figure 3.8(e), these having high quality and being at different frequencies. This shows the real possibility

of generating high-frequency mm-wave carriers with a high tuning capability of up to 80 GHz.

Then, to investigate the effect of SBS using a bidirectional SMF, the signals that are output from the fibre, as shown in Figure 3.8(c), are redirected to the fibre to propagate in the opposite direction so as to have more Brillouin Stokes signal effects. The output signals are shown in Figure 3.8(d). This method also generates a good range of mm-wave carriers, as shown in Figure 3.8(f), but it can only reach 45 GHz with good peak power, for the generated mm-waves with frequencies above this have weak peak power.

The obtained results from using unidirectional fibre show the possibility of generating high-frequency mm-wave carriers with an improving tuning capability of up to 80 GHz, as shown in Figure 3.9(a). The generated mm-wave carriers have good signal to noise ratio of up to 42 dB. That is, these mm-waves have low noise power, which is averaged at -30 dBm, as shown in Figure 3.9(a). So, different mm-wave carries are generated which have a very low noise with good peak power and this is cost-effective in comparison with the method presented in [44, 58]. While in the case of using the bidirectional fibre, the obtained results show lower frequencies, with a signal to noise ratio of up to 40 dB and low noise power, averaging -40 dBm, as can be seen in Figure 3.9(b). Unfortunately, the mm-wave signals above 45 GHz have very low power. As a result, the applying of the unidirectional SMF is preferred to the bidirectional one for this proposed method, as the former gives better generated mm-wave carriers, as is clear from Figure 3.9(a,b).

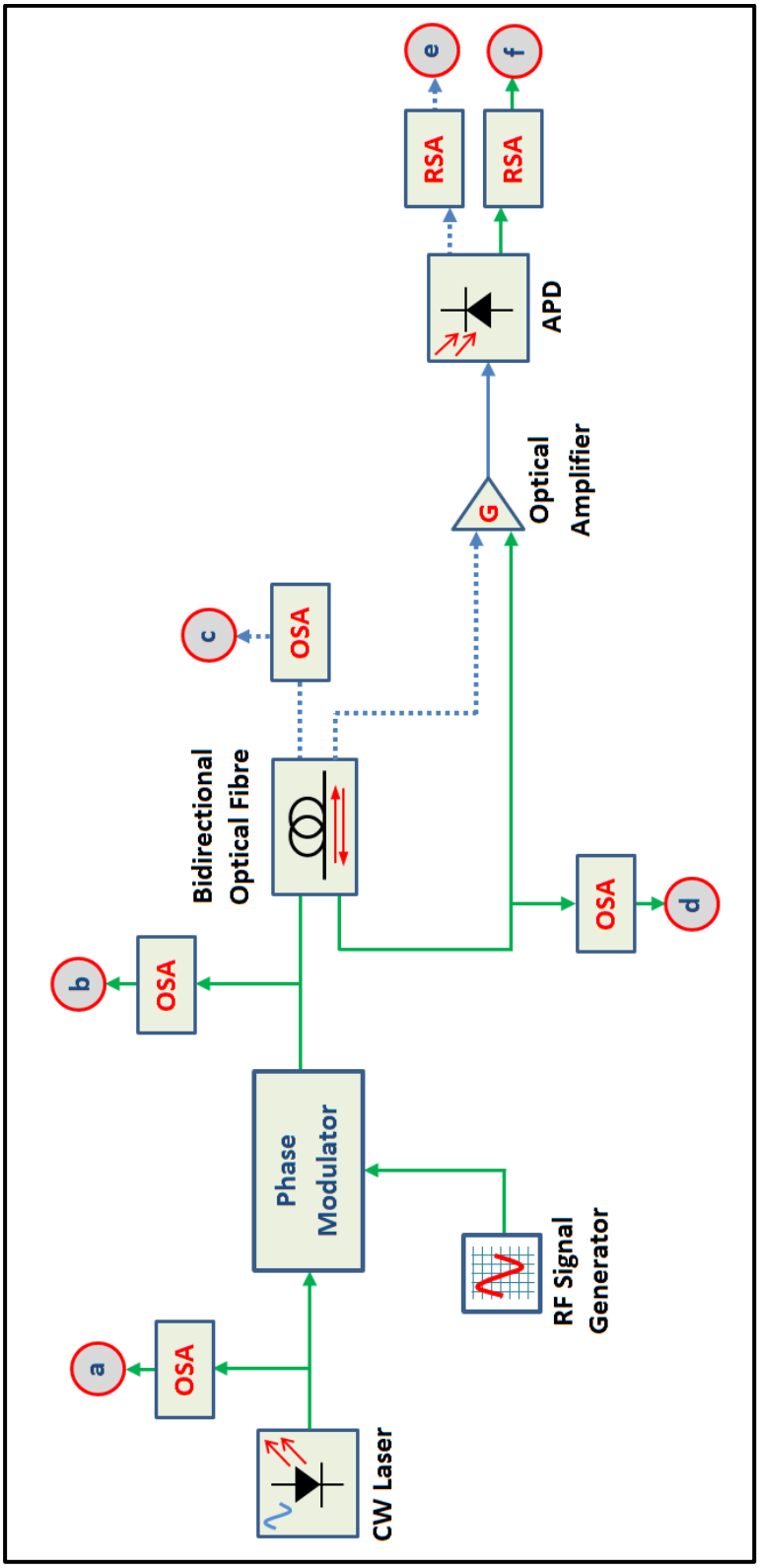

Figure 3.7 The third simulation structure of mm-wave generation.

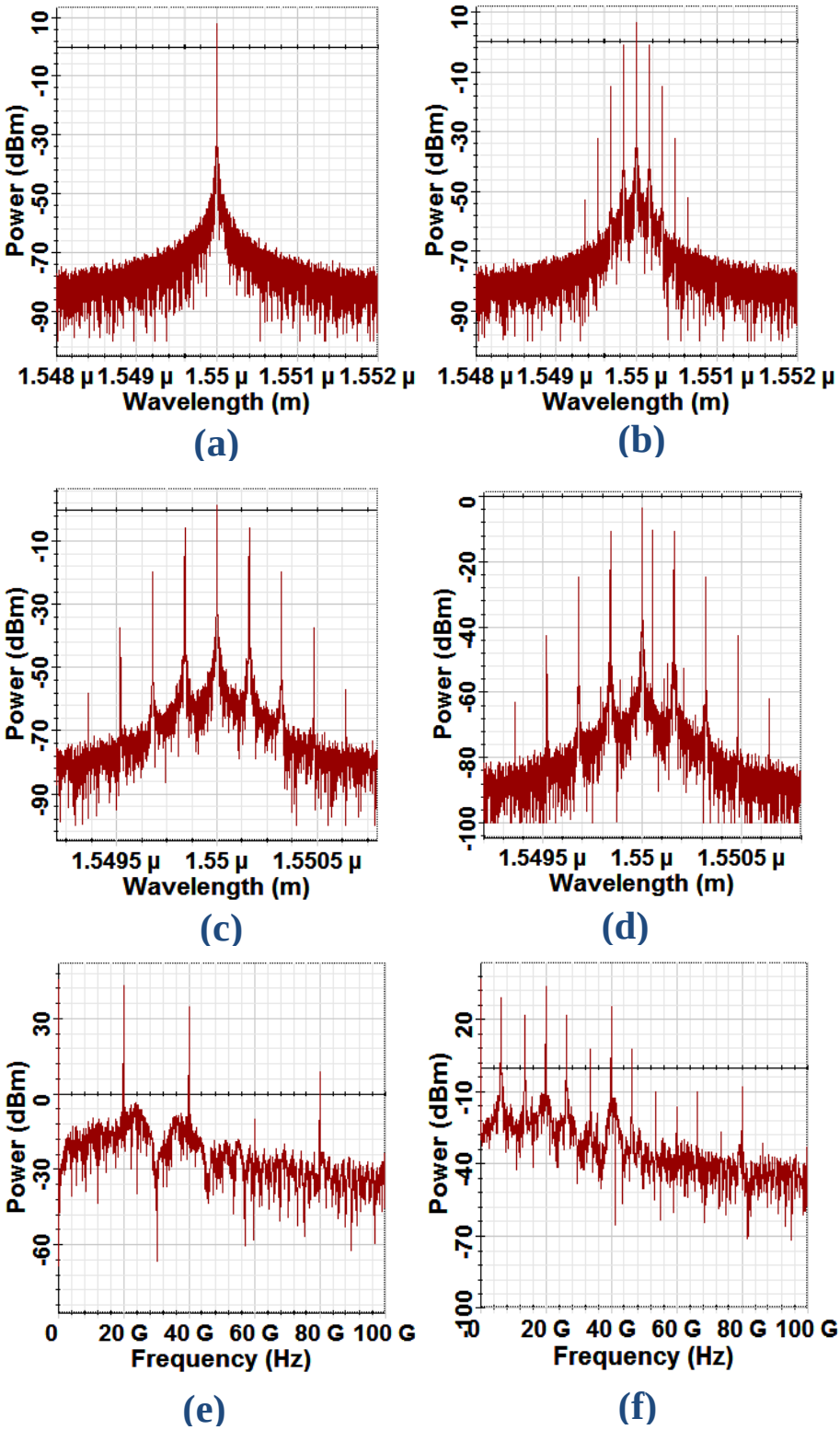

Figure 3.8 The analyser results at the corresponding points (a, b, c, d, e, and f) in Figure 3.7.

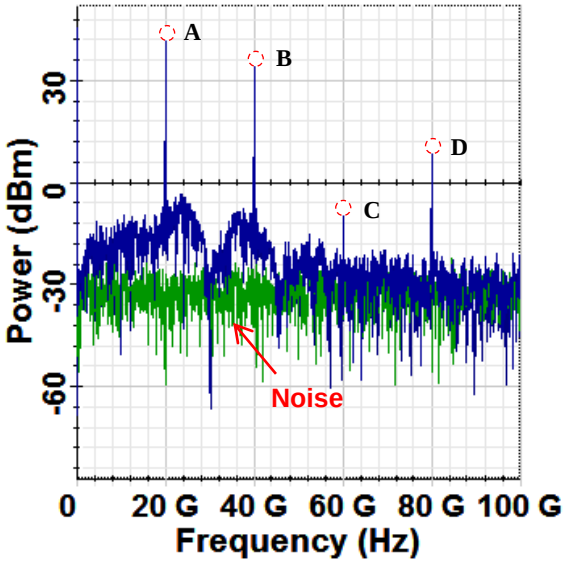

Info-Window
A (20 GHz, 42 dBm)
B (40 GHz, 35 dBm)
C (60 GHz, -10 dBm)
D (80 GHz, 9 dBm)

(a) With Unidirectional Fibre

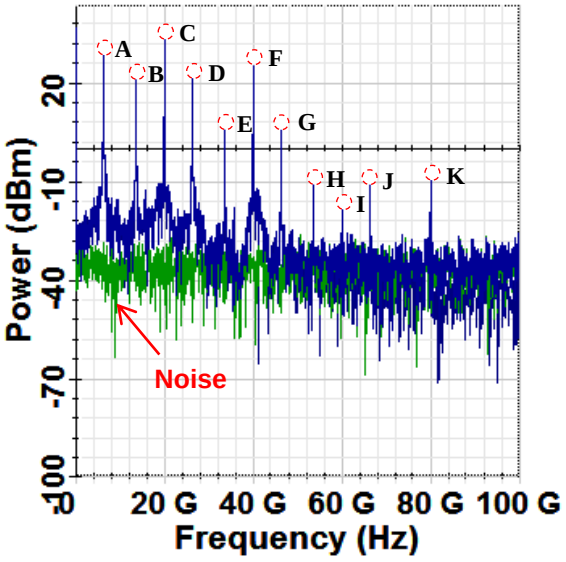

Info-Window
A (5 GHz, 28 dBm)
B (15 GHz, 20 dBm)
C (20 GHz, 33 dBm)
D (25 GHz, 22 dBm)
E (30 GHz, 7 dBm)
F (40 GHz, 25 dBm)
G (45 GHz, 7 dBm)
H (50 GHz, -10 dBm)
I (60 GHz, -16 dBm)
J (65 GHz, -10 dBm)
K (80 GHz, -8 dBm)

(b) With Bidirectional Fibre

Figure 3.9 The generated mm-wave carriers with the noise signal.

3.4 Summary

Millimetre-wave generation systems offer great potential for futuristic 5G communication networks. In this chapter, the SBS theory and concept have been used for mm-wave generation using three different approaches, which are proposed and simulated. The Brillouin scattering effect in optical fibre has been utilised for generating and amplifying high carrier frequency. The design was simulated using a commercial optical system simulator for system performance characterisation in generating mm-wave carriers. The simulation results have demonstrated that an 8 dBm laser light carried over 25 km SMF can successfully generate high-frequency signals with low noise and a tuning capability of up to 90 GHz. Also, the simulation results have shown that all these carriers show good improvement in comparison with the previous methods of generation that have been reported in this thesis. This improvement includes the aspects of stability, availability to apply, and cost.

To sum up, in this work, new schemes of photonic mm-wave generation methods have been proposed, which are based on the SBS effect. In the optical communication link, generating and delivering mm-waves by using these methods could solve the limitations caused by fibre nonlinearity effects. These mm-wave carriers will simplify the optical telecommunication system for data transmission. Also, the physical characteristics of the generated mm-waves are suitable for RoF systems in futuristic 5G networks.

Chapter 4

Proposed mm-Wave over a Full-Duplex RoF System

In this chapter, a full-duplex RoF system with the generation and transmission of 64 GHz mm-wave is investigated. This system is proposed as a solution to cope with the demands of a multi Gbits/s data transmission in 5G and beyond networks. In this chapter, the cost reduction and performance improvement are achieved by simplifying the mm-wave generation and transmission method with a RoF technique. High-frequency radio signals are considered challenging in the electrical generation domain and to address this, the proposed photonic generation method of mm-wave is used. The RoF system design is proposed in addition to the mm-wave generation using both phase modulation and the effect of SBS in the optical fibre. The RoF system, with a transmission rate of 5 Gbits/s, is achieved successfully. In the proposed scheme, one laser source is utilised, and an FBG is used for the wavelength reuse for the uplink connection. That is, a stable mm-wave over fibre link is successfully achieved for up to 100 km fibre length with a high-quality mm-wave carrier. Simulation results show a reduction in fibre nonlinearity effects and the mm-wave signal has good signal power, with low noise power equal to -75 dBm. The outcomes of this study ensure a practical mm-wave over fibre link, which will be appropriate for small cell 5G networks due to a reduction the installation cost.

4.1 Introduction

Recently, the RoF system has been developed to distribute radio signals optically for longer distances [9]. Due to the rapid revolution in wireless networks and mobile technology, the RoF system became a potential option for coping with high demands for this fast growth communication for the new

broadband services [8]. Also, the RoF technique can provide simple antenna front ends and improve wireless access coverage [138].

The overcrowded microwave band and the lack of global bandwidth for wireless communication have encouraged the implementation and improvement of the mm-wave spectrum for futuristic 5G networks [1]. Also, applying mm-wave frequencies will simplify the design of efficient wireless communications, which can offer suitable terminal mobility and high capacity channels [40, 139]. Due to this benefit, mm-waves with the RoF system is seen as one of the promising candidates for delivering high-speed radio transmission with a seamless convergence between the optical and radio signals [140]. Moreover, the RoF technique can directly convert an optical signal to a high-frequency radio signal with a photonic direct up-conversion scheme [15].

The photonic generation and transmission of mm-wave signals over a fibre link is considered essential for keeping the remote cells simple, cost-effective, and energy efficient. It additionally guarantees a low-attenuation transmission for wireless mm-wave signals, thereby potentially providing good flexibility for mobile and broadband access networks [141]. When utilising this system, mm-wave signals will be transmitted from the CS to the RAU directly, which is simplified to deal with only the process of conversion and amplification, while the signal processing can be done at the CS [142]. With this configuration, it is possible to obtain a flexible communication solution for the upcoming high-speed networks. This system can be useful in different applications, such as last-mile broadband access networks and resilient access networks [143, 144].

Another critical point is the possibility of implementing an FSO link with this system. The performance of the FSO communications as being conditional upon the weather is well known, but it still can be considered as an alternative solution for short-range fibre cables [20]. The combination of fibre and mm-wave links is crucial due to its large bandwidth, high capacity, and robust features. Ultimately, to obtain a higher data rate in 5G wireless networks, it is

essential to fulfil the requirement of the transmission latency, which might restrict the length of the fibre link to a few kilometres [145, 146].

The RoF system operating at the free-license mm-wave bands (57-64 GHz), has been considered a promising candidate for meeting the required capacities for wireless backhauling of the future mobile network standards [147]. Accordingly, the demonstration of low-cost systems with a simple setup for generating mm-wave signals over fibre has become necessary for future networks [34]. The primary challenge in implementing such RoF networks is the large size of the optical components and devices [32, 37].

Recently, the need for a multi Gbits/s data transmission system in 5G communications has raised the importance of applying the free licensed 60 GHz frequency band with a RoF system [107]. Hence, in this chapter, a full-duplex RoF system with the photonic generation of mm-waves is proposed and demonstrated as in the recent research by this researcher [67]. This new setup differs from the previous related research by taking into the consideration the generation and transmission performance of the mm-wave over fibre. The mm-wave signal is generated using a phase modulator, and it has been investigated with consideration of the benefits of SBS in the fibre. Exploiting a single laser source with the direct data modulation will reduce the cost and the complexity of the system. Moreover, the use of FBG for wavelength reuse has increased the stability of the mm-wave over a RoF system and reduced the nonlinearity effects as well. In the proposed simulation setup, there is no need to apply expensive components to generate the mm-waves as in some previous techniques that used costly apparatus to reduce the complexity. That is, in this research a simple setup is proposed, which has the potential to support the implementation of mm-waves in 5G futuristic communication systems that are integrated with the optical fibre link.

The rest of this chapter is organised as follows: in Section 4.2, the design of mm-waves over the fibre link is explained with its system principle and architecture. Section 4.3 describes the simulation setup and provides a discussion of the results, whilst Section 4.4 focuses on the evaluation of the

system performance. Finally, the chapter conclusions are presented in Section 4.5.

4.2 Design of mm-Wave Generation and Transmission over a Fibre Link

In this section, the operating principle of the proposed full-duplex RoF system with the photonic generation method of the mm-wave is presented, and evaluation of the system performance is provided. Figure 4.1 illustrates a block diagram of the proposed system design. The full-duplex mm-wave RoF system consists of two main parts: the central station (CS) and the radio access unit (RAU). The CS consists of a directly modulated laser driven by the data signals, a phase modulator driven by RF sinusoidal signals of the local oscillator, and the uplink receiver. The phase modulator can be stably operated without an electrical DC bias control circuit. Moreover, a phase modulator has a small insertion loss, whilst, the RoF system, which uses this modulator, has a larger margin. So, the phase modulator is driven by an appropriate radio frequency signal, which will lead to obtaining a small modulation depth.

The optical signals are then launched into the standard SMF and propagated to the RAU. After the transmission of the optical carrier along the fibre, the optical signal is filtered and amplified in the RAU. The FBG is deployed to reuse the optical carrier for the uplink signal. Therefore, the reuse of the remained optical carrier, which is a strong optical signal, can efficiently realise cost-effective operation. The other part of the optical carrier, which passes through the FBG, will be then detected by the optical receiver to produce the required mm-wave signal. Coherent or incoherent detection methods can be applied, but whilst the latter is simple, its performance is not of the same quality as that of the former [143, 148].

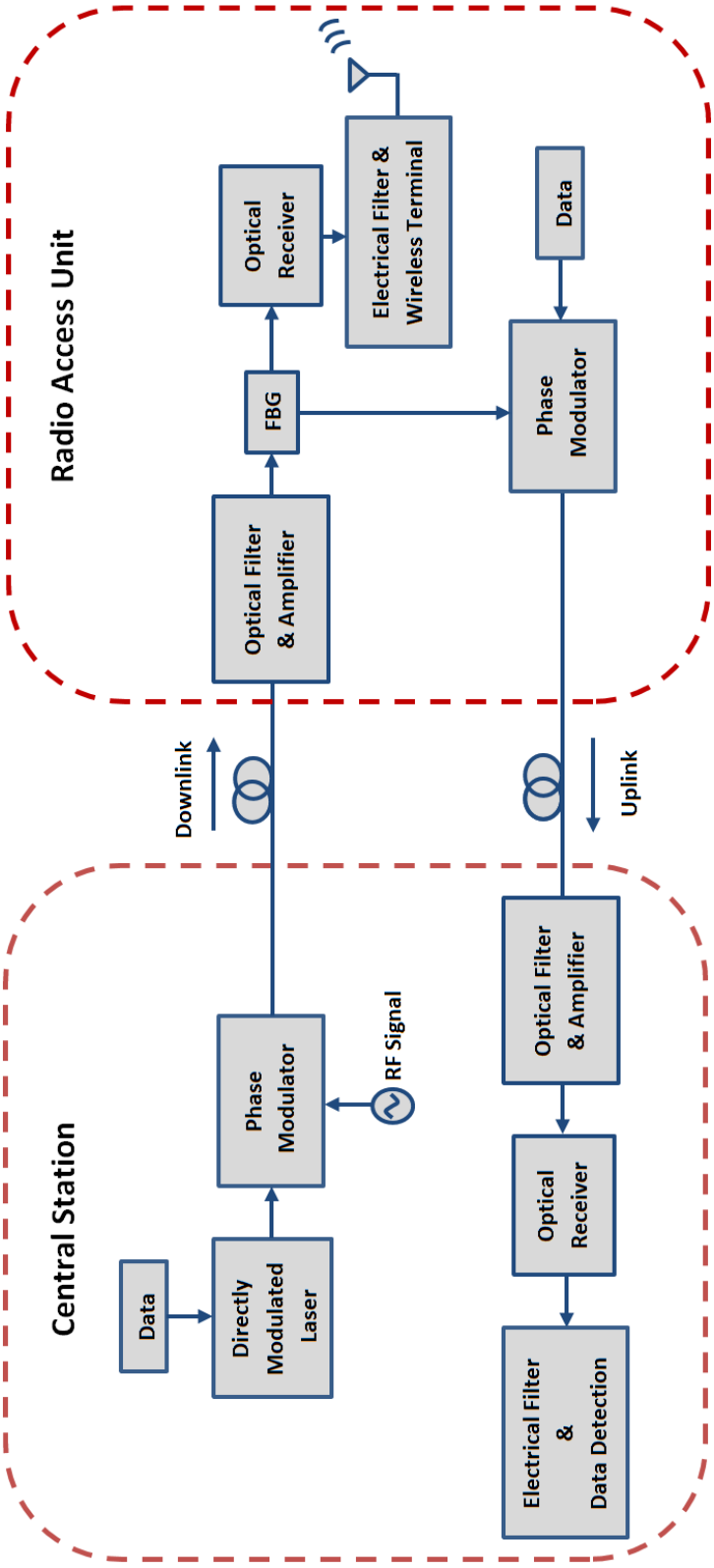

Figure 4.1 A block diagram of the full-duplex RoF with mm-wave photonic generation.

An optical modulation technology based on the phase modulator can generate such a high-quality mm-wave over fibre. Subsequently, an antenna is operated to transmit and receive the mm-wave wireless signal to and from the user terminal. In the uplink direction, after the detection process, the uplink signal is modulated by the optical carrier and then transmitted back to the CS through the optical fibre.

In this chapter, mm-wave generation and transmission over a fibre link based on SBS is proposed. The SBS effect has received significant attention among other fibre nonlinear effects, as has been explained previously in chapters 2 and 3. This transmission of mm-waves over RoF systems offers many advantages. Regarding which, scalability is the main issue that can be solved with mm-wave over fibre systems. Also, the transmission of mm-waves over fibre can offer enormous bandwidth because of the large available optical bandwidth, which can implement a massive increase in signal processing speed. Furthermore, mm-wave over optical fibre has low loss transmission which is very useful to distribute data transmission. This point made mm-waves with RoF technology a viable solution. Moreover, the system cost is reduced because the complicated and expensive equipment is set at the CS, while simpler, smaller and lighter remote antenna units are located at the BSs [149]. This configuration contributes to making the processes of installation and maintenance very easy. Also, a significant amount power can be saved due to the improved and simplified RAU. In 5G networks, this system can be integrated with optical access networks, to reap the benefit of the installed fibre. From another perspective, the centralisation of the network management is suitable for the analogue waves of mobile communication, because all of the computing process is placed in the central stations. This feature means the system complexity can also be simplified with the network arrangement. The use of an SBS fibre laser in these systems can enable dispersion of tolerant signal transport, while also supporting the optical encoding and wireless transmission of high data rate signals [54].

4.3 Simulation Setup and Results

The proposed architecture is built using Optisystem simulation tools to analyse and calculate the results of the system. The simulation results for the proposed scheme are presented and explained using this advanced optical simulation package, which virtually designs and tests the optical link properties in the physical layer of optical networks. This section investigates a full-duplex RoF system based on the simple photonic generation method of mm-waves proposed in chapter 3.

First, the simulation setup of the mm-waves generation method is explained and then, the simulation setup of the full-duplex RoF system for the mm-wave generation and transmission with data is presented.

4.3.1 Simulation Setup for mm-Wave Generation

The configuration of the mm-wave generation method with the simulation optical and electrical spectrum analyser results are shown in Figure 4.2. It is clear from the obtained simulation results that a mm-wave at a frequency of 64 GHz with a power of around 25 dBm has been successfully generated. This generation method is based on the proposed third mm-wave generation method, as explained in chapter 3.

In the simulation setup, a narrowband linewidth laser source (1 MHz linewidth) is used with 8 dBm power at a wavelength of 1550 nm. The continuous wave (CW) laser enters the phase modulator, which is driven by RF sinusoidal signals, having the parameters of 32 GHz frequency, and a phase of 90 degrees. After that, the modulated signals are propagated through the SMF with a sufficient amount of power to generate the Brillouin Stokes. Due to the applied appropriate laser power, First Order Brillouin Stokes (FOBS) are generated regarding the SBS effect in the fibre, where the Brillouin linewidth is set to 31.7 MHz with a frequency shift equal to 11 GHz.

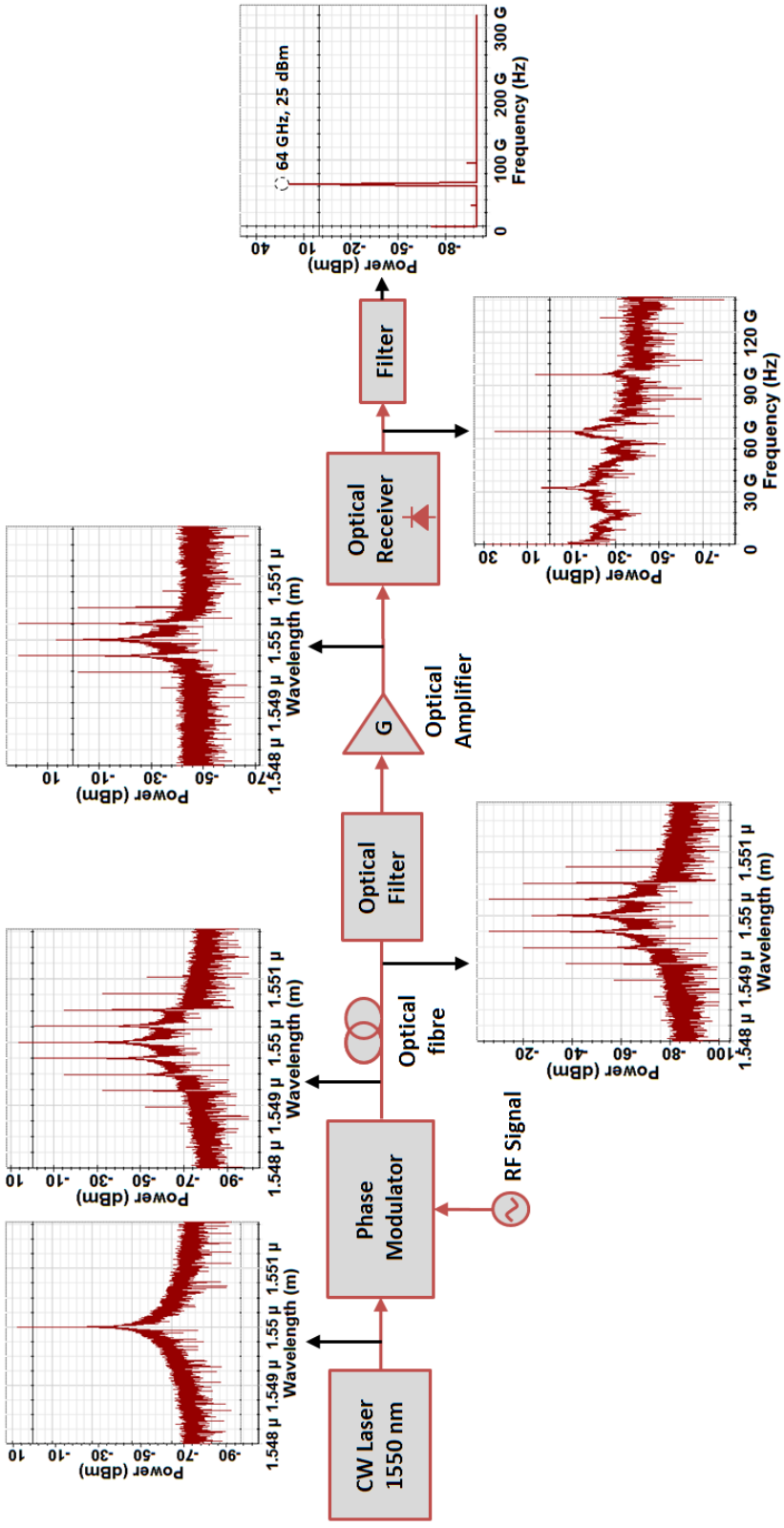

Figure 4.2 The simulation setup of the mm-wave generation method with the spectrum analyser results.

Then, these optical signals are amplified using the EDFA and heterodyned at the APD to generate mm-wave carriers, as explained in Figure 4.2. The obtained mm-wave carriers show good quality at different frequencies. Subsequently, these signals are filtered to obtain the 64 GHz mm-wave.

Due to the SBS effects in the mm-wave generation system, the optical power fluctuates, and this fluctuation will degrade the Q factor and the bit error rate of the optical communication system. This effect will limit the performance of the optical transmission system, and for this reason, the laser input power to the fibre should be kept at the Brillouin threshold. The maximum power transmitted through the fibre can apparently be impacted upon by this effect, which will limit the efficiency of the fibre laser. Figure 4.3 shows the optical input power transmitted through the fibre versus the Q factor, which is obtained by using the Optiwave simulation. The Q factor describes the system performance by suggesting the minimum SNR required to achieve specific BER. To consider the Brillouin scattering effect for mm-wave generation and to avoid the scattering limitations on system performance, the laser input power should be kept under control and should not reach the threshold amount. To specify the maximum amount of input laser power that provides a specific BER, the Q factor has been measured by the Optiwave simulation. So, figure 4.3 shows the simulation results when the input power versus the Q factor is varied, and the BER has been analysed for each amount of laser input power. This graph shows that the Q factor degrades sharply when the optical power is increased to more than 8 dBm. This graph means the Brillouin threshold for the setup is around 8 dBm, and the degradation of the Q factor begins after reaching this value. Due to this, increasing the laser power more than 8 dBm will affect the performance of the proposed system badly and degrade the Q factor.

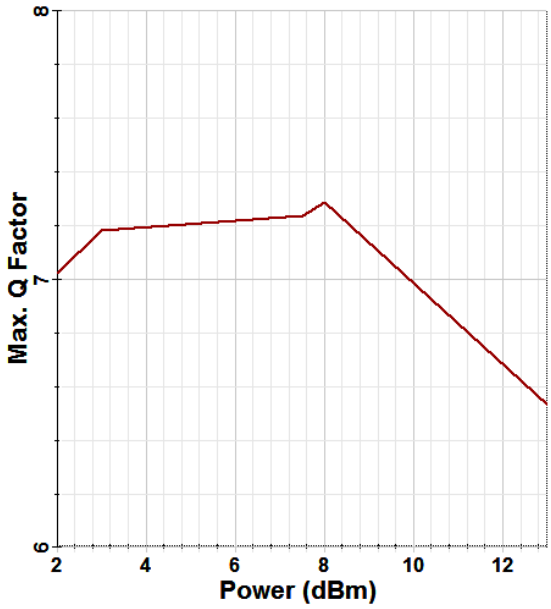

Figure 4.3 Optical power transmitted through the fibre versus the Q factor.

The use of the directly modulated laser has the option of increasing the linewidth of the laser source, but it can increase the dispersion penalty as well. To avoid this, the linewidth of the laser should be modified, which will decrease the SBS threshold power without increasing the dispersion penalty relating to the directly modulated laser. Figure 4.4 shows the relationship between the SBS threshold power and the fibre length for three different linewidths, which is calculated by equation (3.1), according to the simulation parameters. The SBS threshold decreases with an increase of the effective fibre length, but it has higher values when applying a higher laser linewidth. As the effect of SBS is involved in the Optiwave Design Software, the same parameters presented in chapter 3 (Table 3.1 and Table 3.2) are considered.

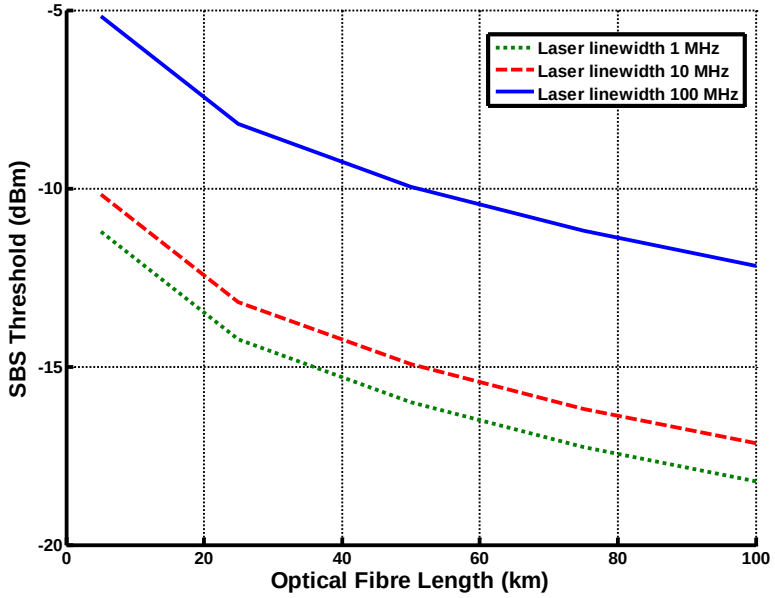

Figure 4.4 SBS threshold power versus fibre length for different laser linewidths.

4.3.2 Simulation Setup for mm-Waves over the Full-Duplex RoF System

With the aim of investigating the performance of the mm-wave generation and transmission with data over the full-duplex RoF system, the simulation setup in this section is first explained. By exploiting a single laser source and an FBG for wavelength reuse, a stable mm-wave RoF system is achieved, and the quality of the carriers is increased with a reduction in the fibre nonlinearity effects. The configuration of the full link of the mm-wave full-duplex RoF is shown in Figure 4.5. The spectrum analyser results in the simulation for each inset in Figure 4.5(a, b, c, d, e, f, g, h, and i) are presented in Figure 4.6(a, b, c, d, e, f, g, h, and i).

In the central station, a directly modulated CW laser source is used with 8 dBm power at 1550 nm and a 1 MHz linewidth. The amount of laser power is set to be at the Brillouin threshold to consider the effect of SBS inside the fibre. The directly modulated laser is driven electrically by the downlink binary data, represented by 5 Gbits/s pseudo-random bit sequences (PRBSs) with a word

length 2^{31}-1. In the Optiwave simulation, PRBSs is generated according to different operation modes. The bit sequence is designed to approximate the characteristics of random data. The directly modulated laser signal enters the phase modulator, which is driven by an RF sinusoidal signal with 32 GHz frequency, and a phase of 90 degrees. Then, the signals are injected into the 100 km SMF, as shown in Figure 4.5. The effects of the phase modulator are added to the proposed setup to improve the mm-wave generation method. Phase modulated signals are combined with the Brillouin Stokes of the SBS in the fibre laser. These signals are heterodyning at the APD and converted into an electrical signal to generate the 64 GHz mm-wave carrier.

The spectrum analyser results at the output of the phase modulator are shown at point (a) in Figure 4.6, while point (b) represents the optical spectrum of the amplified optical signal after propagating via the fibre and the optical filter. Point (c) in Figure 4.6 shows the output of the optical receiver, which is the mm-wave carrier after the electrical filter. These results reveal that the stimulated Brillouin Stokes have affected this generation method by using sufficient Brillouin pump power. As a result, this setup is based on combining the FOBS with the phase modulated signals over a fibre link to generate the mm-wave.

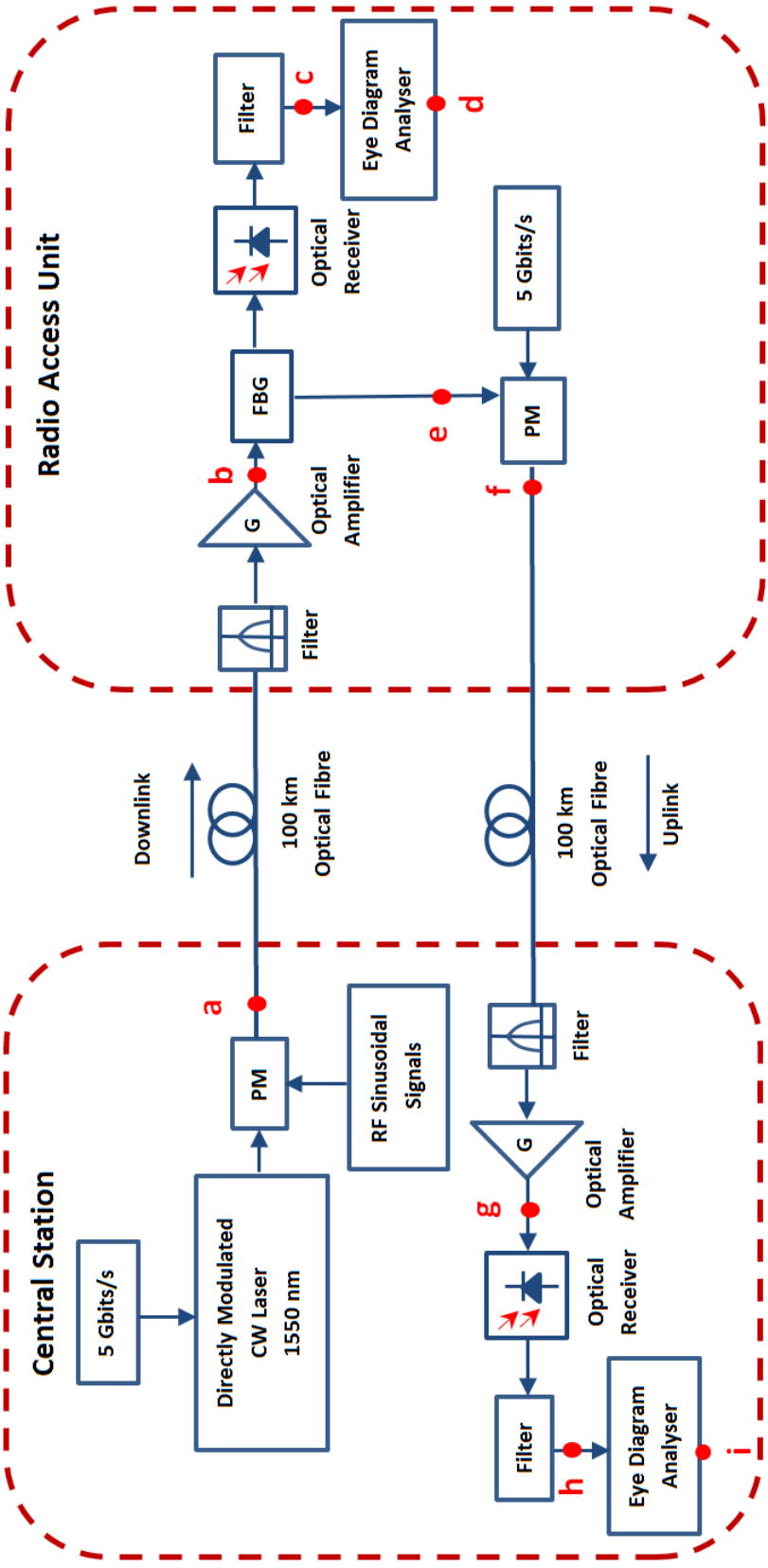

Figure 4.5 Simulation structure of the full-duplex mm-wave over fibre system.

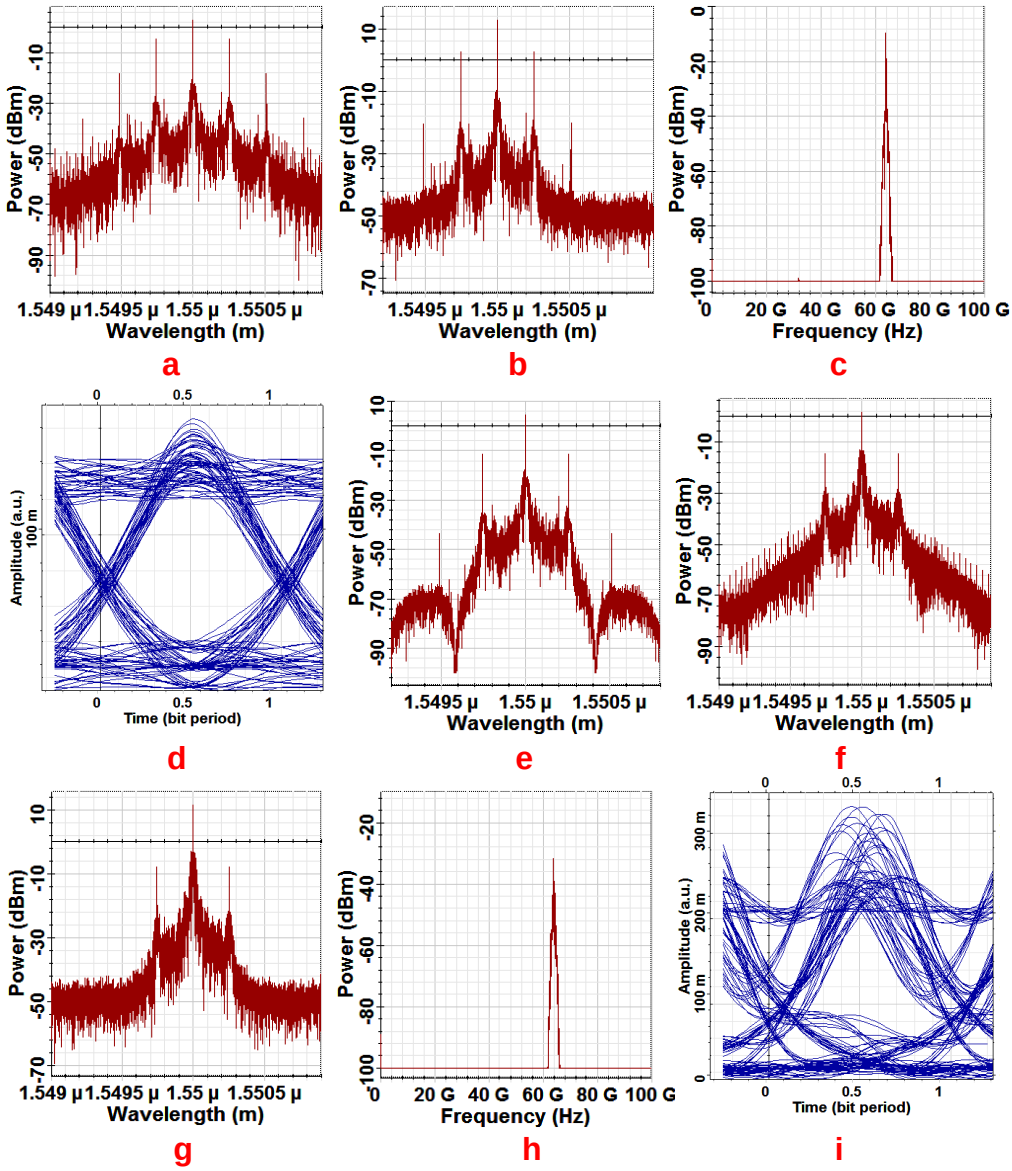

Figure 4.6 The analyser results at the corresponding points in Figure 4.5.

The generated mm-wave carrier is at frequency 64 GHz with good quality, as shown in Figure 4.7, with low noise power approximately equal to -75 dBm. Figure 4.6(d) shows an eye diagram for the RoF downlink, which demonstrates good performance, because the eye still keeps open clearly after the data (5Gbits/s) is transmitted with a 64 GHz mm-wave over a 100 km fibre link length. For the uplink signal, the FBG is used to abstract half of the optical carrier at 1550 nm. For the RoF uplink, the mm-wave wireless uplink data

signal is received by the antenna. Then, this signal is modulated on the optical carrier at 1550 nm via the phase modulator, as shown in Figure 4.6(f). This spectrum of the generated optical signal is transmitted back to the CS over the SMF. Subsequently, the optical signal is amplified, as shown in Figure 4.6(g) and is detected by the APD as in Figure 4.6(h). The eye diagram performance for the RoF uplink is shown in Figure 4.6(i) which is good, for the eye remains open after the uplink data (5Gbits/s) is transmitted with a 64 GHz mm-wave over a 100 km fibre with the wavelength reuse.

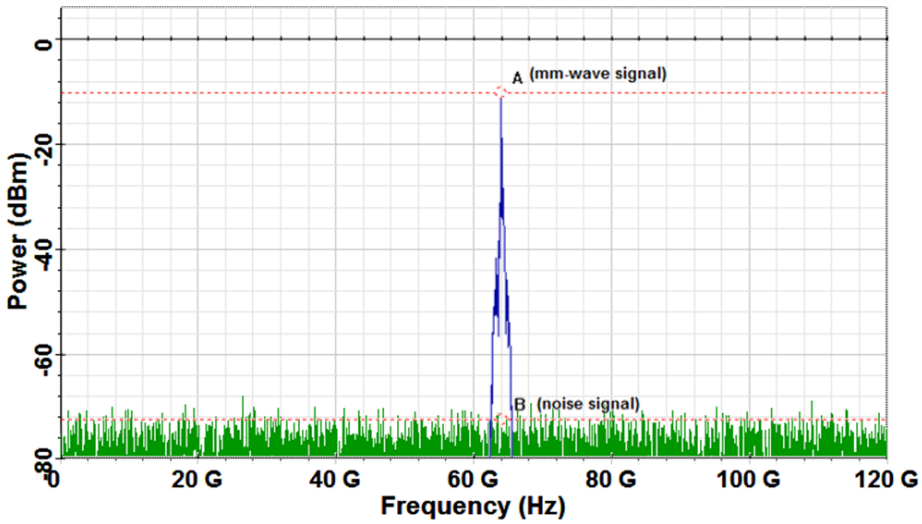

Figure 4.7 The 64 GHz mm-wave carrier with the noise signal.

4.4 System Performance Evaluation and Discussion

To evaluate the performance of the proposed system, a set of simulation results and analysis has been presented. Figure 4.8(a,b) shows the eye diagrams of the downlink and the uplink signals after transmission over different lengths of the fibre link. The results shown in this figure are presented along 20, 60, and 100 km. From these eye diagrams, it can be seen that with an increase in the fibre length, the opening of the eyes decreases, for it is also evident that the

eyelids become thick. This decrease is happened because of the degradation and the phase noise de-correlation of the optical tones.

However, after transmission over 100 km SMF, the eyes clearly look open, which indicates that good performance of both links (down and up) signals can be assured. In this point to improve the performance, the modulation depth should be improved by minimising the difference between the optical carrier and the data-bearing sideband by the FBG.

To calculate the link performance, a BER analyser is applied to the setup. The BER for two data rates, 5 Gbits/s and 7.5 Gbits/s, have been measured. Also, the BERs for both the downlink and the uplink data versus the received power along 100 km fibre link have been measured, as illustrated in Figure 4.9(a, b), respectively. By varying the amount of the input laser power, it can be seen that as the pump power from the laser source goes close to the threshold amount of SBS, the BER in the receiver increases. The reason behind this is that the previous onset of scattering threshold at the long fibre link. This comparison shows that for a data rate of 5 Gbits/s the perfect BER performance ($BER<10^{-9}$) for both downlink and uplink over a 100 km SMF transmission has been obtained. While in the case of the data rate of 7.5 Gbits/s, the performance of the BER seems poor over the long fibre link.

Further analysis has been carried out to evaluate the system performance with Figure 4.10(a,b) showing the BER performance of the downlink and the uplink along different fibre lengths. The tests were carried out with two transmission rates, 5 Gbits/s and 7.5 Gbits/s, along the fibre link from 25 km to 100 km. The nonlinear effects and the attenuation with dispersion were determined by standard industry values (i.e. dispersion of 16.75 ps/nm/km and an attenuation of 0.2 dB/km) to simulate the real environment as closely as possible. The results show the effect of increasing the fibre length on the amount of the received signal power, the losses of which increase when using longer fibre and so for a short fibre link, the data rate should be higher. The critical point in this design a mm-wave RoF system is specifying the maximum fibre length that can achieve a higher data rate with a good system performance.

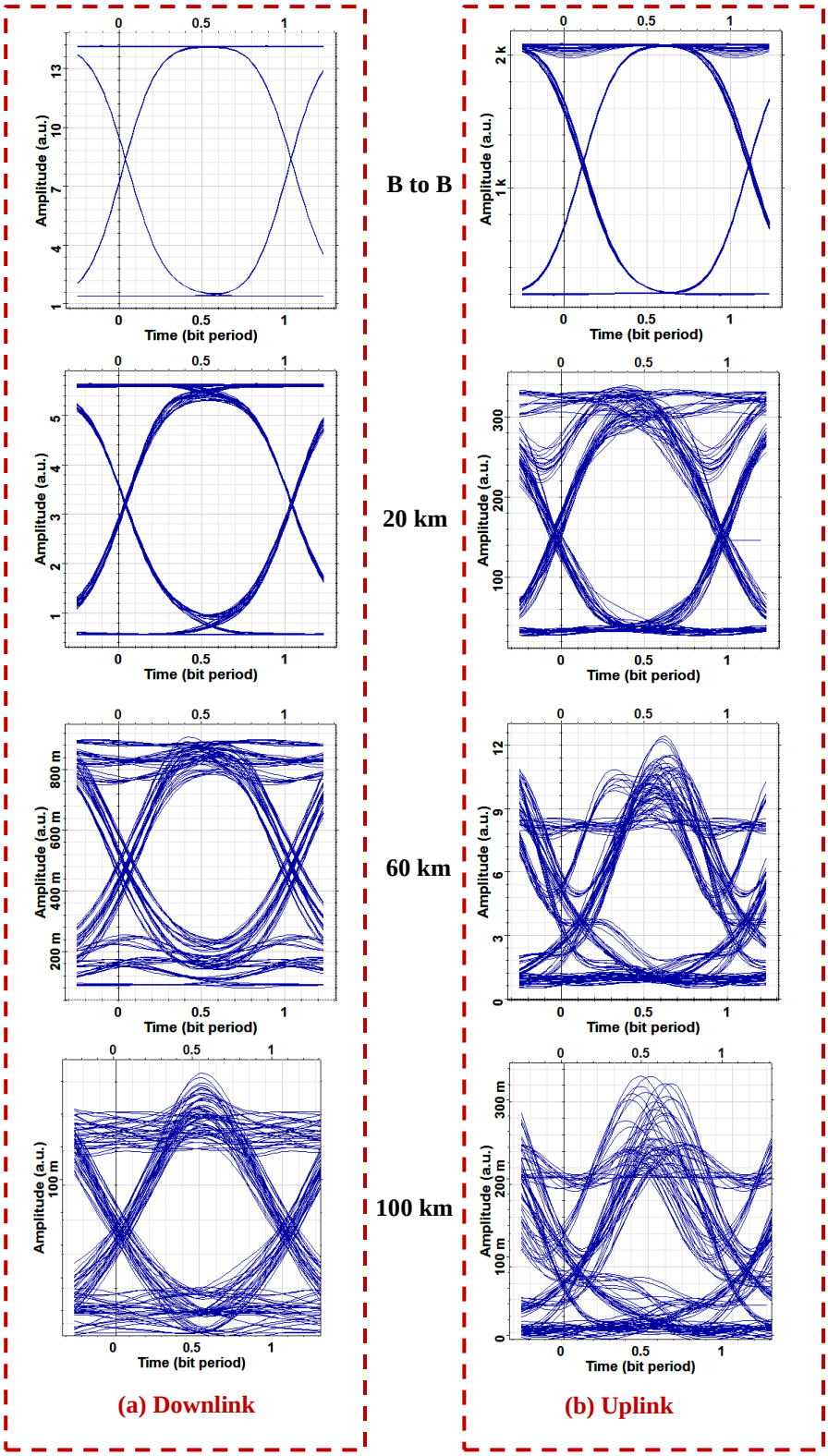

Figure 4.8 Eye diagrams with different transmission lengths along the SMF, for the downlink and the uplink.

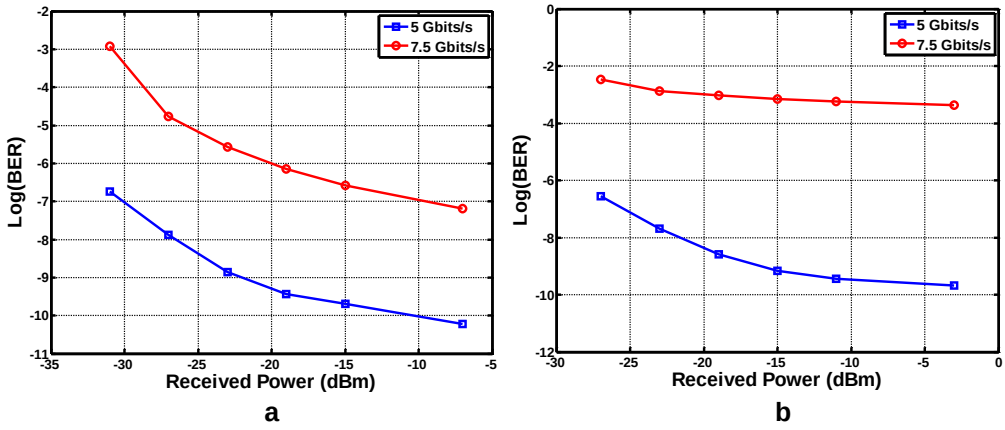

Figure 4.9 BER versus received power: (a) for the downlink (b) for the uplink.

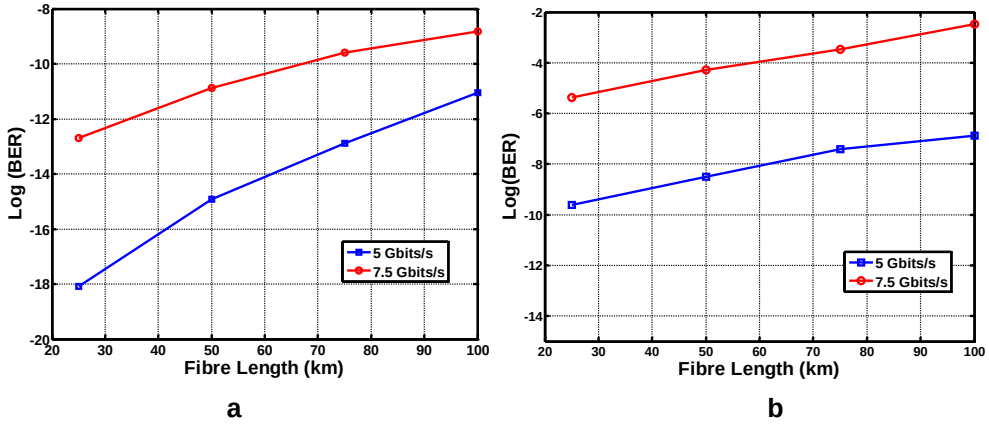

Figure 4.10 BER versus fibre length: (a) for the downlink (b) for the uplink.

4.5 Summary

In this chapter, a full-duplex RoF system for mm-wave photonic generation and transmission with data has been proposed and demonstrated using the Optiwave Design Software. In the proposed scheme, the transmission performance of the mm-wave over fibre which is generated using the phase modulation and SBS effect in the optical fibre has been investigated. A single

laser source is applied in the proposed setup, with an FBG being deployed for wavelength reuse for the uplink connection. This scheme will not only increase the stability and the quality of the generated 64 GHz mm-wave carrier frequency over the RoF system, for the fibre nonlinearity effects are also reduced, thereby generating a mm-wave that has a low noise power of less than -75 dBm. In the setup, the RAU structure is simplified, thus achieving a cost reduction for the system. For instance, the RAU does not need any laser source for the uplink optical carrier by using the FBG. The transmission performance of the full-duplex mm-wave RoF system has been investigated theoretically and verified by the Optisystem simulation.

Also, the simulation results have shown that the proposed system with a data rate of 5 Gbits/s for both the downlink and uplink can successfully reach a transmission distance up to 100 km over the SMF with a good agreement of the optical communication standards. Based on the obtained results, this system is recommended as a promising choice with a simple design setup for the future small cell networks. In sum, the proposed scheme has the potential to support the implementation of the mm-wave in wireless systems integrated with optical fibre link in 5G networks.

Chapter 5

Proposed mm-Wave over Hybrid Fibre/FSO Link

In this chapter, a hybrid Fibre/free-space optical (FSO) system is proposed for the generation and transmission of a 64 GHz millimetre wave (mm-wave). This system can serve as a potential solution for the fifth generation and beyond (5G+) communications to overcome the mm-wave wireless propagation obstacles, especially for the 60 GHz band, such as high path loss and high attenuation. In this chapter, a hybrid system is proposed, which provides an optical link capacity of 10 Gbits/s with an FSO transmission distance of up to 2 km. This new system offers a communication link with low latency (speed of light) and can cope with the problems of high path loss and the blockages effect that face mm-wave wireless propagation. Furthermore, this system will increase the network coverage area by transmitting mm-waves over an FSO link to the areas with natural obstacles where laying fibre cables is impossible. The proposed setup is validated via Optiwave Design Software and MATLAB simulation tools. This chapter also discusses the challenges that may face such a new system and presents some key ideas towards overcoming these.

5.1 Introduction

The next generation communication system promises to deliver high data rates of around 10 Gbits/s for mobile users due to the rapid growth in the use of smart devices and techniques [4, 145]. Providing such a high data rate for users should be ensured with a high QoS anytime and anywhere. As widely agreed, radio over fibre (RoF) has become a feasible technique to provide high capacity requirements for mobile communication systems [9, 54]. However, the bandwidth lack in the current wireless carriers has motivated considering

mm-wave frequencies for next generation communication networks [3, 149]. As explained earlier in this thesis, mm-waves with a RoF system can provide high-speed data transmission and can increase the network capacity by the wide available bandwidth at these frequencies. This integration between the optical fibre and mm-waves has encouraged the implementation of the mm-wave spectrum in the fifth generation (5G) cellular networks to cope with the enormous traffic growth [1, 15].

Whilst mm-wave frequencies are considered attractive for futuristic mobile networks, they have faced serious difficulties in outdoor applications. Unfortunately, mm-wave signals have significant wireless propagation losses [6, 117]. Some of mm-wave bands are appropriate for the application in the outdoor deployment, and others are not due to physical characteristics that vary with changing frequencies, as it is explained previously in chapter 1 (see Figure 1.2) [12, 13, 121]. Moreover, mm-waves are very sensitive to the effect of blockages, so the condition of the line of sight (LoS) propagation is considered a significant factor for these networks [98, 122].

In recent studies, overcoming mm-wave propagation losses has been tackled by using directional antennas with beamforming techniques [25]. These techniques are able to reach about 200 metres of mm-wave wireless transmission in outdoor urban areas [10, 14]. Hence, more fibre infrastructure needs to be added to enhance the network coverage area, but this, unfortunately, will lead to increase the latency and cost of the whole system.

Lately, the FSO system has received considerable attention due to its advantages, such as high security, flexibility, and rapid deployment time [76, 150]. In addition, FSO communication systems have received an interest due to the higher bandwidth and higher capacity in comparison with the traditional radio frequency wireless communication systems. Therefore, FSO technology is successfully utilised in the cognitive radio network based on an asymmetric RF/FSO communication system to increase its performance [151]. The FSO system is efficiently used for the transmission of high data rate between two fixed points over a long distance, instead of applying optical fibre cables [84,

152]. The wide optical bandwidth has allowed the obtaining of much higher data rates by using an FSO link. This system also has attracted the attention for solving the problem of the last mile coverage in remote areas or under disaster emergency [153]. The integration of fibre optic infrastructure with FSO could help in resolving these issues [79, 80]. The performance of the radio frequency with FSO systems has been studied recently by considering separate links. Some researchers have tried to combine RF wireless links and FSO links to improve system performance [75, 85, 82].

Despite the potential of the FSO system, it faces some challenges, and the transmitted optical signal is affected by various factors, as explained previously in chapter 2 [20, 83]. Recently, some literature has proposed different solutions to mitigate these affecting factors [21, 80, 82]. Consequently, RoF technology is considered a vital solution for mm-wave transmission through a fibre link to small cell networks. However, the deployment costs of the fibre, such as installation, digging, and obtaining laying permission, makes the placement of fibre impossible in some situations. On that account, proposing mm-waves over a hybrid Fibre/FSO system, as shown in Figure 5.1, for futuristic 5G+ communications can reduce the cost, enhance performance, and improve the coverage to the last mile.

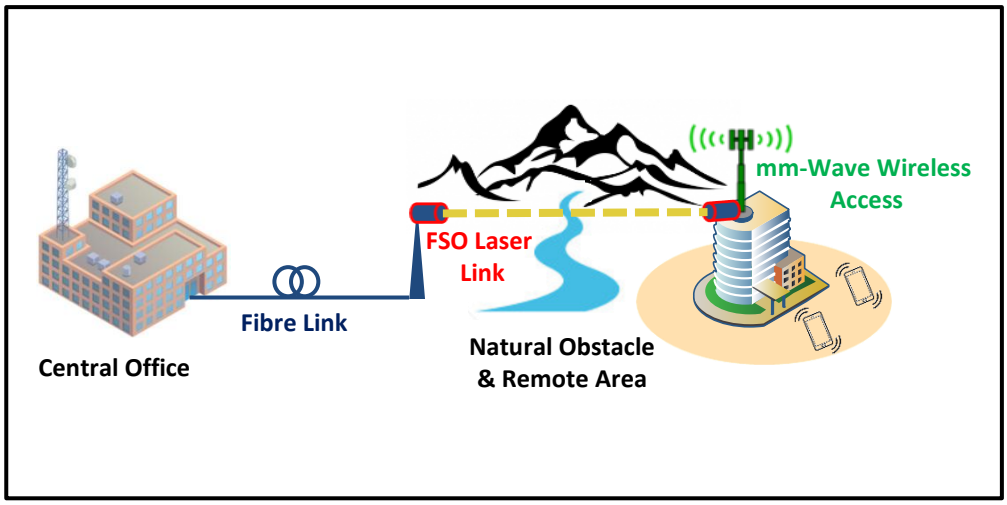

Figure 5.1 The proposed mm-wave over hybrid link for the last mile coverage.

In this chapter, a communications system is proposed that integrates the advantages of both mm-wave and FSO systems, such as free licence spectrum, low-cost system, and higher bandwidth carrier. The proposed system is based on the photonic generation and transmission of mm-waves over a hybrid Fibre/FSO laser link. Figure 5.2 explains the proposed idea of the hybrid Fibre/FSO link with the application of mm-waves. The main idea here, comes with the generating and transmitting of mm-waves optically over fibre, then transmitting mm-waves optically to the BS over the FSO link using laser light instead of mm-wave wireless propagation. Specifically, in this hybrid system, there are two options for mm-wave transmission link, which are fibre link and FSO link. So, fibre link can be used alone for the mm-wave generation and transmission, and if it is impossible laying the fibre cables in some areas like, historical places, areas with natural obstacles, and under emergency disasters, the fibre would be cut and the FSO link could be used instead for mm-wave transmission. The contribution is overcoming the obstacles related to mm-wave wireless propagation by proposing mm-waves over FSO instead and avoiding laying fibre cables to remote areas, which increases the latency, cost, and network complexity. Moreover, the performance of the proposed system has been evaluated and compared with mm-wave wireless propagation to verify the improvement achieved. Finally, latency reduction is also investigated in this work by reducing the fibre link length.

The rest of this chapter is organised as follows: Section 5.2 is a description of the proposed system architecture, whilst in section 5.3, simulation results are provided and discussed. The performance evaluation of the hybrid Fibre/FSO system is discussed in Section 5.4 and finally, Section 5.5 concludes the chapter.

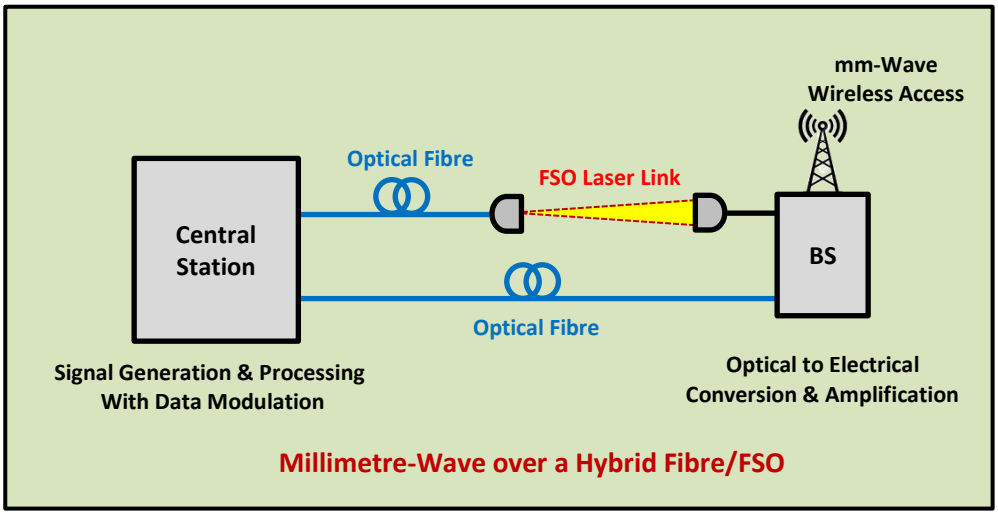

Figure 5.2 Illustration of the proposed mm-wave over the hybrid system.

5.2 Proposed System Architecture

The generation and transmission of a mm-wave over a hybrid Fibre/FSO communication system are proposed in this chapter. This hybrid system can overcome the limitations presented in mm-wave wireless transmission for long distances owing to the high path losses and blockages effects. In this section, the operating principle of the mm-wave generation and transmission over the hybrid Fibre/FSO system is explained, and evaluation of the system performance is discussed. Figure 5.3 contains a block diagram of the proposed system setup, which is built by using the Optisystem simulation tools.

The FSO laser channel and the mm-wave wireless channel have been explained previously in chapter 2, with details of the analytical models and mathematical equations. In this section, the system simulation design is explained with the generation process of a mm-wave over fibre. This generation process consists of a directly modulated continuous wave (CW) laser source working with a 1550 nm wavelength and 1 MHz linewidth. The laser is derived electrically by the downlink binary data signals, which are represented by 10 Gbits/s pseudo-random bit sequences (PRBSs).

Then, the laser signal enters a phase modulator, and an RF sinusoidal signal with 32 GHz frequency is used to drive this phase modulator. After that, the optical signals are launched and propagated through 10 km standard single mode fibre (SMF), which has a dispersion of about 16.75 (ps/nm.km) and an attenuation of about 0.2 dB/km.

The generation process of the mm-wave is based on recent work by this researcher, for which a cost-effective and straightforward mm-wave generation method was proposed, as in [64, 67]. So, a mm-wave generation model has previously been proposed based on SBS with a RoF system. The amount of the laser power needs to be set to 8 dBm, which is equal to the Brillouin threshold to consider the effect of SBS on the fibre, as explained previously in chapter 4. The effects of the phase modulator are added to the proposed setup to improve the mm-wave generation method.

Then, the optical signals, which are the phase modulated signals with the Brillouin Stokes, are filtered by an optical filter to ignore any unwanted sidebands to improve the results. After that, the filtered optical signals are transmitted through the FSO laser channel along a 2 km distance. The proposed FSO channel simulation parameters are summarised in Table 5.1.

On the receiver side, these optical signals are combined by the photo detector and converted into an electrical signal to generate a mm-wave carrier, which has a frequency equal to the frequency difference between the optical signals.

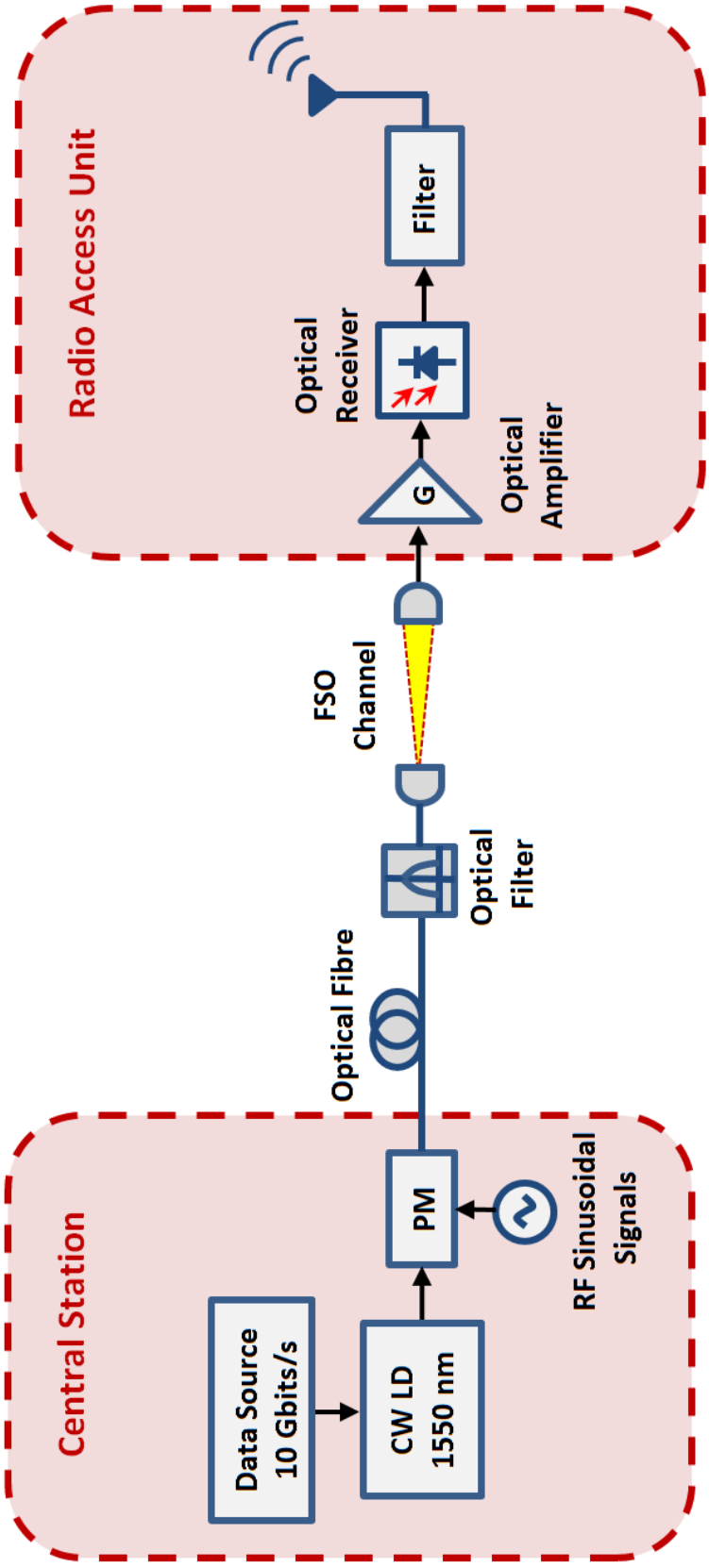

Figure 5.3 Simulation setup of the proposed hybrid Fibre/FSO system.

Table 5.1 FSO channel parameters

Parameter	Value	Unit
Laser wavelength	1550	nm
Range	2	km
Clear weather attenuation	10	dB/km
Heavy rain attenuation	20	dB/km
Moderate fog attenuation	30	dB/km
Index refraction structure	5×10^{-15}	$m^{2/3}$
Transmitter aperture diameter	5	cm
Receiver aperture diameter	25	cm
Beam divergence	0.25	mrad
Transmitter loss	2	dB
Receiver loss	2	dB
Receiver sensitivity	-20	dBm

5.3 Simulation Results and Discussion

In this chapter, the performance of mm-wave transmission over the hybrid Fibre/FSO laser link is investigated. First, the mm-wave transmission through the FSO laser channel has been examined. Then, the effect of the FSO link length on the power of the generated mm-wave has been studied. Figure 5.4 shows the generated mm-wave (64 GHz), which has been transmitted over a 10 km fibre with two different FSO link lengths (1 km, and 2 km). This figure represents the power of the mm-wave signal versus its frequency. It can be seen that there is a decrease in the power of the generated mm-wave with the 2 km FSO link. The atmospheric attenuation reduces the FSO laser power, and this reduction becomes greater as the FSO link length increases. The decrease in the laser power, which is received optically, will affect the power of the generated mm-wave accordingly. Despite the mm-wave power in the 2 km link

being lower than at 1 km by approximately 20 dB, simulation results with the BER analyser show that it still has acceptable performance, for the BER is equal to 2.7×10^{-10} and the Q factor about 6.2. The best performance of the mm-wave as a carrier was achieved with a 1 km FSO link length, with a BER equal to 1.5×10^{-13} and a Q factor of about 7.

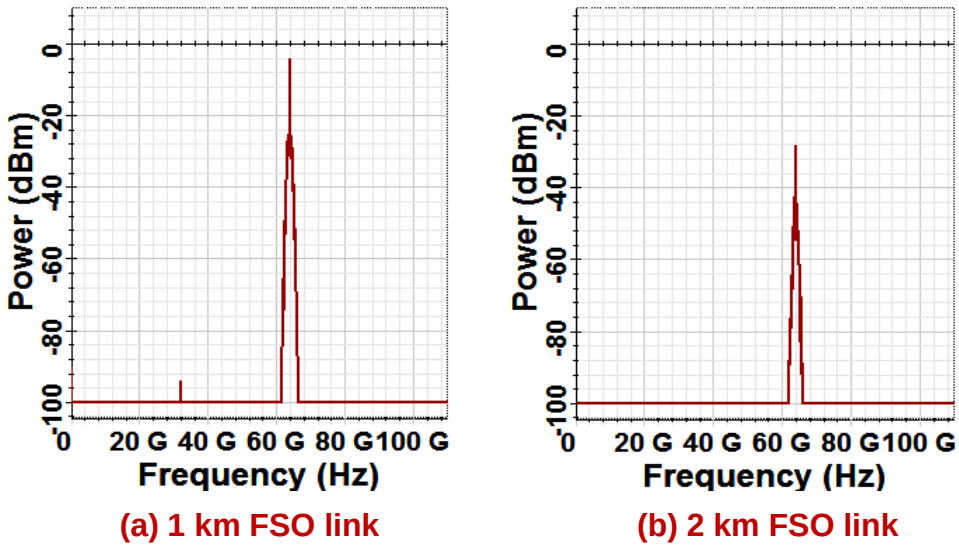

Figure 5.4 The generated mm-waves with different FSO link lengths.

To examine the effect of the fibre link on the overall system, different fibre lengths (1, 10, and 15 km) have been applied. Figure 5.5 shows the eye diagrams of the downlink signals after considering the transmission over different fibre lengths with a 1 km FSO laser link. From these eye diagrams, it can be seen that an increase in the fibre length will lead to a decrease in the opening of the eye. It can also be seen that the eyelids become thick with a 15 km fibre link. This loss happens because of the degradation and the phase noise de-correlation of the optical tones. From these results, the fibre losses can be observed very clearly by increasing the length of the fibre link distance. Moreover, increasing the fibre length will also affect the latency, which is

directly proportional to this length. A significant advantage of applying the FSO link is achieving a low latency link. The transmission of mm-waves over fibre for long distances will increase the latency of the mm-wave network, whilst the applied FSO laser link provides mm-wave transmission at the speed of light. For 5G and beyond communication systems, less than 1 ms of latency is needed, and this can easily be verified by using the FSO laser link.

The proposed hybrid system has been compared with a recent study in [143], in relation to improving mm-wave wireless transmission and providing an efficient optical link. This comparison shows the feasibility of the proposed work in enabling a mm-wave communication link with good performance. The distance of the mm-wave transmission over the proposed FSO link has been improved to reach more than 1 km, while in the research presented in [143], mm-wave wireless transmission could not be more than a few metres.

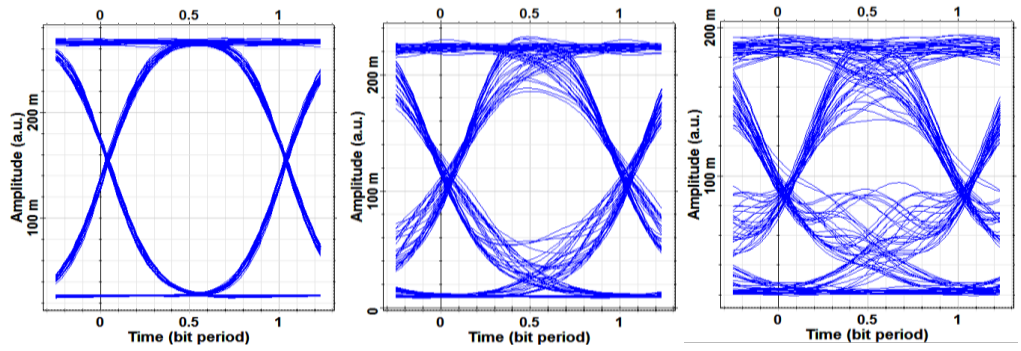

Figure 5.5 Eye diagrams for the transmission along different fibre lengths (1, 10, and 15 km) and a 1 km FSO laser link.

The performance of the mm-wave over an FSO link has also been investigated considering different atmospheric phenomenon, which can be highly variable depending on the different areas and seasons, whereby there can be clear weather, rain, fog etc. These atmospheric conditions will increase the laser optical attenuation and distortion. Hence, the FSO link availability has been examined and the mm-wave received power has been measured along the laser

FSO link under different attenuation coefficients. Figure 5.6 presents the measured log BER versus the mm-wave received power using the Optiwave simulation tools. To calculate the FSO link performance, the BERs have been measured with varying the amount of the laser attenuation coefficient between 5-30 dB/km for different weather conditions (clear, rain, and fog). The received power of the mm-wave has been measured along the 1 km FSO link.

This comparative result shows that the perfect BER performance (BER<10^{-9}) has been obtained by considering a low attenuation coefficient and a short FSO link length. While in the case of a higher attenuation coefficient and long link, the performance of the BER would appear to be poor over the FSO link. This result indicates that the mm-wave performance over an FSO laser link can be very weak under difficult weather conditions, like dense fog or smoke, when the laser attenuation coefficient could reach more than 200 dB/km.

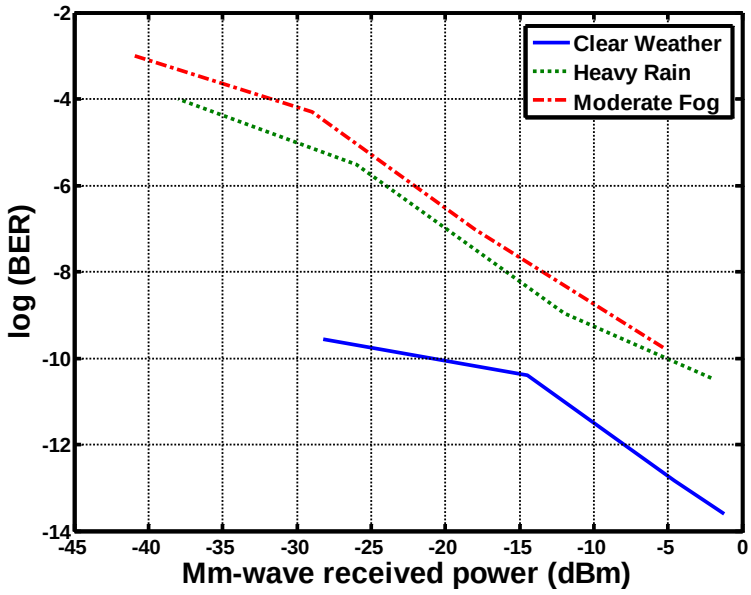

Figure 5.6 BER versus mm-wave received power for different attenuation coefficients of an FSO laser link.

Moreover, the mm-wave wireless transmission as an RF carrier is compared with the performance of this transmission over the FSO laser link in the proposed design. The received electrical power of mm-waves over FSO link is compared with the received power in the case of mm-wave that wirelessly transmitted through a directional antenna. The power of the mm-wave received over the FSO laser link is measured by the Optisystem simulation tool using an electrical power meter, which is set after the optical receiver. While the received power of the mm-wave (P_{rmm}), which is assumed to be transmitted wirelessly with the LoS path condition, is calculated by equation (2.9) using a MATLAB simulation environment. All mm-wave wireless channel simulation parameters are summarised in Table 5.2, which are based on some of the latest research [3, 14, 98].

Figure 5.7 shows a comparison between the received powers for each of mm-wave wireless link and mm-wave over the FSO laser link along a 1 km transmission range. The received power of mm-wave over FSO link, which is measured by using the electrical power metre components in the Optiwave simulation along the FSO link, is considered under clear weather conditions (i.e. 10 dB/km atmospheric attenuation). From this figure, it can be seen that the received power of the mm-wave transmitted over the FSO laser link is higher than that transmitted wirelessly by approximately 120 dB with considering clear weather situation. This enhancement in mm-wave power demonstrates the advantage of using an FSO link for transmitting mm-waves to reduce the higher propagation losses in wireless transmission especially with good weather conditions. The mm-wave band around 60 GHz frequencies has the highest attenuation losses in the atmosphere when compared with other mm-wave bands, because its resonance frequency is very close to the oxygen molecule [97]. As a result, the proposed system of transmitting 64 GHz mm-wave over FSO link will solve this issue of overcoming the wireless path losses. In addition, in remote areas or areas with natural obstacles that make it impossible to lay optical fibre cables, the need to apply an FSO laser link is a matter of urgency. The mm-wave over an FSO link will offer a satisfactory

solution to provide a high capacity connection, as will be discussed in the next section.

Table 5.2 mm-Wave wireless channel parameters

Parameter	Value	Unit
mm-Wave frequency	64	GHz
Transmitted power	30	dBm
Antenna gain	25	dBi
LoS path loss exponent	2	dB
LoS shadow fading	5.8	dB

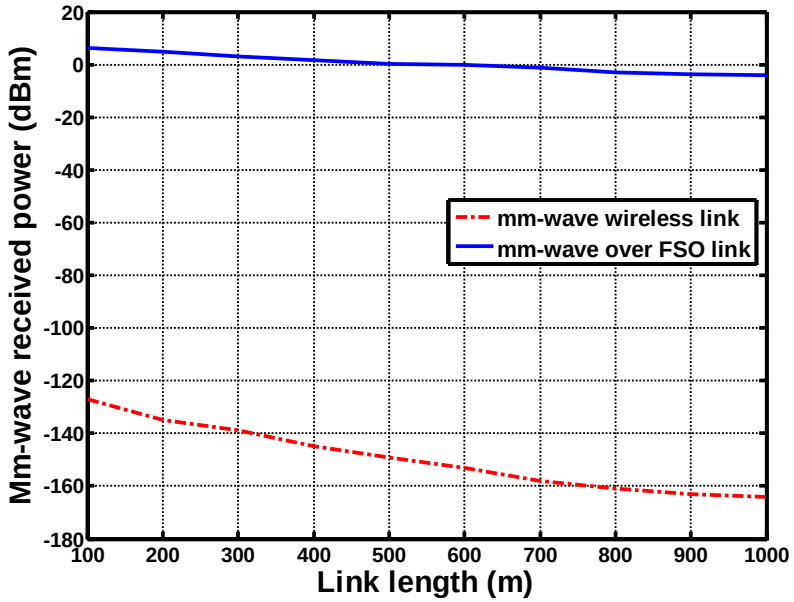

Figure 5.7 Received powers comparison versus transmission length.

5.4 Performance Evaluation of the Hybrid System

The performance of the proposed hybrid Fibre/FSO system for mm-wave generation and transmission demonstrates the importance of applying this new system in futuristic 5G+ communications. In this section, the received power of the FSO laser link has been calculated theoretically by applying equation (2.4). The result is then compared with the measured received laser power by the Optisystem simulation tool using an optical power meter component, which has been deployed after the FSO channel component. Figure 5.8 shows a comparison between the theoretical and simulation received laser FSO power regarding link length. The theoretical curve in the figure has been calculated by using equation (2.4), which calculated the ideal amount of the received power of FSO signal. While the other curve has presented the results obtained from the Optiwave simulation with considering more parameters, which add more realistic considerations about the performance of the FSO link and the amount of the received FSO signal power. Due to this, from this figure, it can be seen that the Optiwave simulation laser power amount, which is measured by the optical meter, is slightly less than the theoretical one amount that calculated by equation (2.4). This slight difference happens typically due to the added measured losses in the Optiwave simulation components that cannot be estimated theoretically by equations.

A significant advantage of using the FSO laser link is the high data rate. Regarding this contribution, transmission of mm-waves with data rate 10 Gbits/s over the hybrid Fibre/FSO link has been achieved successively. To study the performance of the laser FSO link with high data transmission, the predicted capacity of the laser link has been calculated. Figure 5.9 shows the estimated data rate versus the link range, which is calculated by equation (2.6) and, represents a general prediction from the mathematical calculation. The performance of the FSO link has been evaluated with different attenuation coefficient values (5-30 dB/km) to calculate the possible data rate achieved. As appears in this figure, the laser link can provide about a Terabit/s (10^{12} bits/s)

data rate with a 2 km link length in the case of clear weather (attenuation 10 dB/km). Such a high bit rate is necessary for the application of futuristic 5G+ networks [154]. While for a link range of about 1 km with a higher attenuation, the data rate is still in the range of Gigabit/s (10^9 bits/s). It is also observed that when the attenuation increases to 30 dB/km (moderate or heavy fog), the data rate decreases below the acceptable amount of BER for a long link. Hence, weather conditions are considered a challenging issue with an FSO laser link in terms of providing high data rate connectivity.

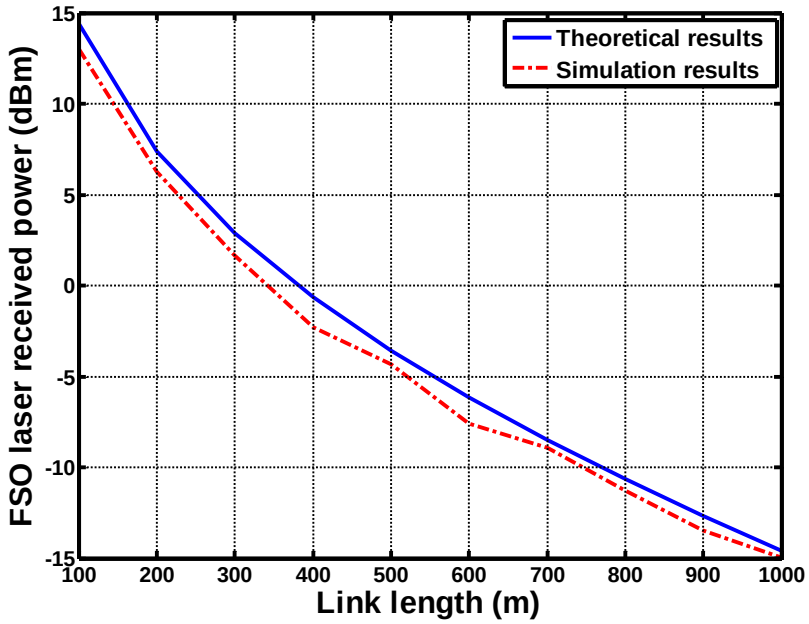

Figure 5.8 Theoretical and simulation FSO laser received power comparison according to transmission length.

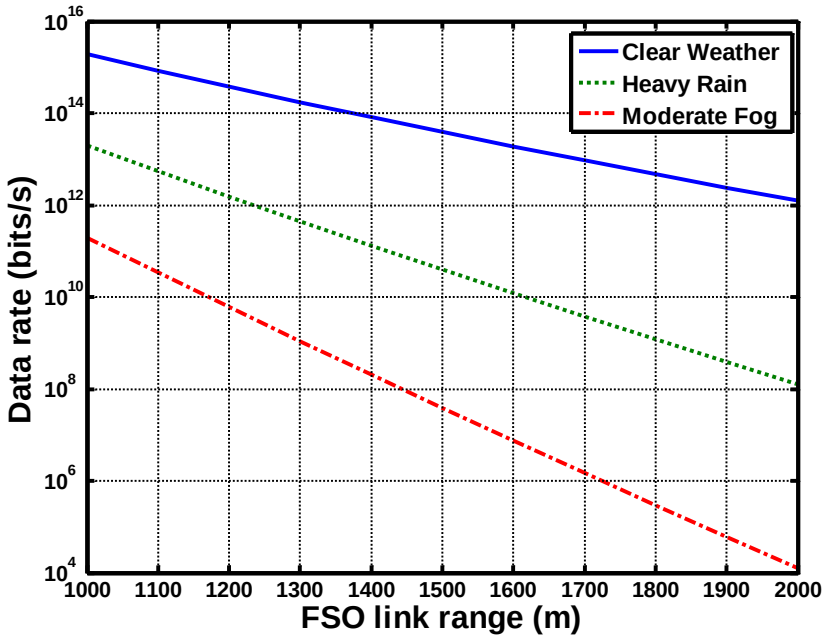

Figure 5.9 The estimated data rate of the FSO laser link versus the link range.

Also, the link margin value has been investigated to show how much the margin range of the proposed system to be able for compensating different FSO link losses. The FSO link margin can be calculated by the equation (2.5), which represents a general prediction from the mathematical calculation. Figure 5.10 shows the estimated link margin versus the FSO link range for achieving the available data rate of 10 Gbits/s with different weather conditions. As seen in this figure, link margin values of 77, 56, and 37 dB are available at an altitude of 2 km for the different attenuation amounts of 10, 20, and 30 dB/km respectively. So, the FSO link will provide successful transmission for the mm-waves with a data rate of about 10 Gbits/s up to 2 km, and this finding supports the proposed hybrid system, by validating the possibility of transmitting the mm-wave with a high data rate.

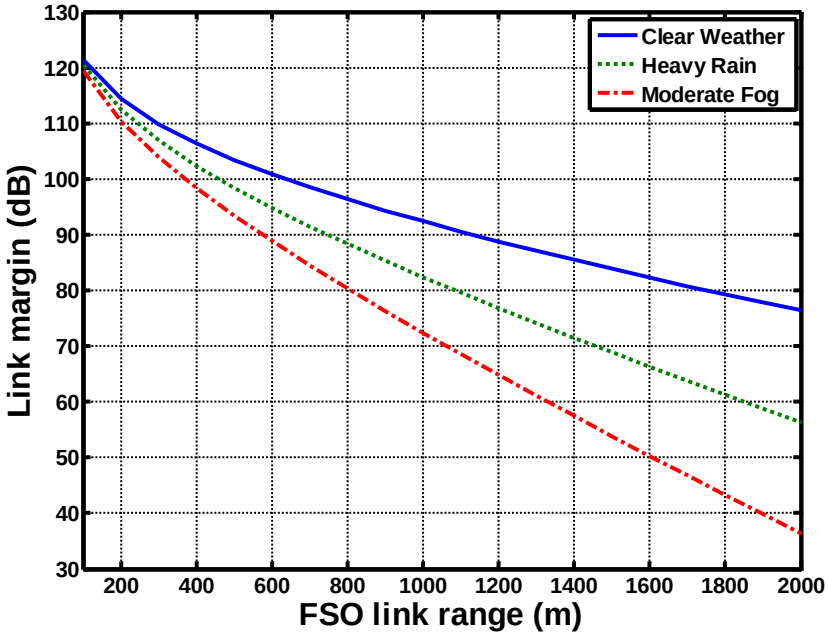

Figure 5.10 The estimated link margin versus FSO link range.

As discussed previously in this chapter, the proposed hybrid Fibre/FSO system for mm-wave generation and transmission is considerably affected by the weather conditions. To solve this issue, it is crucial to adjust the laser transmitted power based on the weather conditions (clear, rain, or fog) in the specified deployment areas. Also, other relevant parameters, such as the FSO laser link divergence angle and link distance should be considered based on the area's environment to verify whether a high QoS communication link is possible.

5.5 Summary

In this chapter, a proposed hybrid Fibre/FSO communication system for mm-wave generation and transmission has been presented. This proposed system enables the reach of mm-waves over the FSO link to the remote areas, where

laying fibre cables is not possible. Also, this new system can provide mm-wave transmission over a high capacity link with latency reduction by decreasing the fibre link length and applying an FSO link instead. The obtained results have shown the successful generation and transmission of a 64 GHz mm-wave over the hybrid Fibre/FSO link with excellent BER equal to 1.5×10^{-13} and a Q factor of about 7.1. Moreover, the performance of the proposed system has been evaluated and compared with mm-wave wireless propagation to address the achieved improvement by using the FSO laser link. The results have shown the availability of transmitting mm-wave over a 2 km FSO link with a stable received signal power in contrast high path losses from mm-wave wireless propagation. Finally, this hybrid system will not only support the requirements of 5G and beyond, such as high bandwidth, low latency, and last-mile coverage area, for it can also be used as a vital solution under emergency disaster conditions.

Chapter 6

Investigation of mm-Wave Wireless Propagation

In this chapter, a comprehensive study of mm-wave wireless propagation is presented. Specifically, the propagation performance of different mm-wave bands of 28, 60, and 73 GHz is investigated and compared with the ultra-high frequency (UHF) 2.4 GHz by evaluating the coverage and rate trends. This investigation is essential for enhancing futuristic cellular networks. The proposed scenario involves applying a map-based model for the deployment of BSs on Brunel University's London campus as an urban area. Different densities of BSs with a random distribution of users in an outdoor environment are considered. A user's association with the BS is based on the strongest received power, while the path loss models are determined by the blockage of the actual buildings' locations within the real campus map. MATLAB Simulation results show that dense deployment of BSs would improve the coverage of all mm-wave frequency bands and will also offer limited noise networks. Comparative results demonstrate that the 73 GHz mm-wave bands will provide good network coverage with the lowest interference effects and the higher data transmission rate is due to the large available bandwidth.

6.1 Introduction

The significant development of cellular networks has led to extensive research on the application of mm-wave frequencies. The growing capacity demand is one of the biggest challenges that faces next generation networks, while mm-wave spectrum has an available wide bandwidth higher than all the current cellular wireless networks [93, 149, 155]. The use of the new mm-wave bands for indoor and outdoor wireless propagation will improve the capacity of the

network [114]. In addition, the integration of mm-waves with the advanced antenna techniques will improve communication systems by applying beamforming and MIMO [14, 117, 119].

A 5G network needs to provide high data rate connectivity for users anytime and anywhere and achieving this will ensure a high QoS [13, 92]. Therefore, using mm-wave wireless links will meet 5G demands, because it could achieve data rates around a multi Gbits/s [6]. While mm-wave frequencies have been considered attractive for indoor applications, mm-waves have faced a serious obstacle in outdoor ones, that of large propagation losses [99, 149]. The physical characteristics of mm-wave propagation vary with changing frequencies [7], which ensures that the successful application of a mm-wave band in a 5G wireless network will mainly depend on the characteristics of that band [6]. It is well-known that mm-waves are very sensitive to the effects of blockage and shadowing, which are considered the main obstacles that face their wireless transmission [121]. Specifically, blockage effects represent the major reason for an increase in mm-wave path losses. The mm-wave signal power decreases due to the reflection and diffraction of mm-waves with building walls or the ground in the environment [24, 149]. Hence, the condition of the non-line of sight (NLoS) is considered a significant factor in all mm-wave bands propagation [149]. So, researchers have focused on studying the blockages model for urban areas by using curve fitting techniques to derive NLoS approximations [98, 112].

Recently, researchers have started to deal with overcoming mm-waves' significant propagation losses by utilising directional antennas with beamforming [13, 26, 92, 116]. These investigations have led reaching up to 200 metres of transmission range in wireless mm-wave propagation for outdoor areas. Some of the latest studies have suggested employing high gain antennas with narrow beams in dense mm-wave cellular networks to ensure the potential of achieving real improvement in data rates [14, 92]. In addition, mm-wave applications for 5G cellular technologies will be supported by manufacturing low-cost mm-wave chips [122, 156].

In this chapter, mm-wave wireless propagation is investigated by an analytical scenario of BSs deployment. The application of the underutilised mm-wave for different spectrum bands is analysed in comparison to the current 4G cellular networks, as found in recent work by this researcher [129]. So, the performance of different mm-wave bands (28, 60, and 73 GHz) propagation as a 5G cellular network is investigated by comparing the coverage and rate trends with UHF (2.4 GHz). The impact of this analytical study is specifying which band among the mm-wave spectrum will achieve a significant increase in the network capacity with good coverage. The proposed scenario involves simulating a real campus map of Brunel University London, as a map-based model to calculate precisely the effect of building blockages. Figure 6.1 shows the area of interest, which is considered in the simulation of this chapter. Accordingly, this study takes into consideration different densities of BSs and users in the outdoor application area. The simulation results pertain to analytical comparisons between mm-wave bands and UHF performances based on calculating the coverage and data transmission rate for each frequency band as a standalone cellular network.

The rest of this chapter is organised as follows: Section 6.2 contains a description of the proposed BSs deployment scenario. In section 6.3, the analytical model and the mathematical analysis are explained. Section 6.4 includes the simulation results and comparisons discussion, whilst Section 6.5 concludes the chapter.

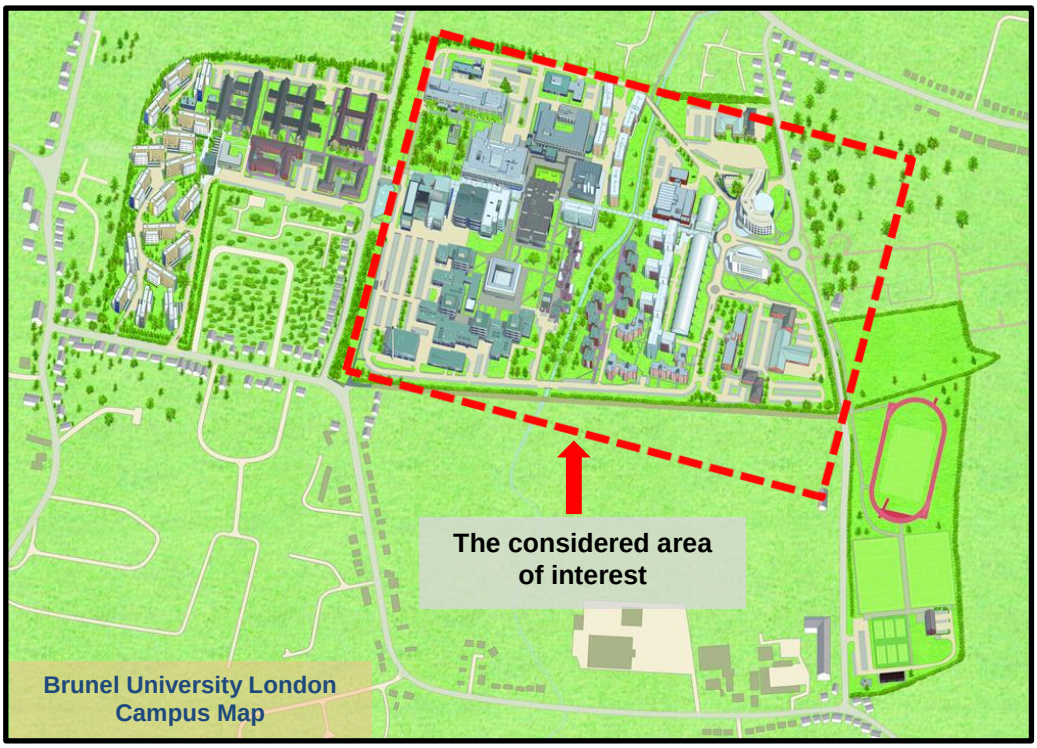

Figure 6.1 The considered area of interest.

6.2 The Proposed BSs Deployment Scenario

The mm-wave propagation depends highly on its physical nature and transmission mechanism. The attenuation and distortion of the mm-wave band are critically affected by the deployment of the BSs and the frequency of that band. As explained previously in chapter 2, some other impacting factors relate to atmospheric effects, like the absorption of oxygen and water vapour as well as fog and rain. Penetration loss is another factor in mm-wave propagation, which is considered the leading cause of reflection and multipath propagation. In addition, the penetration loss is affected by the building wall roughness [99]. Recently, mm-wave outdoor coverage has been considered as an essential research topic when studying multipath propagation [2, 10]. Also, investigation of utilising mm-waves in mobile communication is seen a significant issue for LoS or NLoS conditions [27]. Recent outdoor scenarios have concerned

emergency cases, such as high rate hot spots. These mm-wave hot spots can cover a few tens of metres in areas like parking or suburban places [2].

Proposing a deployment scenario able to provide a higher data rate with a less number of mm-wave BSs is considered very necessary to reduce the cost and complexity of the network. According to Friis Law [93], mm-wave carriers have very high propagation losses due to the high frequencies. Also, the mm-wave signal is highly affected by shadowing and blockage effects, because of low penetration capability and high directivity. To address this, an LoS link has been considered as being very significant in the deployment of mm-wave BSs to eliminate the propagation losses, which are caused by blockages, such as diffraction, scattering, and reflection.

In this chapter, as aforementioned, a scenario for the deployment of BSs on Brunel University's London campus is proposed based on the campus map and real buildings' locations. When applying this scenario, a comprehensive comparison between different mm-wave band networks is presented with the evaluation of users' received power for each. This scenario will be implemented for all frequencies as a standalone network to calculate the coverage in the university campus area. The proposed scenario is based on considering the specified rectangular area of about (600 m × 500 m) divided into 30 virtual zones covered by BSs working together. The shadowing and blockage effects have been calculated for each virtual zone by programming the real buildings' locations using MATLAB simulation tools. Then, the path loss model has been specified with LoS and NLoS link conditions based on the simulation analysis.

Two deployment densities of BSs have been applied in this scenario. In the first, the deployment of 6 BSs has been assumed, while in the second, the number of the BSs has been increased to 12 for improving the coverage by decreasing the mm-wave cell size. The locations of the BSs have been assumed on the buildings' roof-tops by choosing the best that allows for achieving the highest probability of LoS communication links. The proposed MATLAB simulation calculations are presented in Figure 6.2, which shows the flowchart

of the steps used in this simulation study. Figure 6.3 shows the virtual zones division as a red grid of the google map view of the university's campus with the deployment of 6 BSs. In this figure, the specification method of LoS and NLoS links is explained as well by zooming in on one of the virtual zones. Each virtual zone has four numbered edges, as in Figure 6.3, and the possible outdoor links for each zone have been simulated to ensure the accurate calculation of path loss with the LoS and NLoS conditions. While Figure 6.4 shows the deployment of 12 BSs in the specified area. Different users' densities are also applied in this scenario, with random distribution in the specified area. The distribution of 500 and 1000 users/km^2 has been investigated to calculate the rate coverage trends as an urban area. The process of user association with the BS depends on the strength of the signal that the user can receive. While the other BSs that exist in the considered area, are assumed to be interferers. Each user is allowed to connect with any BS, which means an open access association has been assumed for all.

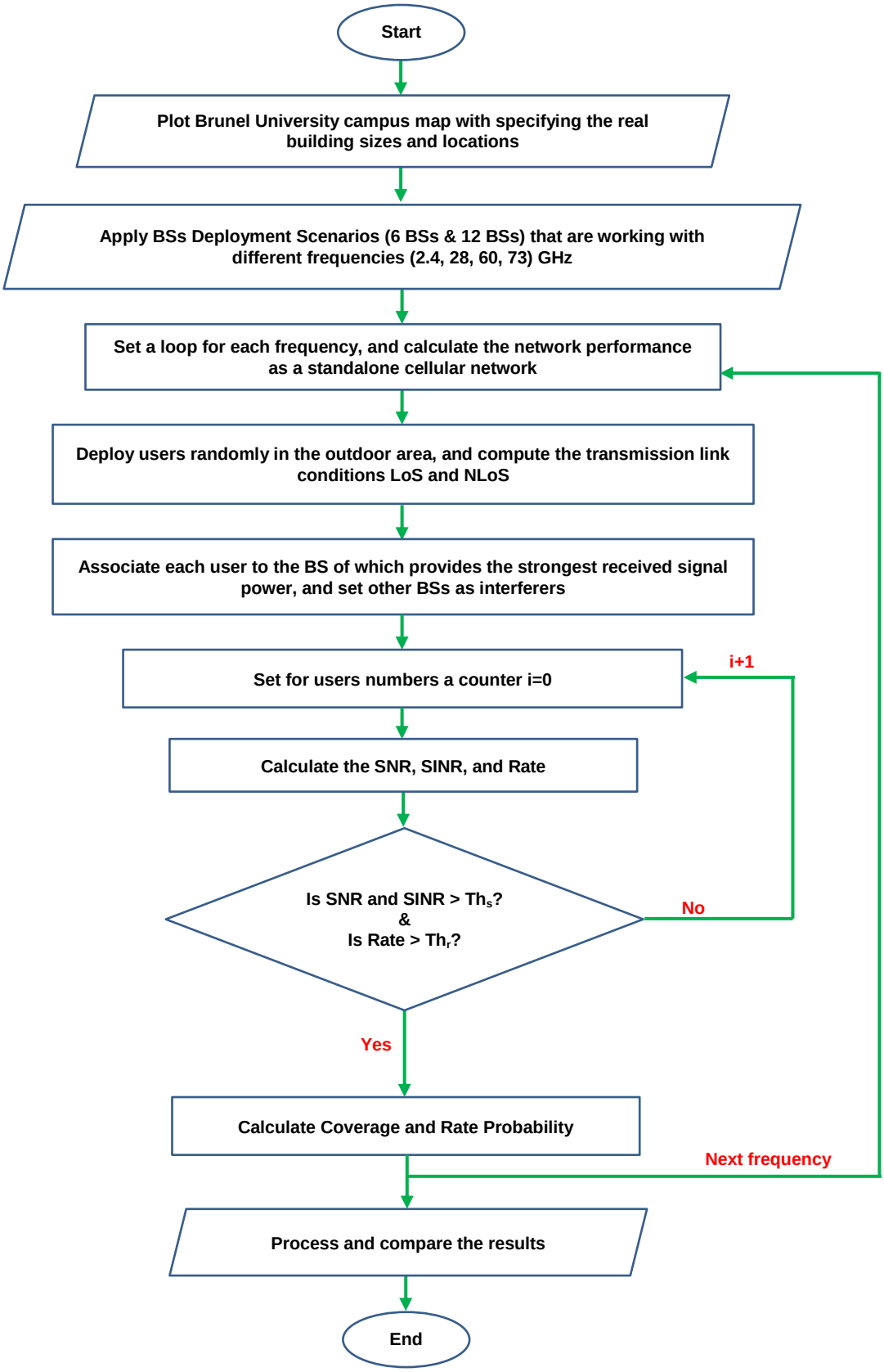

Figure 6.2 Flowchart describes the proposed MATLAB simulation calculations.

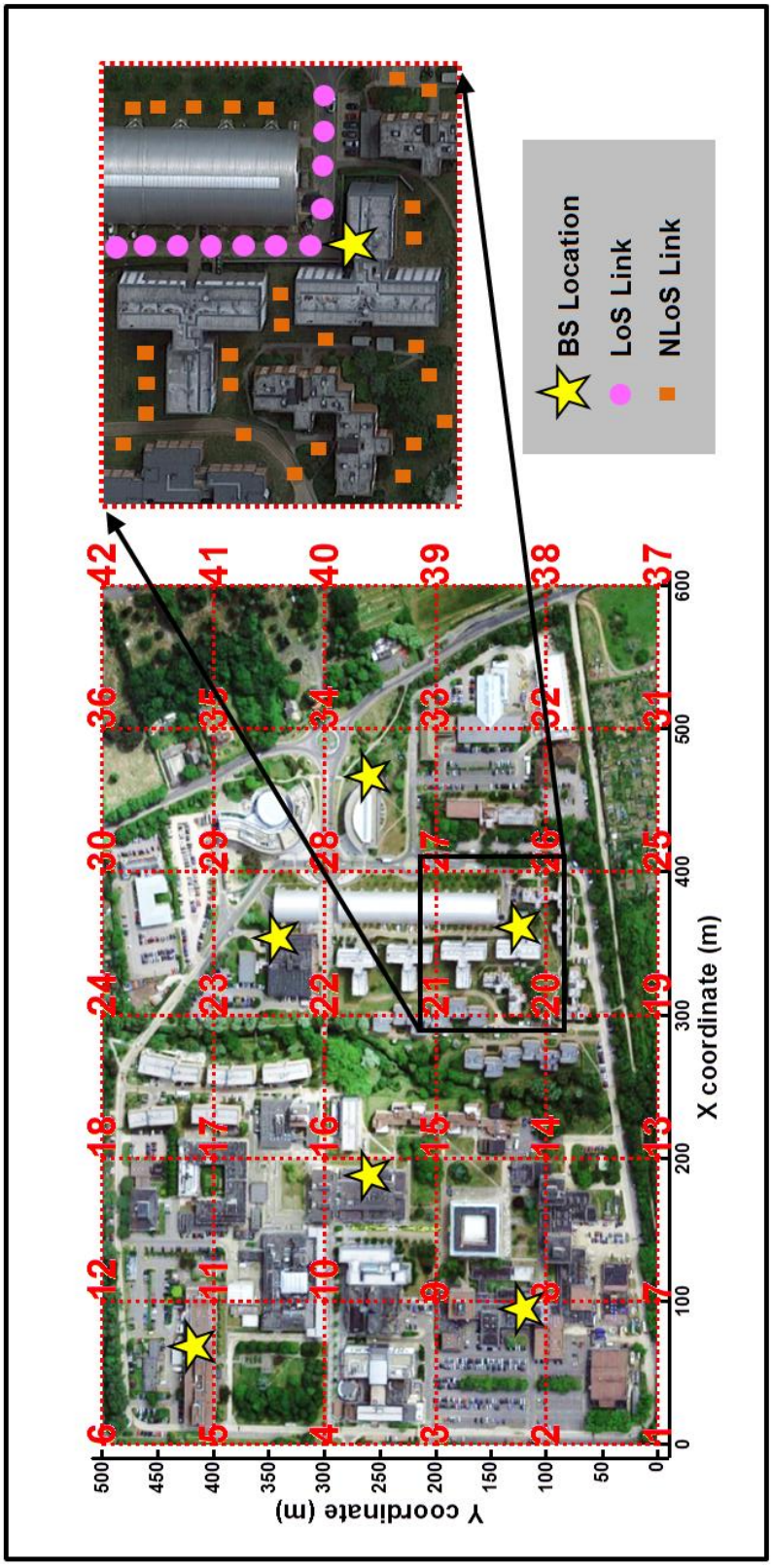

Figure 6.3 Virtual zones division (red grid) of the google map view of the campus, with the deployment of 6 BSs (yellow stars).

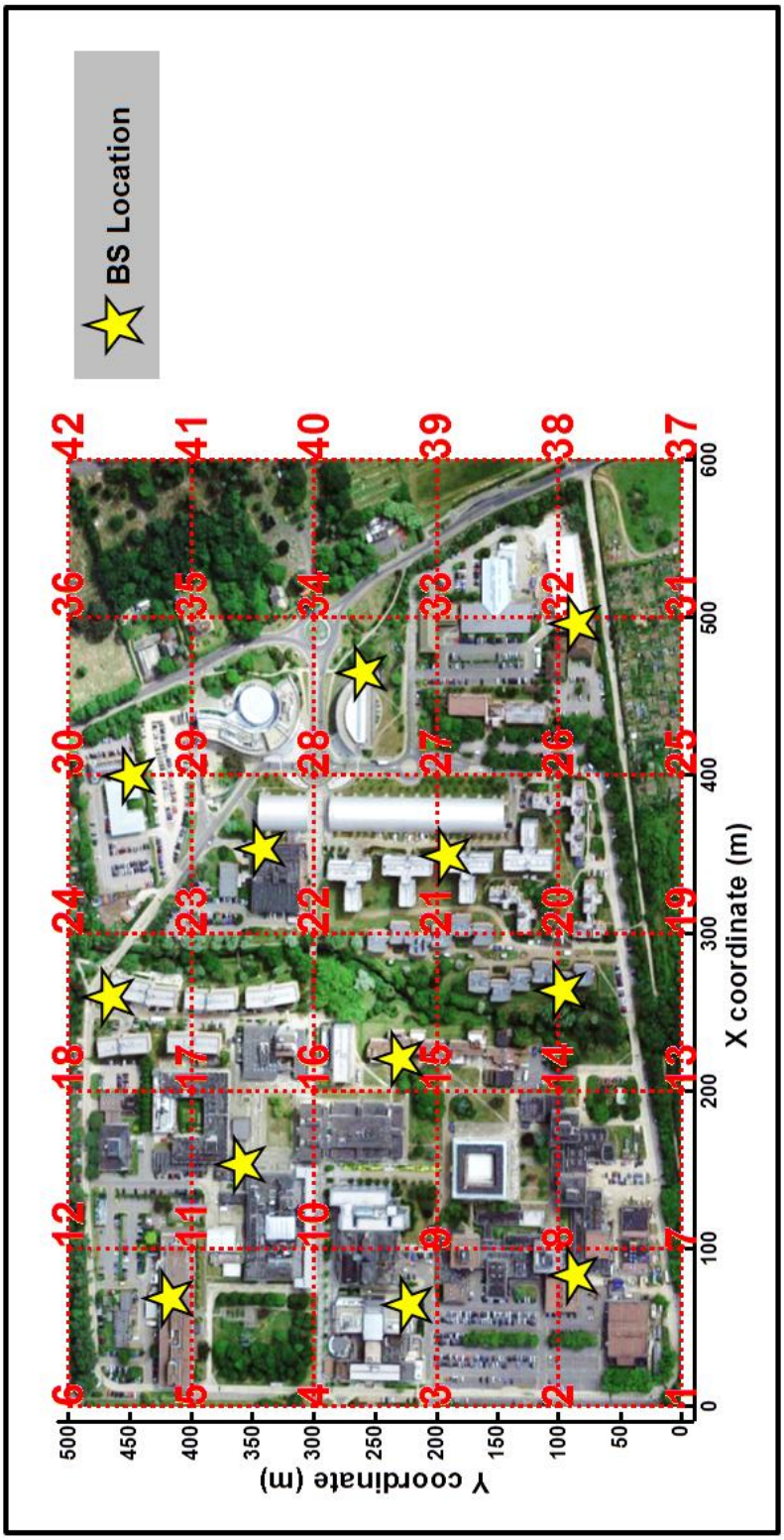

Figure 6.4 Virtual zones division (red grid) of the google map view of the campus, with the deployment of 12 BSs (yellow stars).

6.3 System Analytical Model

In this section, the analytical model for evaluating the performance of cellular networks using mm-waves and UHF is presented. In this chapter, the downlink transmission is considered with the investigation of the coverage and rate trends for outdoor users in urban places. The users within the specified area are distributed randomly. Accordingly, two path loss calculations are assumed based on the communication link between the users and BSs. The calculation of path losses varies from LoS and NLoS based on the simulation of the campus map and real buildings' locations. While the bandwidth is fixed for the users according to their association with each frequency band.

The model of evaluating path loss for UHF link is calculated by [98]:

$$PL_{UHF}(r) = (20\, log_{10}\frac{4\pi}{\lambda_c}) + (10 \propto_{UHF} log_{10}(r)) + X_{UHF} \quad (6.1)$$

where, PL_{UHF} represents the path loss [dB] for a UHF, and λ_c is the wavelength [m] for the carrier frequency f_c [Hz]. While, α_{UHF} is the path loss exponent, r is the distance between the BS and the user [m], and X_{UHF} is the shadow fading in the link.

For the mm-wave link, there are two path loss calculations, one for the LoS and the second for the NLoS, as in the following [98, 156]:

$$PL_{mm}(r) = \begin{cases} \rho + (10\alpha_L\, log_{10}(r)) + X_L & for\ LoS \\ \rho + (10\alpha_N\, log_{10}(r)) + X_N & for\ NLoS \end{cases} \quad (6.2)$$

where, PL_{mm} is the mm-wave path loss [dB] and ρ is the fixed path loss which is given by ($(20log_{10}(4\pi/c))+20log_{10}(f_c)$) [dB]. While α_L and α_N are the path loss exponents for LoS and NLoS respectively in [dB] and their values are specified for each mm-wave frequency band. X_L represents the shadow fading for LoS and X_N is for NLoS [dB], with their values being also specified for each mm-wave frequency band [98, 156].

Based on the distance r between the BS and the user, the received power by the user from the UHF BS is determined the follows [98]:

$$P_{rUHF}(r) = \frac{P_t G \mu}{PL_{UHF}(r)} \times \left(\frac{\lambda}{4\pi}\right)^2 \quad (6.3)$$

where, P_{rUHF} represents the received power [dBm] of the user from the UHF link, P_t is the transmitted power, G is the transmit antenna gain, and μ is the squared envelope of the multipath fading [dB].

The received power by the user from the mm-wave BS is determined as follows [98]:

$$P_{rmm}(r) = \frac{P_t G \mu}{PL_{mm}(r)} \times \left(\frac{\lambda}{4\pi}\right)^2 \quad (6.4)$$

where, P_{rmm} represents the received power in [dBm] of the user from the mm-wave link and G is the transmit antenna gain. The antenna gain depends on the azimuthal angle as a function varying with it [122]. In the calculation, the beam alignment that gives the maximum received power has been considered. Therefore, the beam of the BS is assumed to be perfectly aligned with the user it is serving, so it has the maximum amount of the gain. Whilst in this work, the variation of the gain with the elevation angle is neglected. All users are assumed to be omnidirectional therefore user antenna gain is 0 dB [157].

The following equation calculates the signal to interference plus noise ratio (SINR) of the user [14]:

$$SINR = \frac{P_r(r)}{\sum_{x \neq r} P_r(x) + \sigma^2} \quad (6.5)$$

where, $P_r(x)$ is the power of interfering BS [dBm], and σ^2 is the noise power [dB] [98]. The noise power is calculated by the equation ($\sigma^2 = -174[dBm/Hz] + 10log_{10}B[Hz] + NF$), where NF is the noise figure (equals 10 dB), B is the bandwidth [14].

The SINR coverage probability is evaluated as [98]:

$$C_p(Th_s) = Probability(SINR > Th_s) \quad (6.6)$$

where, $C_p(Th_s)$ is the coverage probability with the *SINR* threshold (Th_s). Each BS is serving a number of users, and its downlink rate (*Rate*) is calculated by [98]:

$$Rate = \frac{B}{N} log_2(1 + SINR) \quad (6.7)$$

where, N represents the total number of users.

The probability of the rate coverage (R_p) is given by [122]:

$$R_p(Th_r) = Probability(Rate > Th_r) \quad (6.8)$$

where, Th_r is the rate threshold.

6.4 Simulation Results and Discussion

In this work, applying four different frequencies in the proposed scenario is assumed, one is the UHF (2.4 GHz), and the remainders are the three different mm-wave bands (28, 60, 73 GHz). The simulation depends on varying the frequencies and the physical properties related to each frequency band. The simulation parameters are based on previous recent studies [3, 14, 98, 122, 158]. Table 6.1 gives the parameters' values for the different mm-wave bands used in the analysis and Table 6.2 provides the UHF parameters' values, while Table 6.3 summarises the parameters of the proposed model with the deployment scenario.

The simulation procedure is explained in Figure 6.5. The performance for each frequency has been analysed by calculating the SNR, SINR and the coverage rate as a standalone cellular network, with the obtained results being compared.

Table 6.1 Millimetre-wave parameters

mm-Wave frequency bands [GHz]	LoS Parameters		NLoS Parameters		Bandwidth [GHz]
	α_L (dB)	X_L (dB)	α_N (dB)	X_N (dB)	
28	2	5.8	2.92	8.7	0.8
60	2	5.8	2.69	7.7	0.75
73	2	5.2	2.3	7.2	2

Table 6.2 UHF parameters

Parameter	UHF	α_{UHF}	X_{UHF}	Bandwidth
Value	2.4 GHz	3 dB	4 dB	20 MHz

Table 6.3 The proposed model parameters

Scenario Architecture	1st BSs Deployment	2nd BSs Deployment
Number of BSs	6 BSs	12 BSs
Environment	(600 m × 500 m) campus area of Brunel University London	
Frequencies	(2.4, 28, 60, 73) GHz	
Buildings Height	(10-20) m	
BSs locations and height	On rooftops of buildings at height 5 m above rooftop level	
BS transmit power	30 dBm	
Antenna gain	18 dBi	
Number of users	(500-1000) total users	
Users locations and height	Random distribution from BSs, 1.5 m above ground level	
Link direction	Downlink (from BS to user)	

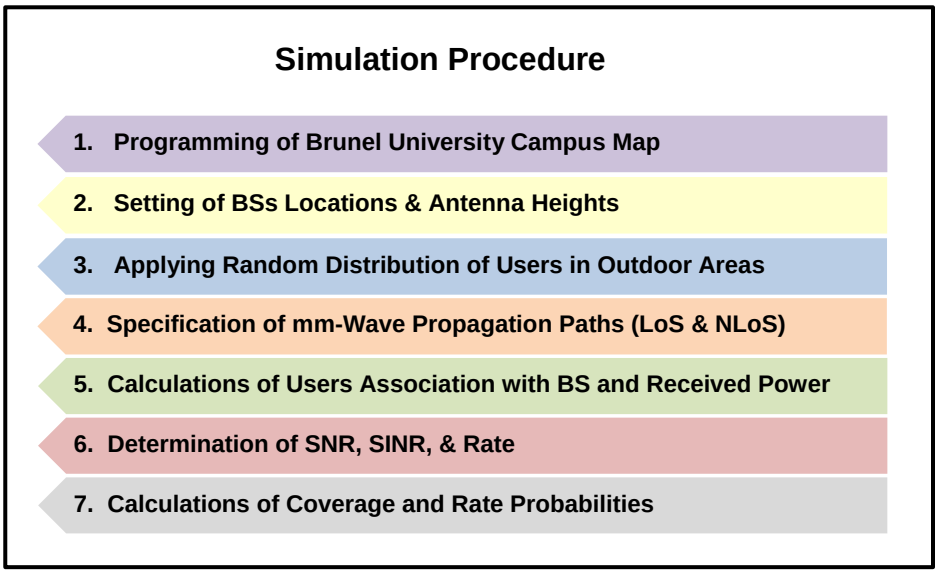

Figure 6.5 Simulation procedure steps.

To analyse the performance of mm-waves, firstly a comparison of the path losses in each frequency band is presented versus the variation of the propagation with the separation distance between the transmitter and receiver as in Figure 6.6(a,b). The transmission link distance in this figure is assumed up to 200 m, which is considered the maximum possible range in mm-wave wireless propagation for outdoor urban areas based on [13]. For mm-wave bands, the path loss is calculated for both the LoS and NLoS links. To obtain an accurate comparison, the path loss calculation is assumed to be under the same environmental conditions and that there is the same separation distance between the transmitter and receiver for each frequency band. Because mm-wave bands are sensitive to the shadowing and blockages, for small cell deployment, it is better to provide the propagation condition as being LoS, as has been explained previously in the deployment scenario (section 6.2). The deployment of BSs with LoS links can improve the overall performance of the mm-wave wireless system. From Figure 6.6, it is clear that the LoS path losses in the 28 GHz frequency band are approximately close the propagation of 2.4 GHz. Also, it is clear from this figure that the increase in the path losses is greater for the 73 GHz frequency band based on Friis' law, in urban areas, as considered here. That is, this loss is bigger than that for 2.4 GHz by 15 dB and 40 dB for LoS and NLoS, respectively, which is considered a significant concern with this band.

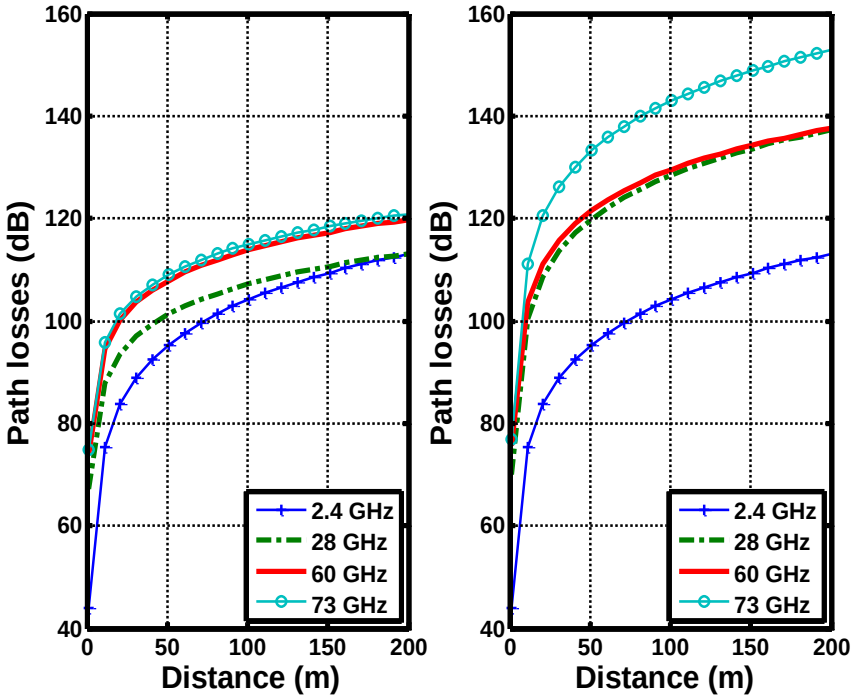

Figure 6.6 Path losses comparisons for different frequency bands as a function of distance.

With regards to simulating the deployment of the BSs, their locations have been chosen by considering the optimal LoS paths. It is challenging to find an advanced set of BSs places, so efforts were made to obtain more LoS paths. Figure 6.7(a,b) presents comparisons of the SINR coverage probability between UHF band and the different mm-wave frequency bands, with densities of 6 and 12 BSs/km^2, with distributions of 1000 users/km^2 in the outdoor area. It can be seen from this figure that the coverage probability in the case of 2.4 GHz is the greater, because in the UHF networks the cell edge still has a high SINR. While in the case of the mm-wave high-frequency band, the coverage probability is lower, because only the users located near to the mm-wave BSs have good SINR, while the others located far from them are affected by blockages. Thus, increasing the number of BSs per area will improve the performance of the mm-wave cellular network by increasing the chance of

more LoS links, which means that the amount of received power will increase as well. Therefore, the number of BSs is increased from 6 to 12, and the simulation analysis is repeated to compare the results. Figure 6.7(b) presents that the coverage probability, which is well improved for all mm-wave frequencies by raising the density of BSs. To reduce the interference effects because of increasing the number of BSs, there are some schemes that might be adopted. For example, applying massive MIMO with beamforming technique will help in this issue by focusing a narrow mm-wave beam in one direction and increase the gain. Also, advanced antenna sectoring is considered beneficial in reducing the interference and with applying different frequencies for the neighbour cells can be used perfectly. Some schemes went through reducing the amount of the transmitted power to avoid the interference, so all the schemes above can improve the cellular network performance.

To assess the interference effects, the coverage probability of the SNR and SINR have been compared for each frequency. Figure 6.8 presents a comparison between SNR and SINR for different frequency bands with a distribution density of 12 BSs/km^2 for 1000 users in the outdoor area. From this comparison, it can be observed that the difference between the coverage probability of SNR and SINR is tiny in higher frequency mm-wave networks (60 GHz and 73 GHz). While in the 2.4 GHz network the difference between SNR and SINR is clear and for 28 GHz the difference is noticeable as well. This comparison shows that low-frequency networks are affected by interference, while mm-wave higher frequencies offer a very noise limited cellular network, specifically in the 73 GHz band. This issue is considered a very advantageous of applying high frequency of mm-wave to diminish the interference.

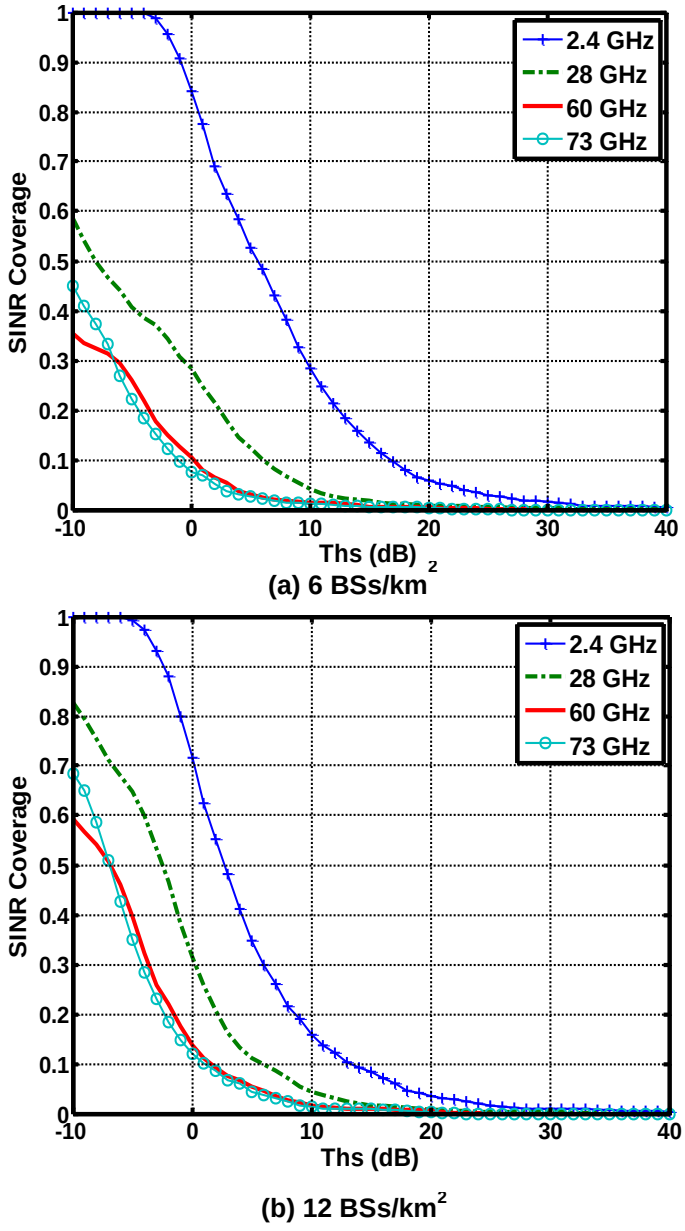

Figure 6.7 Comparison of the SINR coverage probabilities for different frequency bands with 6 and 12 BSs/km^2.

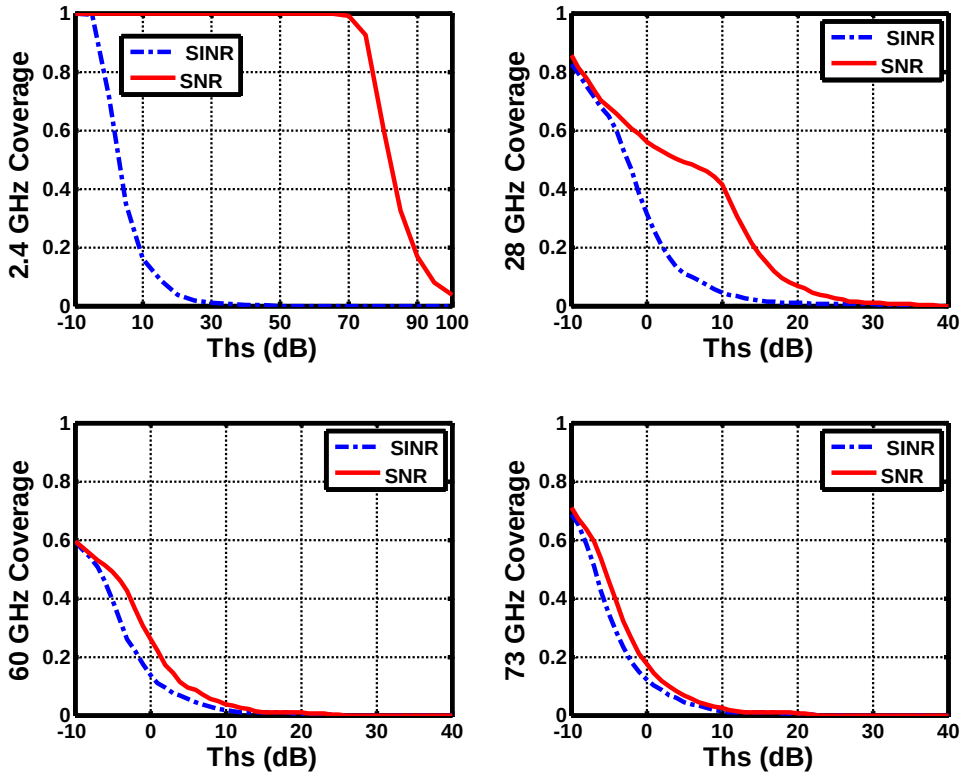

Figure 6.8 Comparison between SNR and SINR for different frequency bands with 12 BSs/km^2.

Further analysis has been carried to determine the rate coverage probabilities. These are shown in Figure 6.9, which compares the rate coverage for different frequency bands between two users densities with the deployment of 12 BSs/km^2. The first case is calculated with 500 users/km^2, whilst the second has 1000 users/km^2. From Figure 6.9, it can be noticed that the mm-wave network operating at 73 GHz can provide data rates in Gbits/s range, which is much higher than those for UHF networks and other mm-wave bands. In UHF, the rate is range around Mbits/s, which is considered low in comparison with all the mm-wave frequencies. Also, it can be observed that increasing the density of users, leads to the data rates decreasing, because the number of users associated with each BS increases as well.

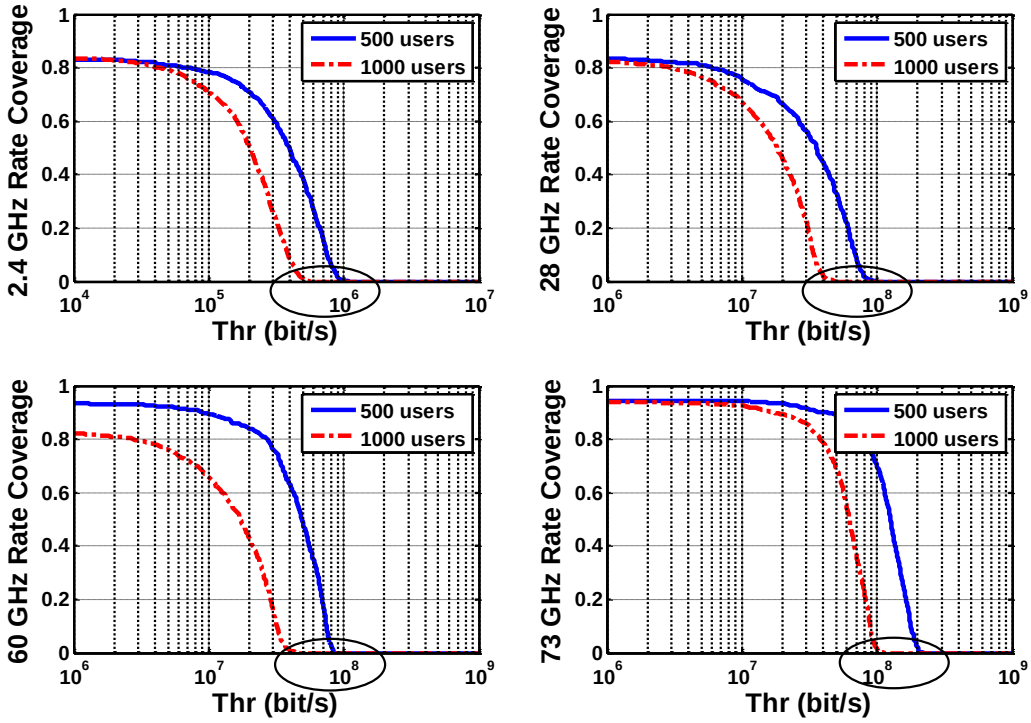

Figure 6.9 Comparisons of the rate coverage probability between two different densities of users for various frequency bands.

Figure 6.10 shows a comparison of the rate coverage probabilities for different frequency bands for two densities of BSs (6 and 12 BSs/km^2), with 1000 users. The results show that a better rate coverage of the network is achieved with the higher density of BSs. This improvement in the network rate coverage relates to the number of users connected to each BS, because the one that serves fewer users can offer a higher rate. Also, the coverage rate has been compared for all the bands in this figure and it can be seen that the highest rate is offered by the 73 GHz mm-wave when compared with the other frequencies.

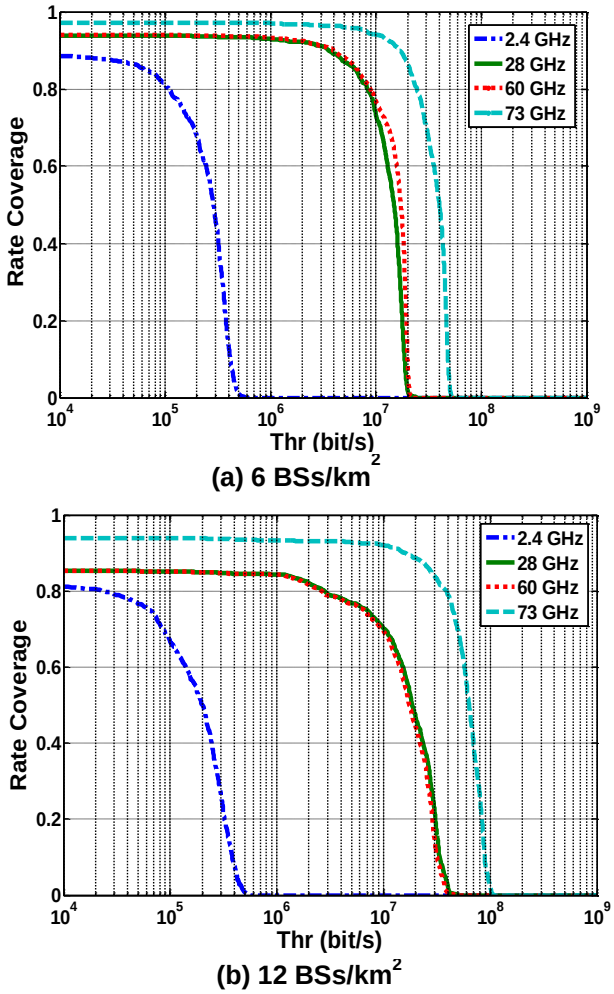

Figure 6.10 Comparisons of the rate coverage probabilities for different frequency bands.

6.5 Summary

In this chapter, the performance of different mm-wave bands as cellular networks has been analysed and compared with UHF by determining the coverage and rate probability calculations. The proposed scenario of BSs deployment is based on a real map with the blockage of the actual buildings' locations being specified. Simulation results have shown that dense

deployment of BSs would enhance the coverage of all mm-wave frequency bands, whilst also offering limited noise networks. Moreover, comparison of the results has elicited that the 73 GHz mm-wave bands with the deployment of 12 BSs could provide good coverage (approximately 75%) for the specified area of interest. Also, the 73 GHz band presents the lowest interference effects and the higher rate due to the large available bandwidth in this band. Moreover, the results have shown that the 28 GHz frequency network with the deployment of 12 BSs offers the highest coverage (up to 80%) of the area of interest, while the 60 GHz gives the lowest (60%).

For this study, there has been the aim of verifying LoS condition by increasing the number of BSs that operating at 73 GHz to cope with the demand of futuristic 5G and beyond networks. That is, this frequency band will enhance the network by offering the highest available bandwidth and the lowest interference ratio. Also, the suggested cell radius at high-frequency should be less than 100 m to ensure good QoS to all users.

Chapter 7

Proposed Simplified mm-Wave Path Loss Model

In this chapter, a simplified path loss model is proposed, which captures the diffraction and specular reflection impacts that affect mm-wave wireless propagation. Also, the proposed path loss model is compared with the traditional one in terms of the performance results. Proposing this simplified model is important for accurately specifying the rate of change in mm-wave signal strength due to these losses. The performance of 28 GHz mm-wave outdoor propagation, which is considered a key component in 5G networks, has been investigated. The proposed scenario for the BSs deployment involved applying a map-based model on Brunel University's London campus with a random distribution of users. Simulation results provide a comparison between the proposed path loss model with the traditional one. The obtained results show that the traditional path loss model has serious implications for describing the real mm-wave propagation for the outdoor applications. In addition, the results reveal the characteristics of mm-wave received signals under both the line of sight (LoS) and non-line of sight (NLoS) conditions. The coverage trends for mm-wave frequency are also evaluated by considering the real distribution of buildings' locations as blockages.

7.1 Introduction

Whilst, mm-wave wireless propagation is more challenging than the microwave frequency, its application in 5G mobile communication systems will enrich the capacity and the data rate. The mm-wave high propagation loss makes its wireless channel more sensitive to blockage and shadowing effects [3, 158]. Understanding the diffraction impact on mm-wave wireless

propagation is important for accurately specifying the rate of change in mm-wave signal strength due to attenuation losses. As the use of new mm-wave bands for outdoor wireless propagation will improve the capacity of futuristic mobile networks, the behaviour of mm-wave wireless propagation has added new aspects to investigate. Regarding which, shadowing and blockage effects are considered the main obstacles that face mm-wave wireless transmission due to the high sensitivity of mm-waves [99, 100]. They are also the major reason for an increase in mm-wave path losses, because the signal power decreases due to reflection and diffraction by building walls or the ground in the environment [24, 149].

In this chapter, a simplified path loss model that provides adequate accuracy for 28 GHz mm-wave wireless propagation is proposed, as in recent work by this researcher [130]. Part of Brunel University's London campus (about 37,175 m^2) is considered the outdoor area of interest for this study, and it is simulated by MATLAB simulation tools. Fixed location of BSs is implemented with a random distribution of users in the specified outdoor area. Figure 7.1 shows the area of interest considered in the simulation analysis of this chapter, while Figure 7.2 presents the simulated map created with the MATLAB tools.

The rest of this chapter is organised as follows: Section 7.2 is a description of the proposed map based scenario, whilst in section 7.3, the proposed simplified mm-wave path loss model is explained. Section 7.4 includes the simulation results and comparisons discussion. Finally, Section 7.5 concludes the chapter.

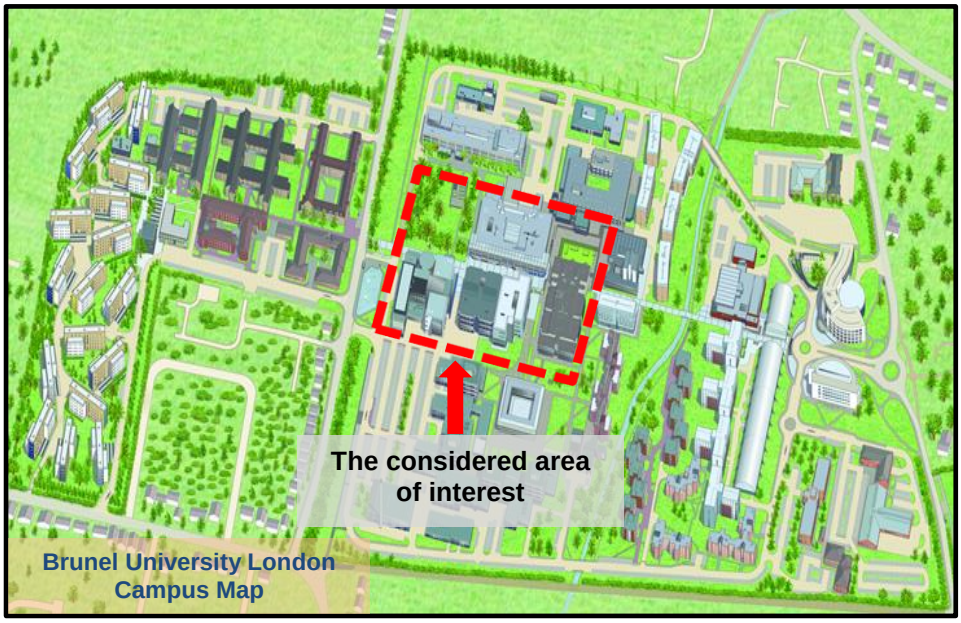

Figure 7.1 The considered area of interest.

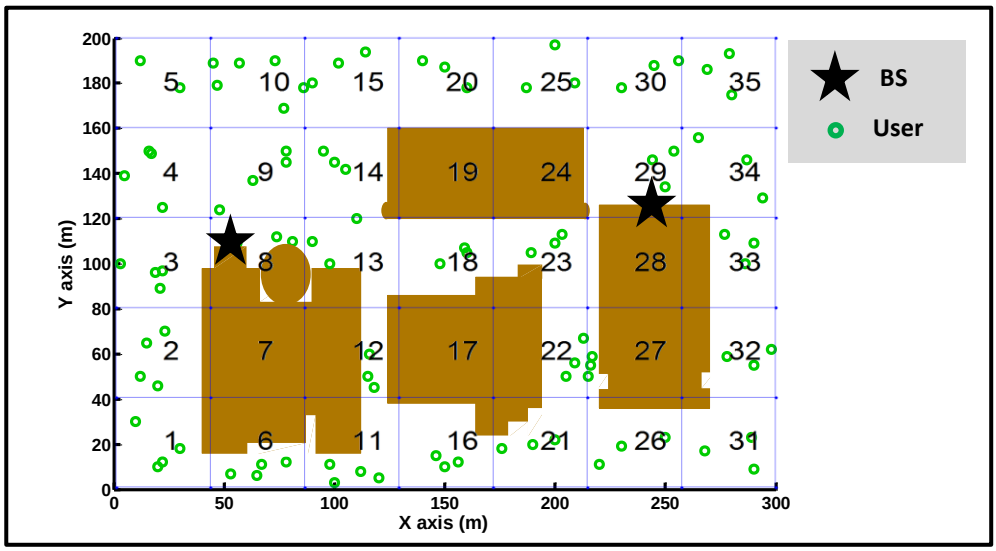

Figure 7.2 The simulated area of interest.

7.2 The Proposed Map Based Scenario

The proposed 3D map scenario is designed based on applying a description of the real buildings' sizes, locations, and walls surfaces. Also, specific materials

properties have been considered to evaluate the proposed path loss model. The mm-wave propagation mechanisms, which include reflection, diffraction, and blockage nature have been considered in this scenario. The area of interest has been virtually divided into 35 zones to specify the LoS link condition and NLoS link. Two mm-wave BSs are deployed with a random distribution of 100 users within the specified area outside the buildings. The process of user association with the BS depends on the strongest signal that the user can receive, while the other BS that exists in the considered area is assumed as being an interferer. Figure 7.3 briefly shows the procedure used to analyse the map based scenario.

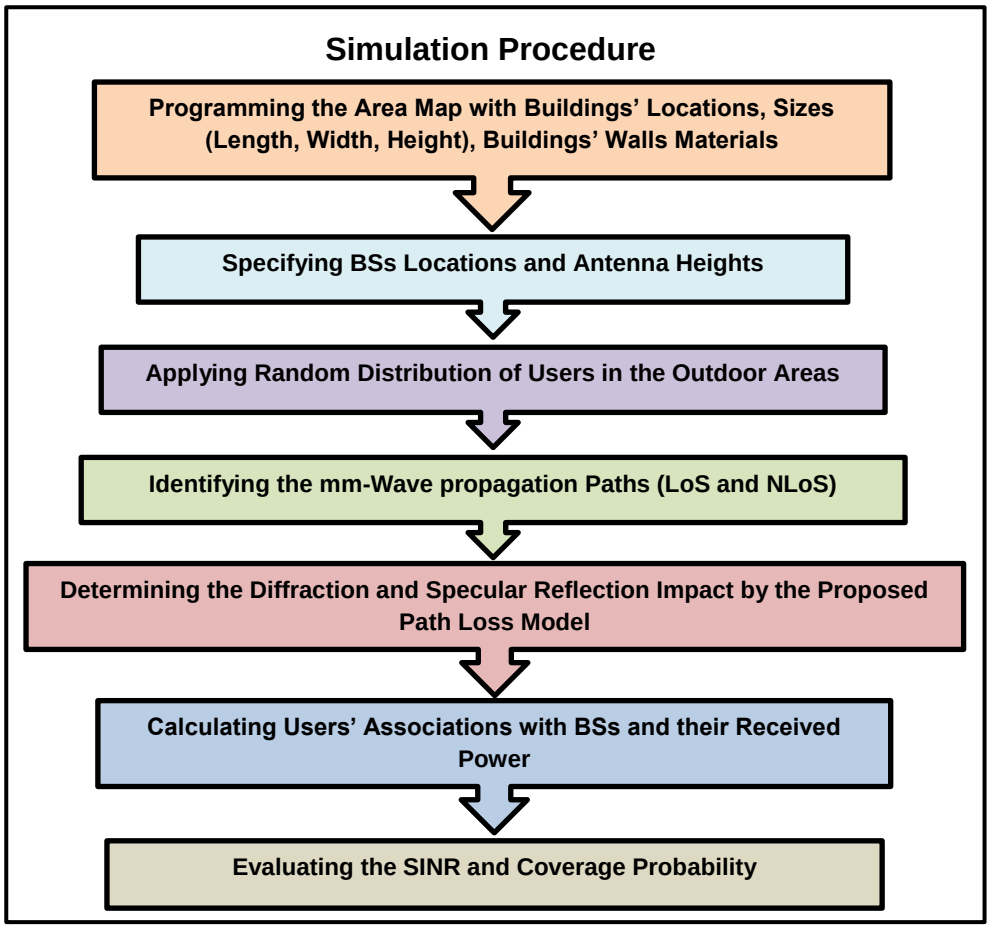

Figure 7.3 Simulation procedure steps.

7.3 The Proposed Simplified mm-Wave Path Loss Model

The proposed simplified path loss model is modified from the traditional path loss model that was presented in chapter 6. In this chapter, the proposed model is calculated by adding the impact of diffraction and specular reflection, whilst also considering the antenna height. The proposed model for evaluating mm-wave path loss for the LoS and the NLoS propagation links is [130]:

$$PL(r) = \begin{cases} \rho + 10\alpha_L \, log_{10}(r) + X_L & for\ LoS \\ \rho + 10\alpha_N \, log_{10}(r) + X_N + D_L + R_L & for\ NLoS \end{cases} \quad (7.1)$$

where, ρ is the fixed path loss which, is given by ($(20log10(4\pi/c))+20log_{10}(f_c)$) [dB] [98, 156], α_L and α_N are path loss exponents for LoS and NLoS, respectively, X_L represents the shadow fading for LoS and X_N is for NLoS and r is the real distance between the antenna and the user location, which is calculated by considering the antenna height (h_A) [130], as explained in Figure 7.4.

$$r = \frac{h_A}{\sin \theta_{AoA}} = \frac{h_A}{tan^{-1}\frac{h_A}{d}} \quad (7.2)$$

where, d is the direct distance between the user and the BS.

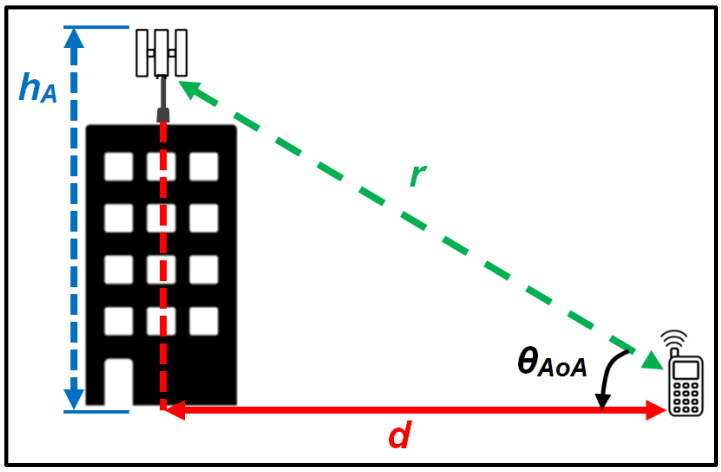

Figure 7.4 The separation distance between the BS and the user.

Due to the knife edge approximation, which is considered one of the simplest ways to model the blockage effects of buildings [124, 159], the calculation of diffraction losses (D_L) [dB] is calculated by [124, 159]:

$$D_L = 20\,log_{10}\,v = 20\,log_{10}(h_B\sqrt{\frac{2}{\lambda}(\frac{1}{r_1}+\frac{1}{r_2})}) \quad (7.3)$$

where, v is the diffraction parameter, h_B is the building height, and λ is the carrier wavelength. r_1 is the terminal distance from the antenna to the blockage, and r_2 is the distance from the blockage to the user, as demonstrated in Figure 7.5. The total distance r is the sum of r_1 and r_2, which can be calculated by applying the knife edge approximation and then substituted in equation (7.1).

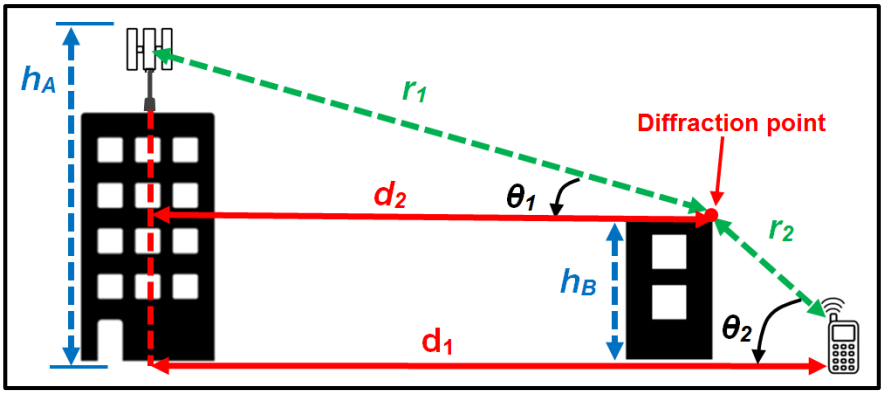

Figure 7.5 Knife edge approximation to evaluate the diffraction losses.

Another important calculation is the reflection losses (R_L), which is based on the reflection coefficient (Γ) and it is presented as [130]:

$$R_L = -20\,log_{10}\,\Gamma = -20\,log_{10}(\left|\frac{n_1-n_2}{n_1+n_2}\right|^2) \quad (7.4)$$

where, n_1 is the air refractive index and n_2 is the refractive index of the surface materials. The main surface materials considered in this study are brick, concrete, and glass, which are based on Brunel University's London buildings in the specified area. The refractive index for each material with the mm-wave

interaction of the building walls is based on practical measurement presented in [160].

The received power of the user from the BS is calculated by the same presented model in chapter 6 using equation (6.4). Also, the SINR calculation and the coverage probability are based on the same models presented as equations (6.5) and (6.6). So, the received power by the user from the BS is given by [122]:

$$P_r(r) = \frac{P_t G \mu}{PL(r)} \times \left(\frac{\lambda}{4\pi}\right)^2 \quad (7.5)$$

where, P_t is the transmitted power, G is the transmit antenna gain, and μ is the squared envelope of the multipath fading. The antenna gain depends on the azimuthal angle as a function varying with it. In the calculation, the beam alignment that gives the maximum received power has been considered. Therefore, the beam of the BS is assumed to be perfectly aligned with the user it is serving, so it has the maximum amount of the gain. Whilst in this work, the variation of the gain with the elevation angle is neglected. All users are assumed to be omnidirectional therefore user antenna gain is 0 dBi [157].

The signal to interference plus noise ratio (SINR) of the user is calculated by [14, 98]:

$$SINR = \frac{P_r(r)}{\sum_{x \neq r} P_r(x) + \sigma^2} \quad (7.6)$$

where, $P_r(x)$ is the power of interfering BS, and σ^2 is the noise power, which is given by ($\sigma^2 = -174[dBm/Hz] + 10log_{10}B[Hz] + NF$), where NF is the noise figure and B is the bandwidth. The $SINR$ coverage probability is evaluated as [14, 98]:

$$C_p(Th_s) = Probability(SINR > Th_s) \quad (7.7)$$

where, $C_p(Th_s)$ is the coverage probability with the $SINR$ threshold (Th_s).

7.4 Simulation Results and Discussion

The proposed path loss model has been simulated using MATLAB simulation tools. The simulation parameters are based on the measurements of recent

studies [3, 14, 98, 122, 158, 160] and Table 7.1 shows those used in the analysis.

The network coverage has been compared in relation to two path loss models: the proposed one and the traditional model presented in chapter 6. Figure 7.6 shows 100% coverage of the mm-wave network by applying the traditional path loss model without considering the diffraction and specular reflection impact. However, by applying the proposed model, which takes into accounts this impact on the mm-wave propagation, the obtained results showed that the coverage area is reduced by approximately 25%, as shown in Figure 7.7. This reduction occurs due to the effects of buildings' blockages, which reduce the amount of the received power to under the threshold limits. Hence, the proposed path loss captures the effects of the added attenuation to the mm-wave signal by diffraction and reflection with buildings' walls in the outdoor environment.

Table 7.1 Simulation Parameters

Parameter	Setting
Frequency	28 GHz
α_L	2 dB
X_L	5.8 dB
α_N	2.92 dB
X_N	8.7 dB
P_t	30 dBm
G	25 dBi
NF	10 dB
Bandwidth	0.8 GHz
Air refractive index	1
Brick complex refractive index	1.18-j0.028
Concrete complex refractive index	1.21-j0.256
Glass complex refractive index	2.77-j0.114

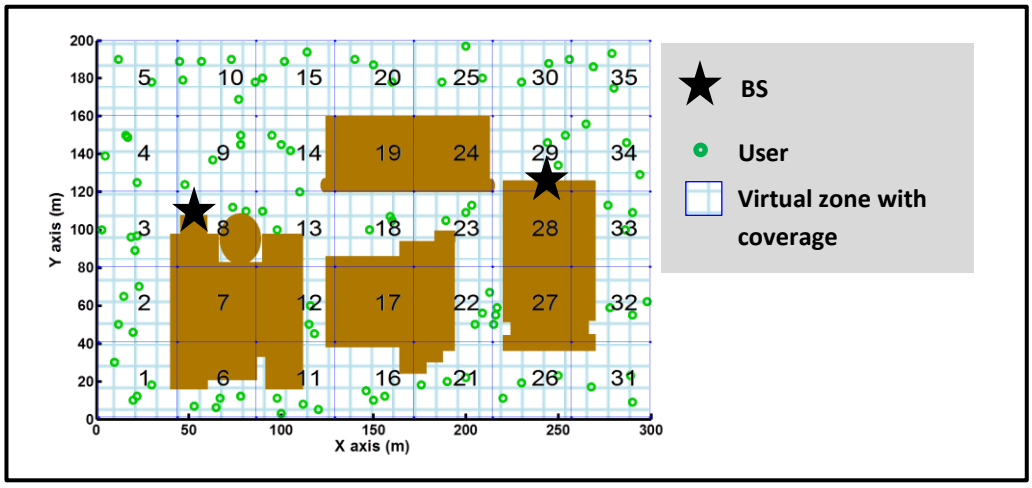

Figure 7.6 The mm-wave network coverage without considering the diffraction and specular reflection impact.

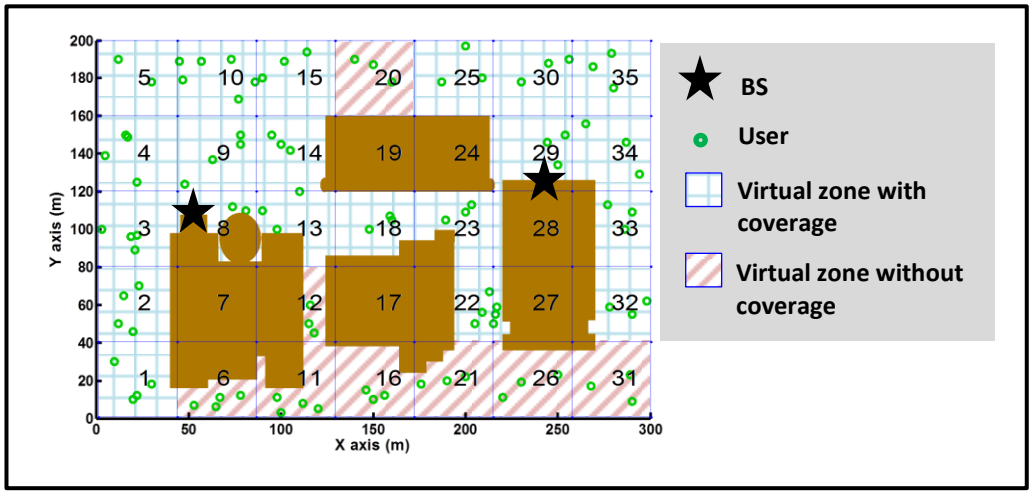

Figure 7.7 The mm-wave network coverage taking into account the diffraction and specular reflection impact.

Figures 7.8 and 7.9 reflect the importance in this study to specify mm-wave wireless propagation for the 5G mobile network accurately. Figure 7.8 presents the path losses comparisons with and without considering the diffraction and specular reflection impact. From the results in this figure, the proposed path loss model shows that the NLoS path loss is increased by more than 45 dB in comparison with the traditional model. While figure 7.9 presents the users'

received power versus the angle of arrival, which are calculated for 30 users randomly deployed in the specified area of interest. This figure is calculated based on applying the knife edge approximation and the calculation of the real separation distance between the user and the base station with considering the angle of arrivals. By calculating the link distance as in equation (7.2) for both the LoS and NLoS cases, the received power is evaluated by specifying the angle of arrival. Figure 7.9 demonstrates that the received power is directly proportional to the angle of arrival in the case of LoS transmission link and that means when the angle is large the user location is near to the base station. But it also reveals the importance of specifying the antenna height in the mm-wave mobile network because applying too high antenna can limit the performance of the cellular network. Due to this, for future networks, the antennas can be placed for example on the light poles in roads.

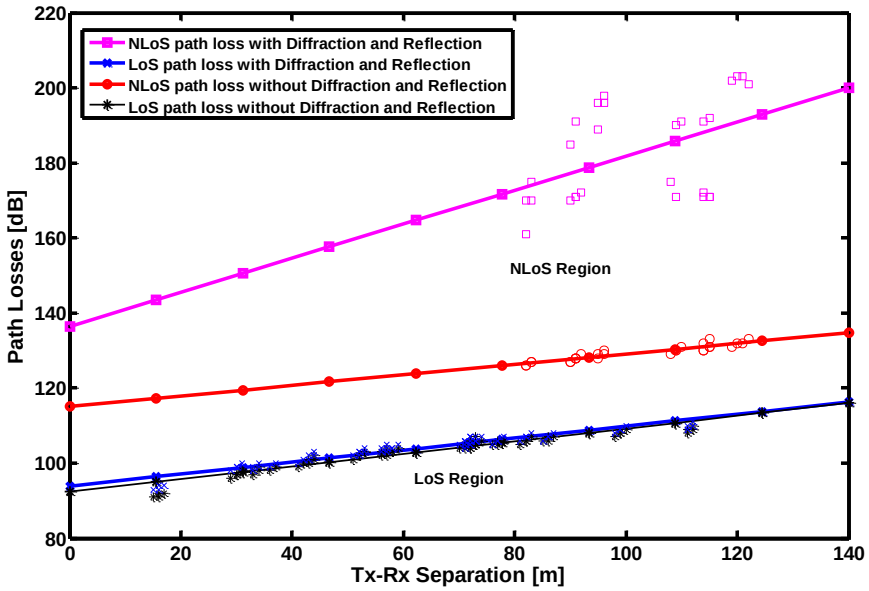

Figure 7.8 Path loss comparisons with and without considering diffraction and specular reflection impact.

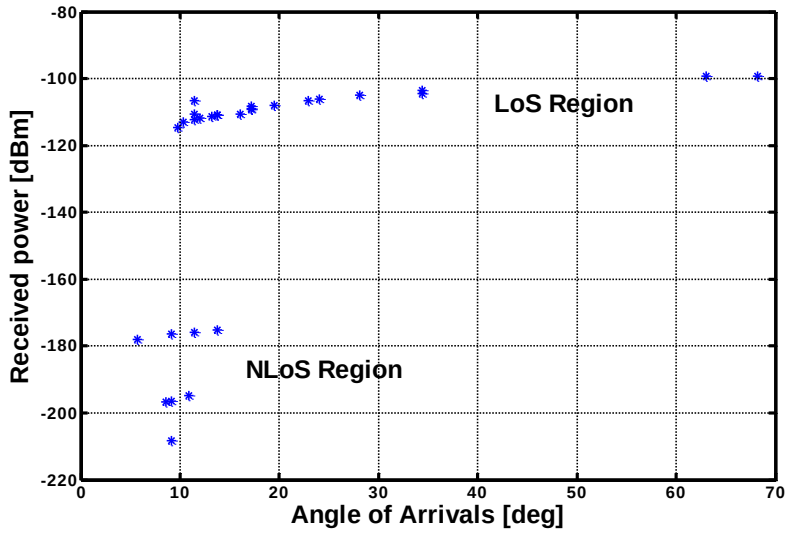

Figure 7.9 User received power vs the angle of arrival of the mm-wave.

Figures 7.10 and 7.11 show the comparisons between the SINR and SNR for the traditional model and the simplified proposed model. Figure 7.11 indicates that the coverage probability of the proposed path loss model is reduced to approximately 0.75 compared with the full coverage in Figure 7.10. This reflects the importance of considering diffraction and specular reflection on mm-wave wireless propagation in 5G networks so as to determine the real coverage probability amount.

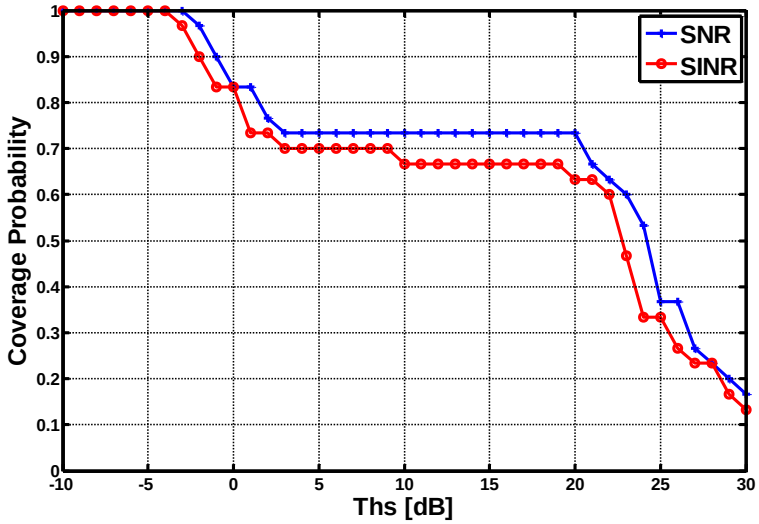

Figure 7.10 Comparison between SNR and SINR without considering the diffraction and specular reflection impact.

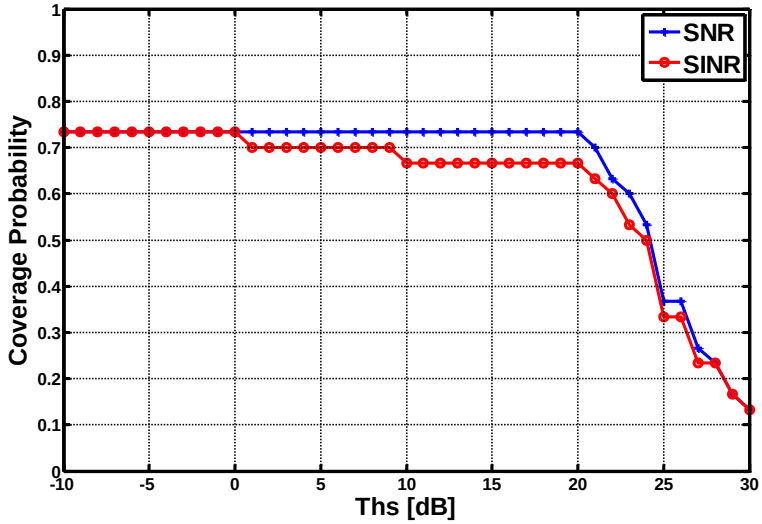

Figure 7.11 Comparison between SNR and SINR in terms of the diffraction and specular reflection impact.

7.5 Summary

In this chapter, the propagation performance of 28 GHz mm-wave has been evaluated based on a proposed simplified path loss model. The impact of diffraction and specular reflection on mm-wave propagation has been calculated by considering the materials of buildings' walls. The applied real map based scenario for the BSs deployment has shown that the coverage area of the mm-wave mobile network is reduced by 25% when taking into account the real building blockages. Also, simulation results have demonstrated that the traditional path loss model would appear to present inaccurate results, which could have serious implications for real mm-wave system applications. This study's findings highlight the importance of verifying more LoS links to assure network coverage to larger areas.

Chapter 8

Conclusions and Future Works

As the use of mm-waves in the futuristic communication networks will significantly help in increasing system capacity, mm-wave communication raises many issues that need to be addressed. In particular, mm-wave signal generation and transmission over fibre and wireless will bring up significant challenges in relation to exploiting them in future communications, including the system design and the application in cellular networks. Hence, designing simple and cost-effective mm-wave generation and transmission methods is essential for improving futuristic networks. In this thesis, a comprehensive mm-wave generation and transmission system have been proposed for futuristic communications. Five main contributions have been presented in five separated chapters according to these perspectives. In this chapter, the main findings of this thesis are summarised along with some suggestions being put forward for future research.

8.1 Conclusions

The main conclusions of this thesis can be summarised as follows. For photonic mm-wave generation, three different approaches are proposed and designed based on the characterisations of Brillouin fibre laser and SBS effects. The Brillouin scattering effect in optical fibre was used with the phase modulation technique for generating the mm-wave carrier with a tuning capability from 5 to 90 GHz. The generated mm-waves are with good SNR up to 51 dB, and low noise signal power of about -40 dBm. These generation methods will help in obtaining stable mm-wave carriers, which are beneficial

for RoF transmission systems and futuristic application in 5G optical networks. Also, a full-duplex RoF system with the generation and transmission of 64 GHz mm-wave was proposed. A single laser source was applied, and an FBG used for the wavelength reuse for the uplink connection. This scheme will not only increase the stability and the quality of the generated 64 GHz mm-wave carrier frequency with the RoF system, but also, the fibre nonlinearity effects are reduced with obtaining mm-wave with a low noise power of less than -75 dBm. Stable mm-wave transmission over a fibre link has been successfully achieved for up to 100 km fibre length with a data rate of 5 Gbits/s. Adopting such a system will help in system cost reduction and provide performance improvement by simplifying the mm-wave generation and transmission technique.

Moreover, a hybrid Fibre/FSO system for the generation and transmission of 64 GHz mm-wave was proposed. The proposed system enables the reach of mm-waves over the FSO link to remote areas, where laying fibre cables is not possible. Also, this new system can provide mm-wave transmission over a high capacity link with latency reduction by decreasing the fibre link length and applying the FSO link instead. Furthermore, the proposed system will overcome mm-wave high path losses. A successful mm-wave transmission is achieved over a 10 km fibre length, and a 2 km FSO link length with good BER of about 1.5×10^{-13} and a data rate of 10 Gbits/s. The performance of the proposed hybrid system was evaluated and compared with the performance of mm-wave wireless transmission to show the achieved improvement by using the FSO laser link. This system will help in increasing the network coverage area by transmitting mm-waves over this FSO link to areas with natural obstacles making impossible to lay fibre cables. Also, it can be used as a vital solution under emergency and disaster conditions.

Regarding the wireless networks, a comprehensive study of the wireless propagation performance for different mm-wave bands (28, 60, and 73 GHz) as cellular networks was undertaken and compared with the UHF (2.4 GHz) by evaluating the coverage and rate trends. A map-based scenario was proposed

for the deployment of BSs on the real map of the Brunel University London, campus to consider real blockage effects. Simulation results showed that dense deployment of BSs would enhance the coverage of all mm-wave frequency bands, whilst also offer limited noise networks. In addition, comparative results showed that the 73 GHz mm-wave bands with the deployment of 12 BSs could provide good coverage approximately (75%) of the specified area of interest. Also, the 73 GHz band presents the lowest interference effects and the higher data transmission rate due to the large available bandwidth in this band. Moreover, the results showed that the 28 GHz frequency network with the deployments of 12 BSs offers the highest coverage (up to 80%) of the area of interest, while the 60 GHz showed the lowest coverage (60%). Comparative results showed the 73 GHz bands achieved the higher data transmission rate with good coverage and the lowest interference effects, while the 28 GHz band provides the best network coverage. This study will help in specifying which mm-wave spectrum can enhance futuristic cellular networks with a higher capacity and the best performance.

In addition, a simplified path loss model was proposed for precisely estimating the 28 GHz mm-wave performance, which is considered a key component in 5G networks in outdoor applications. The impact of diffraction and specular reflection on mm-wave propagation was calculated by considering the materials of the walls of buildings. The applied real map based scenario for the BS deployment showed that the coverage area of the mm-wave mobile network is reduced by 25% due to building blockages. Also, simulation results showed that the traditional path loss model could present inaccurate results, which has serious implications for real mm-wave system applications. This study highlights the importance of verifying more LoS links to assure network coverage to larger areas.

8.2 Future Works

Even though this thesis has addressed the main challenges and opportunities of mm-wave applications in futuristic communications systems, there are still some issues that need to be studied and developed in the future work. Whilst some possible solutions are offered through this research as well as in other works, all of these proposals are still at the first stage, and much further effort will be needed to evaluate these designs so that these systems can become a reality. The below are the future works of this thesis:

1. The development of low cost electronic and optical components to simplify the possibility of deploying mm-wave BSs, with a feasible generation system. The applications of mm-wave for 5G cellular technologies will be supported by manufacturing low-cost mm-wave chips with small size. Also, the power efficiency and thermal control of the components should be considered with the amplifier, which is one of the main challenge;

2. The need to apply dense mm-wave network with integration and management between RoF systems and heterogeneous network. The heterogeneous networks (HetNets) can improve network coverage and capacity in the 5G and beyond. The wireless communications with mm-wave are considered as a promising candidate in 5G HetNets. But the need to apply dense deployment of mm-wave cells will increase the fibre links, and this will increase the infrastructure cost and the latency. So the end to end delay can be minimised by using the HetNets with mm-wave communications by proposing some new strategies;

3. The improvement of mm-wave wireless network efficiency by the application of massive MIMO and beamforming techniques. |So new algorithms will be required to specify the effect of interference and

direction of signal arrivals to obtain the maximum benefit of applying massive MIMO and beamforming technique;

4. The application of mm-wave for vehicular communications with investigating its performance. Several cases will be needed to investigate regarding mm-wave vehicular communications, such as:
   A- If the transmitter is fixed and the receiver is moving;
   B- Both the transmitter and receiver are moving (i.e. vehicle to vehicle communications);
   C- Antenna height;
   D- Penetration losses and diffraction losses (affect the user inside the car).

8.3 Research Impact

The mm-wave frequencies have been considered as being a vital solution to the spectrum congestion in futuristic communication systems. However, despite the underutilised mm-wave frequencies having potential of delivering high capacity communication networks, there is still the need to design an efficient generation and transmission system with simple infrastructure, low cost, and consideration of size issues. The contributions made by this thesis can deal with three main issues, namely: photonic generation, optical transmission; and wireless propagation. The impact of the proposed photonic mm-wave generation methods is obtaining stable mm-wave carriers, which is beneficial for RoF transmission systems and application in 5G optical networks. Whilst verifying the mm-wave over fibre system helps in cost reduction and performance improvement, by simplifying the mm-wave generation and transmission with the proposed RoF technique. Also, it ensures a useful communication link that will be appropriate for small cell networks. Furthermore, the proposed hybrid Fibre/FSO system can increase the network

coverage area by transmitting mm-waves over the FSO link to areas with natural obstacles that make it impossible to lay fibre cables. In addition, it can be used as a vital solution under emergency and disaster conditions. The final contributions of this thesis help in specifying which mm-wave spectrum can provide the futuristic cellular networks with a higher capacity and the best performance. This work also deals with the misdirection in the traditional mm-wave path loss model by proposing a simplified model able to capture the diffraction and specular reflection impacts on mm-wave wireless propagation. All these contributions improve the overall mm-wave communication system's performance. In sum, this research work contributes to the ongoing efforts towards 5G communications and beyond by offering a new mm-wave system design and solutions.

References

[1] M. Agiwal, A. Roy and N. Saxena, "Next generation 5G wireless networks: A comprehensive survey," *IEEE Communications Surveys & Tutorials,* vol. 18, no. 3, pp. 1617-1655, 2016.

[2] N. Al-Falahy and O. Y. Alani, "Technologies for 5G networks: challenges and opportunities," *IT Professional,* vol. 19, no. 1, pp. 12-20, 2017.

[3] T. S. Rappaport, S. Sun, R. Mayzus, H. Zhao, Y. Azar, K. Wang, G. N. Wong, J. K. Schulz, M. Samimi and F. Gutierrez, "Millimeter wave mobile communications for 5G cellular: It will work!," *IEEE access,* vol. 1, pp. 335-349, 2013.

[4] J. G. Andrews , S. Buzzi, W. Choi, S. V. Hanly, A. Lozano, A. C. Soong and J. C. Zhang, "What will 5G be?," *IEEE Journal on selected areas in communications,* vol. 32, no. 6, pp. 1065-1082, 2014.

[5] D. Liu, L. Wang, Y. Chen, M. Elkashlan, K. K. Wong, R. Schober and L. Hanzo, "User association in 5G networks: A survey and an outlook," *IEEE Communications Surveys & Tutorials,* vol. 18, no. 2, pp. 1018-1044, 2016.

[6] F. Boccardi , R. W. Heath , A. Lozano and T. Marzetta, "Five disruptive technology directions for 5G," *IEEE Communications Magazine,* vol. 52, no. 2, pp. 74-80, 2014.

[7] Z. Pi and F. Khan, "An introduction to millimeter-wave mobile broadband systems," *IEEE communications magazine,* vol. 49, no. 6, pp. 101-107, 2011.

[8] J. Beas, G. Castanon , I. Aldaya, A. Aragón-Zavala and G. Campuzano, "Millimeter-wave frequency radio over fiber systems: a survey," *IEEE Communications surveys & tutorials,* vol. 15, no. 4, pp. 1593-1619,

2013.

[9] H. Al-Raweshidy and S. Komaki , Radio over fiber technologies for mobile communications networks, Artech House, 2002.

[10] Y. Niu, Y. Li, D. Jin, L. Su and A. V. Vasilakos, "A survey of millimeter wave (mmWave) communications for 5G: Opportunities and challenges," *arXiv preprint arXiv:1502.07228,* 2015.

[11] T. S. Rappaport, J. N. Murdock and F. Gutierrez, "State of the art in 60-GHz integrated circuits and systems for wireless communications," *Proceedings of the IEEE,* vol. 99, no. 8, pp. 1390-1436, 2011.

[12] L. Frenzel, "Millimeter waves will expand the wireless future," *Electron. Des. Mag,* vol. 61, no. 4, pp. 30-36, 2013.

[13] W. Roh, J. Y. Seol , J. Park, B. Lee, J. K. Lee, Y. Kim, J. Cho, K. Cheun and F. Aryanfar, "Millimeter-wave beamforming as an enabling technology for 5G cellular communications: Theoretical feasibility and prototype results," *IEEE communications magazine,* vol. 52, no. 2, pp. 106-113, 2014.

[14] S. Kutty and D. Sen, "Beamforming for millimeter wave communications: An inclusive survey," *IEEE Communications Surveys & Tutorials,* vol. 18, no. 2, pp. 949-973, 2016.

[15] V. A. Thomas, M. El-Hajjar and L. Hanzo, "Millimeter-wave radio over fiber optical upconversion techniques relying on link nonlinearity," *IEEE Communications Surveys & Tutorials,* vol. 18, no. 1, pp. 29-53, 2016.

[16] N. Mohamed, S. M. Idrus and A. B. Mohammad, "Review on system architectures for the millimeter-wave generation techniques for RoF communication link," in *IEEE International RF and Microwave Conference*, 2008.

[17] R. Ford, M. Zhang, M. Mezzavilla, S. Dutta, S. Rangan and M. Zorzi, "Achieving ultra-low latency in 5G millimeter wave cellular networks," *IEEE Communications Magazine,* vol. 55, no. 3, pp. 196-203, 2017.

[18] A. Osseiran, F. Boccardi, V. Braun, K. Kusume, P. Marsch, M. Maternia, O. Queseth, M. Schellmann, H. Schotten, H. Taoka and H. Tullberg, "Scenarios for 5G mobile and wireless communications: the vision of the METIS project," *IEEE Communications Magazine,* vol. 52, no. 5, pp. 26-35, 2014.

[19] R. N. Mitra and D. P. Agrawal, " 5G mobile technology: A survey," *ICT Express,* vol. 1, no. 3, pp. 132-137, 2015.

[20] A. Mansour, R. Mesleh and M. Abaza, "New challenges in wireless and free space optical communications," *Optics and Lasers in Engineering,* vol. 89, pp. 95-108, 2017.

[21] I. S. A. Alimi, V. Ribeiro, A. Sousa, P. Monteiro and A. Teixeira, "Channel characterization and empirical model for ergodic capacity of free-space optical communication link," *Optics Communications,* vol. 390, pp. 123-129, 2017.

[22] N. A. M. Nor, Z. F. Ghassemlooy, J. Bohata, P. Saxena, M. Komanec, S. Zvanovec, M. R. Bhatnagar and M. A. Khalighi, "Experimental Investigation of All-Optical Relay-Assisted 10 Gb/s FSO Link Over the Atmospheric Turbulence Channel," *Journal of Lightwave Technology,* vol. 35, no. 1, pp. 45-53, 2017.

[23] J. Bohata, M. Komanec, J. Spáčil, Z. Ghassemlooy, S. Zvánovec and R. Slavík, "24–26 GHz radio-over-fiber and free-space optics for fifth-generation systems," *Optics letters,* vol. 43, no. 5, pp. 1035-1038, 2018.

[24] Z. Pi, J. Choi and R. Heath, "Millimeter-wave gigabit broadband evolution toward 5G: fixed access and backhaul," *IEEE Communications Magazine,* vol. 54, no. 4, pp. 138-144, 2016.

[25] Z. Gao, L. Dai, D. Mi, Z. Wang, M. A. Imran and M. Z. Shakir, "MmWave massive-MIMO-based wireless backhaul for the 5G ultra-dense network," *IEEE Wireless Communications,* vol. 22, no. 5, pp. 13-21, 2015.

[26] S. Sun, T. S. Rappaport, R. W. Heath, A. Nix and S. Rangan, "MIMO for millimeter-wave wireless communications: beamforming, spatial multiplexing, or both?," *IEEE Communications Magazine,* vol. 52, no. 12, pp. 110-121, 2014.

[27] T. E. Bogale and L. B. Le, "Massive MIMO and mmWave for 5G wireless HetNet: Potential benefits and challenges," *IEEE Vehicular Technology Magazine,* vol. 11, no. 1, pp. 64-75, 2016.

[28] V. A. Thomas, M. El-Hajjar and L. Hanzo, "Performance improvement and cost reduction techniques for radio over fiber communications," *IEEE Communications Surveys & Tutorials,* vol. 17, no. 2, pp. 627-670, 2015.

[29] J. Karjalainen, M. Nekovee, H. Benn, W. Kim, J. Park and H. Sungsoo, "Challenges and opportunities of mm-wave communication in 5G networks," in *IEEE International Conference Cognitive Radio oriented Wireless networks and communications (CROWNCOM),* 2014.

[30] C. Lim, A. Nirmalathas, M. Bakaul, P. Gamage, K. L. Lee, Y. Yang, D. Novak and R. Waterhouse, "Fiber-wireless networks and subsystem technologies," *Journal of Lightwave Technology,* vol. 28, no. 4, pp. 390-405, 2010.

[31] X. N. Fernando, Radio over fiber for wireless communications: from fundamentals to advanced topics, John Wiley & Son, 2014.

[32] S. E. Alavi, M. R. K. Soltanian, I. S. Amiri, M. Khalily, A. S. M. Supa'at and H. Ahmad, "Towards 5G: A photonic based millimeter wave signal generation for applying in 5G access fronthaul," *Scientific reports,* vol. 6, p. 19891, 2016.

[33] A. J. Seeds, H. Shams, M. J. Fice and C. C. Renaud, "Terahertz photonics for wireless communications," *Journal of Lightwave Technology,* vol. 33, no. 3, pp. 579-587, 2015.

[34] J. K. R. Z. X. a. W. K. 2. .. Yao, "Millimeter-wave photonic techniques:

Part I-Photonic generation of millimeter-wave signals," *International Journal of Microwave and Optical Technology* , vol. 1, no. 1, pp. 204-214, 2006.

[35] P. Hartmann, X. Qian, A. Wonfor, R. V. Penty and I. H. White, "1-20 GHz directly modulated radio over MMF link," in *IEEE International Topical Meeting In Microwave Photonics MWP*, 2005.

[36] S. Mikroulis, S. Karabetsos, E. Pikasis and A. A. Nassiopoulos, "Performance evaluation of a Radio over Fiber (ROF) system subject to the transmitter's limitations for application in broadband networks," *IEEE Transactions on Consumer Electronics*, vol. 54, no. 2, 2008.

[37] C. T. Tsai, C. H. Lin, C. T. Lin, Y. C. Chi and G. R. Lin, "60-GHz millimeter-wave over fiber with directly modulated dual-mode laser diode," *Scientific reports*, vol. 6, p. 27919, 2016.

[38] T. Schneider, Nonlinear optics in telecommunications, Springer Science & Business Media, 2013.

[39] G. Qi, J. Yao, J. Seregelyi, S. Paquet and C. Belisle, "Generation and distribution of a wide-band continuously tunable millimeter-wave signal with an optical external modulation technique," *IEEE Transactions on Microwave Theory and Techniques*, vol. 53, no. 10, pp. 3090-3097, 2005.

[40] M. Weiß, M. Huchard, A. Stohr, B. Charbonnier, S. Fedderwitz and D. S. Jager, "60-GHz photonic millimeter-wave link for short-to medium-range wireless transmission up to 12.5 Gb/s," *Journal of Lightwave Technology*, vol. 26, no. 15, pp. 2424-2429, 2008.

[41] Z. Jia, J. Yu, G. Ellinas and G. K. Chang, "Key enabling technologies for optical–wireless networks: optical millimeter-wave generation, wavelength reuse, and architecture," *Journal of Lightwave Technology*, vol. 25, no. 11, pp. 3452-3471, 2007.

[42] G. Cheng, B. Guo, S. Liu and W. Fang, " A novel full-duplex radio-over-

fiber system based on dual octupling-frequency for 82GHz W-band radio frequency and wavelength reuse for uplink connection," *Optik-International Journal for Light and Electron Optics,* vol. 125, no. 15, pp. 4072-4076, 2014.

[43] M. Zhou and J. Ma, "The influence of fiber dispersion on the transmission performance of a quadruple-frequency optical millimeter wave with two signal modulation formats," *Optical Switching and Networking,* vol. 9, no. 4, pp. 343-350, 2012.

[44] Z. Wei, R. Wang, T. Pu, T. Fang and J. Xiong, "Microwave frequency sextupling generation based on modulator and brillouin-assisted sideband-filtering," in *IEEE International Conference on Microwave and Millimeter Wave Technology (ICMMT),* 2012.

[45] Z. Zhu, S. Zhao, Y. Li, X. Chen and X. Li, "A novel scheme for high-quality 120GHz optical millimeter-wave generation without optical filter," *Optics & Laser Technology,* vol. 65, pp. 29-35, 2015.

[46] Y. Chen, A. Wen, X. Yin, L. Shang and Y. Wang, "Generation of frequency-doubling mm-wave signal using a Mach–Zehnder modulator with three arms to overcome fiber chromatic dispersion," *Optical Fiber Technology,*, vol. 18, no. 1, pp. 1-6, 2012.

[47] A. Islam, M. Bakaul, A. Nirmalathas and G. E. Town, "Simplification of millimeter-wave radio-over-fiber system employing heterodyning of uncorrelated optical carriers and self-homodyning of RF signal at the receiver," *Optics express,* vol. 20, no. 5, pp. 5707-5724, 2012.

[48] I. G. Insua, D. Plettemeier and C. G. Schäffer, "Simple remote heterodyne radio-over-fiber system for gigabit per second wireless access," *Journal of lightwave technology,* vol. 28, no. 16, pp. 2289-2295, 2010.

[49] R. Mohamad, S. M. Idrus, A. S. Supaat, S. Yaakob, A. K. Zamzuri and S. N. A. Sukito, "Millimeter wave carrier generation based on Brillouin

fiber laser with improved tuning capability," *Optik-International Journal for Light and Electron Optics,* vol. 125, no. 1, pp. 205-207, 2014.

[50] R. Chuenchom, X. Zou, V. Rymanov, B. Khani, M. Steeg, S. Dülme, S. Babiel, A. Stöhr, J. Honecker and A. G. Steffan, "Integrated 110 GHz coherent photonic mixer for CRoF mobile backhaul links," in *IEEE International Topical Meeting on Microwave Photonics (MWP)*, 2015.

[51] C. Browning, E. P. Martin, A. Farhang and L. P. Barry, "60 GHz 5G Radio-Over-Fiber Using UF-OFDM With Optical Heterodyning," *IEEE Photonics Technology Letters,* vol. 29, no. 23, pp. 2059-2062, 2017.

[52] M. Wang, C. Chen, Q. Li, K. Huang and H. Chen, " Photonic generation of tunable microwave signal using a passively Q-switched dual-wavelength fiber laser," *Microwave and Optical Technology Letters,* vol. 57, no. 1, pp. 166-168, 2015.

[53] J. A. Nanzer, P. T. Callahan, M. L. Dennis, T. R. Clark, D. Novak and R. B. Waterhouse, "Millimeter-wave wireless communication using dual-wavelength photonic signal generation and photonic upconversion," *IEEE Transactions on Microwave Theory and Techniques,* vol. 59, no. 12, pp. 3522-3530, 2011.

[54] D. Novak, R. B. Waterhouse, A. Nirmalathas, C. Lim, P. A. Gamage, T. R. Clark, M. L. Dennis and J. A. Nanzer, " Radio-over-fiber technologies for emerging wireless systems," *IEEE Journal of Quantum Electronics,* vol. 52, no. 1, pp. 1-11, 2016.

[55] S. Preussler, A. Zadok, Y. Stern and T. Schneider, "Microwave-photonic filters," in *IEEE Microwave Conference (GeMiC)*, 2016.

[56] G. P. Agrawal, Nonlinear Fiber Optics, Academic Press, 2012.

[57] Y. G. Shee, M. H. Al-Mansoori, S. Yaakob, A. Man, A. K. Zamzuri, F. M. Adikan and M. A. Mahdi, "Millimeter wave carrier generation based on a double-Brillouin-frequency spaced fiber laser," *Optics express,* vol. 20, no. 12, pp. 13402-13408, 2012.

[58] B. Chen, S. Zheng, H. Chi, X. Zhang and X. Jin, "An optical millimeter-wave generation technique based on phase modulation and Brillouin-assisted notch-filtering," *IEEE Photonics Technology Letters,* vol. 20, no. 24, pp. 2057-2059, 2008.

[59] M. C. Gross, P. T. Callahan, T. R. Clark, D. Novak, R. B. Waterhouse and M. L. Dennis, "Tunable millimeter-wave frequency synthesis up to 100 GHz by dual-wavelength Brillouin fiber laser," *Optics express,* vol. 18, no. 13, pp. 13321-13330, 2010.

[60] H. Al-Taiy, S. Preußler, S. Brückner, J. Schoebel and T. Schneider, "Generation of highly stable millimeter waves with low phase noise and narrow linewidth," in *IEEE Photonics Conference (IPC)*, 2015.

[61] W. S. Tsai, Y. L. Chen and G. C. Lin, "Optical single sideband modulation using fiber nonlinearity and injection locked technology in radio-on-fiber systems," *Microwave and Optical Technology Letters,* vol. 56, no. 2, pp. 274-278, 2014.

[62] S. Preussler, A. Zadok, A. Wiatrek, M. Tur and T. Schneider, " Enhancement of spectral resolution and optical rejection ratio of Brillouin optical spectral analysis using polarization pulling," *Optics express,* vol. 20, no. 13, pp. 14734-14745, 2012.

[63] S. Preußler, N. Wenzel, R. P. Braun, N. Owschimikow, C. Vogel, A. Deninger, A. Zadok, U. Woggon and T. Schneider, " Generation of ultra-narrow, stable and tunable millimeter-and terahertz-waves with very low phase noise," *Optics express,* vol. 21, no. 29, pp. 23950-23962, 2013.

[64] R. K. Al-Dabbagh and H. S. Al-Raweshidy, "Photonic methods of millimeter-wave generation based on Brillouin fiber laser," *Optics & Laser Technology,* vol. 79, pp. 124-131, 2016.

[65] Y. Jiang, J. Yu, B. Han, L. Zhang, W. Wang, L. Zhang and E. Yang, " Millimeter-wave subcarrier generation utilizing four-wave mixing and dual-frequency Brillouin pump suppression," *Optical Engineering,* vol.

48, no. 3, p. 030502, 2009.

[66] B. B. Tiwari, V. Prakash, V. Tripathi and N. Malaviya, "Nonlinear effects in optical fiber transmission system," *IETE Technical Review*, vol. 16, no. 5, pp. 461-479, 1999.

[67] R. K. Al-Dabbagh and H. S. Al-Raweshidy, "64-GHz millimeter-wave photonic generation with a feasible radio over fiber system," *Optical Engineering*, vol. 56, no. 2, p. 026117, 2017.

[68] Z. Jia, J. Yu and G. K. Chang, "A full-duplex radio-over-fiber system based on optical carrier suppression and reuse," *IEEE Photonics Technology Letters*, vol. 18, no. 16, pp. 1726-1728, 2006.

[69] R. P. Braun, G. Grosskopf, D. Rohde and F. Schmidt, "Low-phase-noise millimeter-wave generation at 64 GHz and data transmission using optical sideband injection locking," *IEEE Photonics Technology Letters*, vol. 10, no. 5, pp. 728-730, 1998.

[70] L. Chen, H. Wen and S. Wen, "A radio-over-fiber system with a novel scheme for millimeter-wave generation and wavelength reuse for up-link connection," *IEEE Photonics Technology Letters*, vol. 18, no. 19, pp. 2056-2058, 2006.

[71] G. H. Smith and D. Novak, "Broad-band millimeter-wave (38 GHz) fiber-wireless transmission system using electrical and optical SSB modulation to overcome dispersion effects," *IEEE Photonics Technology Letters*, vol. 10, no. 1, pp. 141-143, 1998.

[72] A. Nirmalathas, P. A. Gamage, C. Lim, D. Novak and R. Waterhouse, "Digitized radio-over-fiber technologies for converged optical wireless access network," *Journal of Lightwave Technology*, vol. 28, no. 16, pp. 2366-2375, 2010.

[73] T. Schneider, M. Junker and D. Hannover, "Generation of millimetre-wave signals by stimulated Brillouin scattering for radio over fibre systems," *Electronics Letters*, vol. 40, no. 23, pp. 1500-1502, 2004.

[74] S. Bloom, E. Korevaar, J. Schuster and H. Willebrand, " Understanding the performance of free-space optics," *Journal of optical Networking,* vol. 2, no. 6, pp. 178-200, 2003.

[75] M. Alzenad, M. Z. Shakir, H. Yanikomeroglu and M. S. Alouini, "FSO-based vertical backhaul/fronthaul framework for 5G+ wireless networks," *IEEE Communications Magazine,* vol. 56, no. 1, pp. 218 - 224, 2018.

[76] X. Feng, Z. Wu, T. Wang, P. Zhang, X. Li, H. Jiang, Y. Su, H. He, X. Wang and S. Gao, " Experimental demonstration of bidirectional up to 40 Gbit/s QPSK coherent free-space optical communication link over~ 1 km," *Optics Communications,* vol. 410, pp. 674-679, 2018.

[77] J. Wells, " Faster than fiber: The future of multi-G/s wireless," *IEEE microwave magazine,* vol. 10, no. 3, pp. 104-112, 2009.

[78] C. B. Issaid, K. H. Park, M. S. Alouini and R. Tempone, "Fast Outage Probability Simulation for FSO Links with a Generalized Pointing Error Model," in *IEEE Global Communications Conference (GLOBECOM)*, 2016.

[79] K. Takahashi, "Next Generation Optical Wireless Communication Systems Using Fiber Direct Coupled Optical Antennas," in *Optical Communication*, Intech, 2012.

[80] M. A. Khalighi and M. Uysal, " Survey on free space optical communication: A communication theory perspective," *IEEE Communications Surveys & Tutorials,* vol. 16, no. 4, pp. 2231-2258, 2014.

[81] A. K. Majumdar and J. C. Ricklin, Free-space laser communications: principles and advances, Springer Science & Business Media, 2010.

[82] H. K. Al-Musawi, T. Cseh, J. Bohata, P. Pesek, W. P. Ng, Z. Ghassemlooy, E. Udvary, S. Zvanovec and M. Ijaz, "Fundamental investigation of extending 4G-LTE signal over MMF/SMF-FSO under

controlled turbulence conditions," in *IEEE 10th International Symposium on Communication Systems, Networks and Digital Signal Processing (CSNDSP)*, 2016.

[83] A. E. Morra, K. Ahmed and S. Hranilovic, " Impact of Fiber Nonlinearity on 5G Backhauling via Mixed FSO/Fiber Network," *IEEE Access*, vol. 5, pp. 19942-19950, 2017.

[84] A. Jurado-Navas, A. Tatarczak, X. Lu, J. J. V. Olmos, J. M. Garrido-Balsells and I. T. Monroy, " 850-nm hybrid fiber/free-space optical communications using orbital angular momentum modes," *Optics express*, vol. 23, no. 26, pp. 33721-33732, 2015.

[85] B. Makki, T. Svensson and M. S. Alouini, " On the performance of millimeter wave-based RF-FSO links with HARQ feedback," in *IEEE 27th Annual International Symposium on Personal, Indoor, and Mobile Radio Communications (PIMRC)*, 2016.

[86] T. P. McKenna, J. C. Juarez, J. A. Nanzer and T. R. Clark, " Hybrid millimeter-wave/free-space optical system for high data rate communications," in *IEEE Photonics Conference (IPC)*, 2013.

[87] A. Malik and P. Singh, " Free space optics: current applications and future challenges," *International Journal of Optics*, 2015.

[88] M. Ijaz, Z. Ghassemlooy, S. Rajbhandari, H. Le Minh, J. Perez and A. Gholami, "Comparison of 830 nm and 1550 nm based free space optical communications link under controlled fog conditions," in *IEEE 8th International Symposium on Communication Systems, Networks & Digital Signal Processing (CSNDSP)*, 2012.

[89] A. Malik and P. Singh, "Comparative analysis of point to point FSO system under clear and haze weather conditions," *Wireless personal communications*, vol. 80, no. 2, pp. 483-492, 2015.

[90] M. A. Khalighi, F. Xu, Y. Jaafar and S. Bourennane, "Double-laser differential signaling for reducing the effect of background radiation in

free-space optical systems," *Journal of Optical Communications and Networking*, vol. 3, no. 2, pp. 145-154, 2011.

[91] M. M. Abadi, Z. Ghassemlooy, M. R. Bhatnagar, S. Zvanovec, M. A. Khalighi and A. R. Maheri, " Using differential signalling to mitigate pointing errors effect in FSO communication link," in *IEEE International Communications Workshops (ICC)*, 2016.

[92] R. Rajashekar and L. Hanzo, " Iterative matrix decomposition aided block diagonalization for mm-wave multiuser MIMO systems," *IEEE Transactions on Wireless Communications,* vol. 16, no. 3, pp. 1372-1384, 2017.

[93] M. R. Akdeniz, Y. Liu, M. K. Samimi, S. Sun, S. Rangan, T. S. Rappaport and E. Erkip, "Millimeter wave channel modeling and cellular capacity evaluation," *IEEE journal on selected areas in communications,* vol. 32, no. 6, pp. 1164-1179, 2014.

[94] F. Khan, Z. Pi and S. Rajagopal, "Millimeter-wave mobile broadband with large scale spatial processing for 5G mobile communication," in *IEEE 50th Annual Allerton Conference on Communication, Control, and Computing*, 2012.

[95] J. Bae, Y. S. Choi, J. S. Kim and M. Y. Chung, "Architecture and performance evaluation of MmWave based 5G mobile communication system," in *IEEE International Conference on Information and Communication Technology Convergence (ICTC)*, 2014.

[96] P. Adhikari, "Understanding millimeter wave wireless communication," *Loea Corporation, White paper*, 2008.

[97] M. Marcus and B. Pattan, "Millimeter wave propagation: spectrum management implications," *IEEE Microwave Magazine,* vol. 6, no. 2, pp. 54-62, 2005.

[98] M. S. Omar, M. A. Anjum, S. A. Hassan, H. Pervaiz and Q. Niv, "Performance analysis of hybrid 5G cellular networks exploiting

mmWave capabilities in suburban areas," in *IEEE International Conference on Communications (ICC)*, 2016.

[99] T. S. Rappaport, Y. Xing, G. R. MacCartney, A. F. Molisch, E. Mellios and J. Zhang, "Overview of Millimeter Wave Communications for Fifth-Generation (5G) Wireless Networks—With a Focus on Propagation Models," *IEEE Transactions on Antennas and Propagation*, vol. 65, no. 12, pp. 6213-6230, 2017.

[100] H. Xu, T. S. Rappaport, R. J. Boyle and J. H. Schaffner, "Measurements and models for 38-GHz point-to-multipoint radiowave propagation," *IEEE journal on selected areas in communications*, vol. 18, no. 3, pp. 310-321, 2000.

[101] C. R. Anderson and T. S. Rappaport, "In-building wideband partition loss measurements at 2.5 and 60 GHz," *IEEE transactions on wireless communications*, vol. 3, no. 3, pp. 922-928, 2004.

[102] C. X. Wang, F. Haider, X. Gao, X. H. You, Y. Yang, D. Yuan, H. Aggoune, H. Haas, S. Fletcher and E. Hepsaydir, "Cellular architecture and key technologies for 5G wireless communication networks," *IEEE Communications Magazine*, vol. 52, no. 2, pp. 122-130, 2014.

[103] Z. Muhi-Eldeen, L. P. Ivrissimtzis and M. Al-Nuaimi, "Modelling and measurements of millimetre wavelength propagation in urban environments," *IET microwaves, antennas & propagation*, vol. 9, no. 4, pp. 1300-1309, 2010.

[104] T. S. Rappaport, F. Gutierrez, E. Ben-Dor, J. N. Murdock, Y. Qiao and J. I. Tamir, "Broadband millimeter-wave propagation measurements and models using adaptive-beam antennas for outdoor urban cellular communications," *IEEE transactions on antennas and propagation*, vol. 61, no. 4, pp. 1850-1859, 2013.

[105] Z. Genc, U. H. Rizvi, E. Onur and I. Niemegeers, "Robust 60 GHz indoor connectivity: is it possible with reflections?," in *IEEE Vehicular*

Technology Conference (VTC), 2010.

[106] S. Collonge, G. Zaharia and G. Zein, "Influence of the human activity on wide-band characteristics of the 60 GHz indoor radio channel," *IEEE Transactions on Wireless Communications* , vol. 3, no. 6, pp. 2396-2406, 2004.

[107] C. Liu, L. Zhang, M. Zhu, J. Wang, L. Cheng and G. K. Chang, "A novel multi-service small-cell cloud radio access network for mobile backhaul and computing based on radio-over-fiber technologies," *Journal of Lightwave Technology,* vol. 31, no. 17, pp. 2869-2875, 2013.

[108] V. Jungnickel, K. Manolakis, W. Zirwas, B. Panzner, V. Braun, M. Lossow, M. Sternad, R. Apelfrojd and T. Svensson, " The role of small cells, coordinated multipoint, and massive MIMO in 5G," *IEEE Communications Magazine,* vol. 52, no. 5, pp. 44-51, 2014.

[109] H. Elshaer, M. N. Kulkarni, F. Boccardi, J. G. Andrews and M. Dohler, " Downlink and uplink cell association with traditional macrocells and millimeter wave small cells," *IEEE Transactions on Wireless Communications,* vol. 15, no. 9, pp. 6244-6258, 2016.

[110] P. Smulders, "Exploiting the 60 GHz band for local wireless multimedia access: Prospects and future directions," *IEEE communications magazine,* vol. 40, no. 1, pp. 140-147, 2002.

[111] Z. Cao, Q. Ma, A. B. Smolders, Y. Jiao, M. J. Wale, C. W. Oh, H. Wu and A. M. J. Koonen, "Advanced integration techniques on broadband millimeter-wave beam steering for 5G wireless networks and beyond," *IEEE Journal of Quantum Electronics,* vol. 52, no. 1, pp. 1-20, 2016.

[112] A. Ghosh, T. A. Thomas, M. C. Cudak, R. Ratasuk, P. Moorut, F. W. Vook, T. S. Rappaport, G. R. MacCartney, S. Sun and S. Nie, "Millimeter-wave enhanced local area systems: A high-data-rate approach for future wireless networks," *IEEE Journal on Selected Areas in Communications,* vol. 32, no. 6, pp. 1152-1163, 2014.

[113] S. G. Larew, T. A. Thomas, M. Cudak and A. Ghosh, " Air interface design and ray tracing study for 5G millimeter wave communications," in *IEEE Globecom Workshops (GC Wkshps)*, 2013.

[114] G. R. Maccartney, T. S. Rappaport, S. Sun and S. Deng, "Indoor office wideband millimeter-wave propagation measurements and channel models at 28 and 73 GHz for ultra-dense 5G wireless networks," *IEEE Access*, vol. 3, pp. 2388-2424, 2015.

[115] V. Degli-Esposti, F. Fuschini, E. M. Vitucci, M. Barbiroli, M. Zoli, L. Tian, X. D. D. A. Yin, R. Müller, C. Schneider and R. S. Thomä, " Ray-tracing-based mm-wave beamforming assessment," *IEEE Access*, vol. 2, pp. 1314-1325, 2014.

[116] S. Habib, S. A. Hassan, A. A. Nasir and H. Mehrpouyan, "Millimeter wave cell search for initial access: Analysis, design, and implementation," in *IEEE 13th International Wireless Communications and Mobile Computing Conference (IWCMC)*, 2017.

[117] T. Bai and R. Heath, "Asymptotic SINR for millimeter wave massive MIMO cellular networks," in *IEEE 16th International Workshop on Signal Processing Advances in Wireless Communications (SPAWC)*, 2015.

[118] E. Torkildson, H. Zhang and U. Madhow, " Channel modeling for millimeter wave MIMO," in *IEEE Information theory and applications workshop (ITA)*, 2010.

[119] V. Raghavan, A. Partyka, A. Sampath, S. Subramanian, O. H. Koymen, K. Ravid, J. Cezanne, K. Mukkavilli and J. Li, "Millimeter wave MIMO prototype: Measurements and experimental results," *IEEE Communications Magazine* , vol. 56, no. 1, pp. 202 - 209, 2018.

[120] M. Kyro, V. M. Kolmonen and P. Vainikainen, "Experimental propagation channel characterization of mm-wave radio links in urban scenarios," *IEEE Antennas and Wireless Propagation Letters*, vol. 11,

pp. 865-868, 2012.

[121] Y. Lu, H. W. Hsu and L. C. Wang, “Performance model and deployment strategy for mm-Wave multi-cellular systems,” in *IEEE 25th Wireless and Optical Communication Conference (WOCC)*, 2016.

[122] M. N. Kulkarni, S. Singh and J. G. Andrews, “Coverage and rate trends in dense urban mmWave cellular networks,” in *IEEE Global Communications Conference (GLOBECOM)*, 2014.

[123] T. Bai and R. W. Heath, “ Coverage and rate analysis for millimeter-wave cellular networks,” *IEEE Transactions on Wireless Communications*, vol. 14, no. 2, pp. 1100-1114, 2015.

[124] Z. Yun and M. F. Iskander, “ Ray tracing for radio propagation modeling: principles and applications,” *IEEE Access*, vol. 3, pp. 1089-1100, 2015.

[125] T. S. Rappaport, E. Ben-Dor, J. N. Murdock and Y. Qiao, “ 38 GHz and 60 GHz angle-dependent propagation for cellular & peer-to-peer wireless communications,” in *IEEE International Conference on Communications (ICC)*, 2012.

[126] T. Wu, T. S. Rappaport and C. M. Collins, “Safe for generations to come: Considerations of safety for millimeter waves in wireless communications,” *IEEE microwave magazine*, vol. 16, no. 2, pp. 65-84, 2015.

[127] A. R. Guraliuc, M. Zhadobov, R. Sauleau, L. Marnat and L. Dussopt, “Millimeter-wave electromagnetic field exposure from mobile terminals,” in *IEEE European Conference on Networks and Communications (EuCNC)*, 2015.

[128] G. R. MacCartney and T. S. Rappaport, “Rural Macrocell Path Loss Models for Millimeter Wave Wireless Communications,” *IEEE Journal on Selected Areas in Communications*, 2017.

[129] R. K. Al-Dabbagh, H. S. Al-Raweshidy and N. A. Al-Aboody,

"Performance Comparison of Exploiting Different Millimetre-Wave Bands in 5G Cellular Networks," in *IEEE International Conference on on Performance Evaluation and Modeling in Wired and Wireless Networks (PEMWN)*, Paris, 2017.

[130] R. K. Al-Dabbagh, N. A. Al-Aboody and H. S. Al-Raweshidy, "A Simplified Path Loss Model for Investigating Diffraction and Specular Reflection Impact on Millimetre Wave Propagation," in *IEEE International Conference on Network of the future (NOF)*, King's College London, 2017.

[131] A. M. J. Koonen and M. G. Larrodé, " Radio-over-MMF techniques—Part II: Microwave to millimeter-wave systems," *Journal of Lightwave Technology*, vol. 26, no. 15, pp. 2396-2408, 2008.

[132] J. Ma and Y. Li, " A full-duplex multiband access radio-over-fiber link with frequency multiplying millimeter-wave generation and wavelength reuse for upstream signal," *Optics Communications*, vol. 334, pp. 22-26, 2015.

[133] L. Hu, A. Kaszubowska and L. P. Barry, " Investigation of stimulated Brillouin scattering effects in radio-over-fiber distribution systems," *Optics communications*, vol. 255, no. 4, pp. 253-260, 2005.

[134] S. Preu, G. H. Döhler, S. Malzer, L. J. Wang and A. C. Gossard, " Tunable, continuous-wave terahertz photomixer sources and applications," *Journal of Applied Physics*, vol. 109, no. 6, p. 4, 2011.

[135] S. Preussler, R. P. Braun, M. Grigat and T. Schneider, "Generation of high-quality carrier waves for future high-bitrate THz links," in *Photonic Networks Proceedings of ITG Symposium*, 2014.

[136] H. Chi and J. Yao, " Power distribution of phase-modulated microwave signals in a dispersive fiber-optic link," *IEEE Photonics Technology Letters*, vol. 20, no. 4, pp. 315-317, 2008.

[137] K. Nakkeeran and K. Porsezian, "Solitons in an erbium-doped nonlinear

fibre medium with stimulated inelastic scattering.," *Journal of Physics A: Mathematical and General*, vol. 28, no. 13, p. 3817, 1995.

[138] S. R. A.-R. Abdollahi, S. F. H., M. S. and R. Nilavalan, "Digital radio over fibre for future broadband wireless access network solution," in *IEEE 6th International Conference on Wireless and Mobile Communications (ICWMC)*, 2010.

[139] L. Cheng, M. Zhu, M. M. U. Gul, X. Ma and G. K. Chang, "Adaptive photonics-aided coordinated multipoint transmissions for next-generation mobile fronthaul," *Journal of Lightwave Technology*, vol. 32, no. 10, pp. 1907-1914, 2014.

[140] C. Y. Li, H. H. Lu, C. L. Ying, J. R. Zheng, C. Lin, Y. and Z. W. Wan, "Two-way fiber-wireless convergence systems based on two-stage injection-locked VCSELs transmitter and optical interleaver," *Optics express*, vol. 23, no. 4, pp. 5244-5252, 2015.

[141] M. P. Thakur, S. Mikroulis, C. C. Renaud, J. V. Olmos, M. C. R. Medeiros and J. E. Mitchell, "Cost-efficient DWDM-PON/Mm-wave wireless integration using coherent radio-over-fiber (CRoF)," in *IEEE International Topical Meeting on Microwave Photonics (MWP)*, 2015.

[142] P. T. Dat, A. Kanno and K. ,. K. T. Inagaki, "High-capacity wireless backhaul network using seamless convergence of radio-over-fiber and 90-GHz millimeter-wave," *Journal of Lightwave Technology*, vol. 32, no. 20, pp. 3910-3923, 2014.

[143] P. T. Dat, A. Kanno, N. Yamamoto and T. Kawanishi, "Full-duplex transmission of LTE-A carrier aggregation signal over a bidirectional seamless fiber-millimeter-wave system," *Journal of Lightwave Technology*, vol. 34, no. 2, pp. 691-700, 2016.

[144] Y. Xu, J. Yu, X. Li, J. Xiao and Z. Zhang, "Experimental investigation on fiber-wireless MIMO system with different LO at W band," *IEEE Photonics Journal*, vol. 7, no. 2, pp. 1-7, 2015.

[145] R. Waterhouse and D. Novack, “Realizing 5G: Microwave photonics for 5G mobile wireless systems,” *IEEE Microwave Magazine,* vol. 16, no. 8, pp. 84-92, 2015.

[146] L. Cheng, M. M. U. Gul, F. Lu, M. Zhu, J. Wang, M. Xu, X. Ma and G. K. Chang, “Coordinated multipoint transmissions in millimeter-wave radio-over-fiber systems,” *Journal of Lightwave Technology,* vol. 34, no. 2, pp. 653-660, 2016.

[147] P. T. Dat, A. Kanno and T. Kawanishi, “ Radio-on-radio-over-fiber: efficient fronthauling for small cells and moving cells,” *IEEE Wireless Communications,* vol. 22, no. 5, pp. 67-75, 2015.

[148] Y. Xu, Z. Zhang, X. Li, J. Xiao and J. Yu, “ Demonstration of 60 Gb/s W-band optical mm-wave signal full-duplex transmission over fiber-wireless-fiber network,” *IEEE Communications Letters,* vol. 18, no. 12, pp. 2105-2108, 2014.

[149] S. Rangan, T. S. Rappaport and E. Erkip, “Millimeter-wave cellular wireless networks: Potentials and challenges,” *Proceedings of the IEEE,* vol. 102, no. 3, pp. 366-385, 2014.

[150] H. Dahrouj, A. Douik, F. Rayal, T. Y. Al-Naffouri and M. S. Alouini, “Cost-effective hybrid RF/FSO backhaul solution for next generation wireless systems,” *IEEE Wireless Communications,* vol. 22, no. 5, pp. 98-104, 2015.

[151] I. S. Ansari, M. M. Abdallah, M. S. Alouini and K. A. Qaraqe, “Outage performance analysis of underlay cognitive RF and FSO wireless channels,” in *IEEE 3rd International Workshop in Optical Wireless Communications (IWOW),* 2014.

[152] E. Zedini, I. S. Ansari and M. S. Alouini, “On the performance of hybrid line of sight RF and RF-FSO fixed gain dual-hop transmission systems,” in *IEEE In Global Communications Conference (GLOBECOM),* 2014.

[153] M. Uysal and H. Nouri, “Optical wireless communications—An

emerging technology," in *IEEE 16th International Conference on Transparent Optical Networks (ICTON)*, 2014.

[154] R. Prasad, "5G Revolution through WISDOM," *Wireless Personal Communications,* vol. 81, no. 4, pp. 1351-1357, 2015.

[155] S. A. Busari, K. M. S. Huq, S. Mumtaz, L. Dai and J. Rodriguez, "Millimeter-Wave Massive MIMO Communication for Future Wireless Systems: A Survey," *IEEE Communications Surveys & Tutorials,* 2017.

[156] I. Rodriguez, E. P. Almeida, R. Abreu, M. Lauridsen, A. Loureiro and P. Mogensen, "Analysis and comparison of 24 GHz cmWave radio propagation in urban and suburban scenarios," in *IEEE Wireless Communications and Networking Conference (WCNC)*, 2016.

[157] F. Devoti, I. Filippini and A. Capone, " Facing the Millimeter-Wave Cell Discovery Challenge in 5G Networks With Context-Awareness," *IEEE Access,* vol. 4, pp. 8019-8034, 2016.

[158] I. Hemadeh, S. Katla, M. El-Hajjar and L. Hanzo, "Millimeter-wave communications: physical channel models, design considerations, antenna constructions and link-budget," *IEEE Communications Surveys and Tutorials,* 2017.

[159] D. U. P. L. Erricolo, "Propagation path loss-a comparison between ray-tracing approach and empirical models," *IEEE Transactions on Antennas and Propagation,* vol. 50, no. 5, pp. 766-768, 2002.

[160] L. Li, Y. Wang and K. Gong, "Measurements of building construction materials at Ka-band," *International journal of infrared and millimeter waves,* vol. 19, no. 9, pp. 1293-1298, 1998.

Publications and Presentations

Journal Papers

1. **R. K. Al-Dabbagh** and H. S. Al-Raweshidy, "Photonic methods of millimeter-wave generation based on Brillouin fiber laser," *Elsevier Journal of Optics & Laser Technology*, vol. 79, pp. 124-131, 2016.
2. **R. K. Al-Dabbagh** and H. S. Al-Raweshidy, "64-GHz millimeter-wave photonic generation with a feasible radio over fiber system," *SPIE Journal of Optical Engineering*, vol. 56, no. 2, p. 026117, 2017.

Conferences papers

3. **R. K. Al-Dabbagh**, N. A. Al-Aboody and H. S. Al-Raweshidy, "A Simplified Path Loss Model for Investigating Diffraction and Specular Reflection Impact on Millimetre Wave Propagation," in *IEEE International Conference on Network of the future (NOF)*, King's College London, 2017.
4. **R. K. Al-Dabbagh**, H. S. Al-Raweshidy and N. A. Al-Aboody, "Performance Comparison of Exploiting Different Millimetre-Wave Bands in 5G Cellular Networks," in *IEEE International Conference on on Performance Evaluation and Modeling in Wired and Wireless Networks (PEMWN)*, Paris, 2017.

Poster Presentations and Research Seminars

5. **R. K. Al-Dabbagh**, "A Simplified Path Loss Model for Investigating Diffraction and Specular Reflection Impact on Millimetre Wave Propagation," *Poster in IEEE International Conference on Network of the future (NOF)*, King's College London, Nov., 2017.
6. **R. K. Al-Dabbagh**, "Performance Comparison of Exploiting Different Millimetre-Wave Bands in 5G Cellular Networks," in *Electronic and*

Computer Engineering (ECE) Seminar, Brunel University London, Nov., 2017.

7. **R. K. Al-Dabbagh**, "Futuristic Mobile Communication Systems Using Millimetre-Wave," in *three minute thesis (3MT) competition presentation*, Brunel University London, Jan. 2016.

Awards

8. **R. K. Al-Dabbagh**, *Vice-Chancellor's Travel Prize for Postgraduate Research Students*, Brunel University London, Oct., 2017.